

Alma Mater Studiorum Università di Bologna
Archivio istituzionale della ricerca

A review of cretaceous smooth-slopes extensional basins along the Iberia-Eurasia plate boundary: How pre-rift salt controls the modes of continental rifting and mantle exhumation

This is the final peer-reviewed author's accepted manuscript (postprint) of the following publication:

Published Version:

Yves Lagabriele, Riccardo Asti, Thibault Duret, Camille Clerc, Serge Fourcade, Antonio Teixell, et al. (2020). A review of cretaceous smooth-slopes extensional basins along the Iberia-Eurasia plate boundary: How pre-rift salt controls the modes of continental rifting and mantle exhumation. EARTH-SCIENCE REVIEWS, 201(103071), 1-24 [10.1016/j.earscirev.2019.103071].

Availability:

This version is available at: <https://hdl.handle.net/11585/943166> since: 2023-09-27

Published:

DOI: <http://doi.org/10.1016/j.earscirev.2019.103071>

Terms of use:

Some rights reserved. The terms and conditions for the reuse of this version of the manuscript are specified in the publishing policy. For all terms of use and more information see the publisher's website.

This item was downloaded from IRIS Università di Bologna (<https://cris.unibo.it/>).
When citing, please refer to the published version.

(Article begins on next page)

This is the final peer-reviewed accepted manuscript of:

Yves Lagabrielle; Riccardo Asti; Thibault Duretz; Camille Clerc; Serge Fourcade; Antonio Teixell; Pierre Labaume; Benjamin Corre; Nicolas Saspiturry: *A review of cretaceous smooth-slopes extensional basins along the Iberia-Eurasia plate boundary: How pre-rift salt controls the modes of continental rifting and mantle exhumation*

EARTH-SCIENCE REVIEWS VOL. 201 ISSN 0012-8252

DOI: 10.1016/j.earscirev.2019.103071

The final published version is available online at:

<https://dx.doi.org/10.1016/j.earscirev.2019.103071>

Terms of use:

Some rights reserved. The terms and conditions for the reuse of this version of the manuscript are specified in the publishing policy. For all terms of use and more information see the publisher's website.

This item was downloaded from IRIS Università di Bologna (<https://cris.unibo.it/>)

When citing, please refer to the published version.

7
8 **A review of Cretaceous smooth-slopes extensional basins along the Iberia-**
9 **Eurasia plate boundary: how pre-rift salt controls the modes of continental**
10 **rifting and mantle exhumation**
11
12

13
14
15 by :

16
17
18 9 Yves Lagabriele¹, Riccardo Asti¹, Thibault Duretz¹, Camille Clerc², Serge Fourcade¹, Antonio
19
20 Teixell⁴, Pierre Labaume³, Benjamin Corre¹, Nicolas Saspiturry⁵
21

22
23
24
25 13 Addresses

26 14 1. Université de Rennes, CNRS, UMR 6118 Géosciences Rennes, Campus de Beaulieu, 35000 Rennes, France
27

28
29 16 2. ISEA, Université de la Nouvelle Calédonie, 98800 Nouméa, Nouvelle Calédonie
30

31
32 18 3. Géosciences Montpellier, CNRS-Université de Montpellier-Université des Antilles, 34095 Montpellier, France
33

34
35 20 4. Dept. de Geologia, Universitat Autònoma de Barcelona, 08193 Bellaterra, Spain
36

37
38 22 5. EA4592 Géoressources & Environnement, Bordeaux INP, Université Bordeaux Montaigne, 1 Allée Daguin,
39 33607 Pessac, France
40

41
42 25 Riccardo Asti riccardo.asti@univ-rennes1.fr, Duretz Thibault thibault.duretz@univ-rennes1.fr, Camille Clerc
43 camille.clerc@univ-nc.nc, "Serge Fourcade; sg.fourcade@orange.fr" sg.fourcade@orange.fr, Antonio Teixell
44 antonio.teixell@uab.cat, "Pierre Labaume" labaueme@gm.univ-montp2.fr, "Benjamin Corre"
45 benjcorre@hotmail.fr, Saspiturry Nicolas saspiturry.nicolas@gmail.com,
46
47
48
49
50

51 31 *Corresponding author: Yves Lagabriele. yves.lagabriele@univ-rennes1.fr*
52
53
54
55
56
57
58
59
60

61
62
63 **34 Key words** : Smooth-slopes basins; symmetrical profile; Iberia; Eurasia; Triassic evaporites;
64
65 décollement layer; thermal anomaly; sedimentary burial; dominating-ductile tectonic
66
67 regime.

68 **37 Short abstract (for submission)**

69 We enhance a striking correlation between the paleogeography of Upper Triassic deposits
70 and the mode of crustal stretching of the north Iberia plate during the Cretaceous
71 transtensional event. The basins which opened during the mid-Cretaceous times along the
72 Iberia-Eurasia plate boundary (like the emblematic Parentis basin) exhibit a peculiar
73 synclinal-shaped profile and are devoid of prominent block faulting. The top of the basement
74 is characterized by gentle slopes dipping symmetrically towards the basin center. Based on a
75 comparison with rifting models established from the North Pyrenean Zone, this architecture
76 appear to result from the thinning of the central basin continental crust under dominating-
77 ductile deformation in greenschist facies conditions. The common character shared by all
78 the pre-rift sequences of the studied basins is the presence of a thick low-strength Upper
79 Triassic evaporites and clays layer belonging to the Keuper group and forming a thick pre-rift
80 low-strength unit. Efficient décollement along this layer triggers mechanical decoupling and
81 gliding of the pre-rift cover remaining in the basin center as the continental crust is laterally
82 extracted. Using recent paleogeographic reconstructions, we show that the distribution of
83 the Keuper sediments remarkably matches the distribution of the Pyrenean and peri-
84 Pyrenean, Parentis-type basins. This allows for the first time to propose a genetic link
85 between the distribution of evaporite-bearing pre-rift sedimentary formations and the
86 development of smooth-slopes rift basins.
87
88
89

90
91 56

92 57

93 **58 Abstract**

94 59

95 This article enhances for the first time a striking correlation between the paleogeography of
96
97 Upper Triassic deposits and the mode of crustal stretching around and inside the Iberia plate
98 during the Cretaceous transtensional event. In a first step, we propose a review of the
99 architecture of the basins which opened during the mid-Cretaceous times along the Iberia-
100 Eurasia plate boundary. Like the emblematic Parentis basin, all these basins exhibit a
101 peculiar synclinal-shaped profile and are devoid of prominent block faulting. The top of the
102 basement is characterized by gentle slopes, which dip symmetrically towards the center of
103 the basins. Based on a comparison with recent geologically-based rifting models established
104 from the North Pyrenean Zone, we propose that this architecture results from the thinning
105 of the central basin continental crust under dominating-ductile deformation in greenschist
106 facies conditions. The common character shared by all the pre-rift sequences of the studied
107 basins is the presence of a thick low-strength Upper Triassic evaporites and clays layer
108 belonging to the Keuper group and forming a specific pre-rift salt unit. In the studied basins,
109
110
111
112
113
114
115
116
117
118
119
120

121
122
123 73 efficient décollement along the Keuper evaporites and clays triggers mechanical decoupling
124
125 74 and gliding of the pre-rift cover that remains in the center of the basin as the continental
126
127 75 crust is laterally extracted. Thus, during the early rifting phase, the basement undergoes
128
129 76 thinning while the pre-rift cover remains preserved in the basin center. In response to hyper-
130
131 77 thinning and horizontal extraction of the continental crust, hot mantle material approaches
132
133 78 the detached pre-rift cover. The major consequences of this central basin thermal anomaly
134
135 79 are twofolds: (i) the ductile deformation of the thinned continental crust beneath the
136
137 80 detached pre-rift units, and (ii) the development of HT-LP metamorphic conditions in the
138
139 81 pre-rift sediments and at the base of the syn-rift flysch levels. This thermal event is well
140
141 82 recorded in the axial portion of the Pyrenean realm (future North Pyrenean Zone) as well as
142
143 83 in the pre-rift sediments of the Cameros basin (northern Spain). Continental stretching is
144
145 84 accommodated by shearing in the bulk upper and middle crust leading to the formation of
146
147 85 thin tectonic lenses of mylonitic crustal material remaining welded on the exhuming mantle.
148
149 86 The architecture of the smooth-slopes, Parentis-type basins studied in this article thus
150
151 87 contrasts with the structure of the Iberia-Newfoundland Atlantic margins which are
152
153 88 characterized by (i) top-basement detachment faults accommodating crustal extension
154
155 89 through rotation and translation of undeformed basement blocks, and (ii) by the
156
157 90 individualization of continental extensional allochthons lying tectonically over exhumed
158
159 91 lower crust or mantle rocks. Finally, using recent paleogeographic reconstructions, we show
160
161 92 that the distribution of the Keuper evaporites and clays remarkably matches the distribution
162
163 93 of the Pyrenean and peri-Pyrenean, Parentis-type basins. This allows for the first time to
164
165 94 propose a genetic link between the distribution of evaporite-bearing pre-rift sedimentary
166
167 95 formations and the development of smooth-slopes rift basins.
168
169
170
171
172
173
174
175
176
177
178
179
180

181
182
183 **97 Introduction**

184 98

185 99 More than 30 years ago, important steps in our understanding of the mechanisms of
186
187 100 continental rifting were achieved through the acquisition and interpretation of ECORS
188
189 101 seismic reflection profiles (1983-1994) (Damotte et al., 1998). New images of crustal and
190
191 102 Moho geometries beneath stretched continental crusts were obtained, shading light on
192
193 103 important discrepancies between structural patterns at the base of rift systems. In
194
195 104 particular, ECORS profiles from the Rhine graben and the Parentis basin displayed
196
197 105 contrasting images of the thinned upper lithosphere. In the first case, the upper crust
198
199 106 appears clearly rifted and offset by stepping normal faults (Brun et al., 1991) whilst, despite
200
201 107 slight tectonic inversion, the second case exhibits a smooth basement top, with gentle
202
203 108 slopes dipping symmetrically towards the basin center (Bois et al., 1997). Because only few
204
205 109 cases of Parentis-type architecture were observed worldwide, little attention has been paid
206
207 110 to this symmetrical, smooth-slopes type of continental rift, which apparently lacks major
208
209 111 upper crustal faulting and block tilting. Rather, most of the current models of rift-related
210
211 112 crustal thinning generally point to the individualization of a series of tilted continental blocks
212
213 113 indicating that the upper crustal levels behave in a dominant brittle mode in the proximal (or
214
215 114 continentward) as well as in the distal (or oceanward) margin domains. In such models,
216
217 115 shallow detachment faults accommodate the upper crustal extension through the rotation
218
219 116 and the translation of undeformed basement blocks. In the distal margin, these blocks,
220
221 117 referred to as extensional allochthons, are covered by syn-rift and post-rift sediments and
222
223 118 may lie tectonically over exhumed lower levels, including subcontinental mantle (Reston et
224
225 119 al., 1995; Manatschal et al., 2001; Jammes et al., 2010c; Osmundsen and Peron-Pinvidic,
226
227 120 2018, and references therein).

228
229 121 Recent geological investigations in the northern units of the Pyrenean belt forming the
230
231 122 North Pyrenean Zone (NPZ) as well as in the Basque-Cantabrian basin (fig. 1) show that
232
233 123 Parentis-type basins of mid-Cretaceous age were distributed all along the boundary between
234
235 124 the northern Iberia and southern Eurasia plates, thus introducing doubts regarding the
236
237 125 ubiquitous character of Iberia-Newfoundland-type margins (Lagabrielle et al., 2010 ; Clerc
238
239 126 and Lagabrielle, 2014; Teixell et al., 2016; 2018; Asti et al., 2019). In this article, we first list
240
127 the main characteristics of these Parentis-type basins, based on the analysis of detailed
128 geological reconstructions from areas exposed all along the northern flank of the Pyrenean

241
242
243 129 belt. Then we review the distribution of such basins at the scale of the Iberia and Eurasia
244
245 130 plates. We finally discuss some of the key-factors controlling the evolution of smooth-slopes
246
247 131 basins and we evaluate how such information increases our understanding of the
248
249 132 mechanisms of continental rifting and passive margin formation.

250 133

252 134 **I. Symmetrical, smooth-slopes basins of the north Iberia margin: insights from the North**
253 135 **Pyrenean Zone (NPZ) and the Basque-Cantabrian range**

254
255 136

256
257 137 The Pyrenees and the Cantabrian mountain (fig. 1) form a narrow, N110 trending fold-and-
258
259 138 thrust belt resulting from the collision of the northern edge of the Iberia plate (north Iberia
260
261 139 margin) with the southern edge of the Eurasia plate during the Late Cretaceous-Tertiary
262
263 140 (Choukroune and ECORS team, 1989; Muñoz, 1992; Deramond et al., 1993; Roure and
264
265 141 Choukroune, 1998; Teixell, 1998; Vergés and Garcia-Senz, 2001; Pedrera et al., 2017; Teixell
266
267 142 et al., 2018). Convergence initiated ca. 83 Ma, following an almost 40 Ma long period of
268
269 143 transtensional motion in relation with the counterclockwise rotation of Iberia relative to
270
271 144 Eurasia, also leading to oceanic spreading in the Bay of Biscaye between Chron M0 and A33o
272
273 145 (ca. 125-83 Ma) (Le Pichon et al., 1971; Choukroune and Mattauer, 1978; Olivet, 1996;
274
275 146 Sibuet et al., 2004). Convergence led to the partial or complete tectonic inversion of
276
277 147 discontinuous Cretaceous rift basins opened along the Iberia-Eurasia plate boundary during
278
279 148 the transtensional episode (Puigdefàbregas and Souquet, 1986; Debroas, 1990). Rotation
280
281 149 was achieved just before the Albian according to paleomagnetic data collected onland (Gong
282
283 150 et al., 2008). Earlier Triassic and Jurassic rifting events preceded the development of the
284
285 151 Cretaceous rifts (Canérot, 2017, and references therein).

286
287 152 Along the northern flank of the Pyrenees, more than forty, up to km-sized exposures of
288
289 153 subcontinental lherzolites are widespread within the Mesozoic pre-rift and syn-rift
290
291 154 sediments forming the NPZ (Monchoux, 1970; Vielzeuf and Kornprobst, 1984; Fabriès *et al.*,
292
293 155 1991, 1998). The NPZ is bounded by two major post-metamorphic thrusts, the North
294
295 156 Pyrenean Fault (NPF) to the South and the North Pyrenean Frontal Thrust (NPFT) to the
296
297 157 North. The NPF represents the tectonic boundary between the NPZ and the prominent axial
298
299 158 zone of the belt (AZ) constituted of a stack of Paleozoic basement units (Choukroune, 1976a;
300 159 1976b; 1978b).

300 160 Based on field and geophysical evidence from the central and western NPZ, exhumation of

301
302
303 161 sub-continental mantle is shown to have occurred coevally with extreme thinning of the
304 162 continental crust in the Pyrenean realm during the mid-Cretaceous (Lagabrielle and
305 163 Bodinier, 2008; Jammes et al., 2009; Masini et al., 2014). Therefore, mantle exhumation
306 164 (locally followed by peridotite exposure up to the floor of the Pyrenean basins) is now
307 165 considered as a general mechanism accounting for the presence of ultramafic material
308 166 within the NPZ. It is established that the well-known regional high temperature and low
309 167 pressure (HT-LP) Pyrenean metamorphism (Ravier, 1957; Azambre & Rossy, 1976; Bernus-
310 168 Maury, 1984) developed along the southern NPZ in relation with continental thinning during
311 169 the major Cretaceous extensional event (Vielzeuf and Kornprobst, 1984; Dauteuil and Ricou,
312 170 1989; Golberg & Leyreloup 1990; Clerc et al., 2015b; 2016). Following the early ECORS
313 171 profiles (Choukroune and ECORS team, 1989), additional information on the architecture of
314 172 the paleo-margin of Northern Iberia in the Pyrenees is provided by recent interpretation of
315 173 tomographic data acquired during the temporary PYROPE and IBERARRAY experiments
316 174 across the Pyrenees (Chevrot et al., 2015; 2018; fig. 1). Based on such data set, Wang et al.
317 175 (2016) suggest the inversion of a northern Iberia margin characterized by a short necking
318 176 domain and a large distal domain made of strongly attenuated crust (less than 10 km thick)
319 177 overlying a large volume of subcontinental mantle. As discussed further in this article, this
320 178 domain can be compared to large sheets of hyper-extended continental crust found in the
321 179 distal portions of present-day passive continental margins (see section III C)

322
323
324
325
326
327
328
329
330
331
332
333
334
335
336
337
338
339
340
341
342
343
344
345
346
347
348
349
350
351
352
353
354
355
356
357
358
359
360

180

181 Various models of continental crust thinning and associated mantle exhumation have been
182 proposed recently to account for geological constraints collected inside the metamorphic
183 NPZ. In figure 2 (profiles a to e), we present a selection of reconstructions extracted from
184 recent literature, which highlights numerous similarities between recently published models
185 of Cretaceous NPZ basins structure (Lagabrielle et al., 2010; Clerc and Lagabrielle, 2014;
186 Masini et al., 2014; Tugend et al., 2014; 2015; Clerc et al., 2016; Teixell et al., 2016, 2018;
187 Corre et al., 2016; Lagabrielle et al., 2016; DeFelipe et al., 2017; Pedrera et al., 2017; Espurt
188 et al., 2019; Saspiturry et al., 2019; Asti et al., 2019; Ducoux et al., in review). Most of these
189 architecture models stress the role played by a major cover décollement layer during the
190 Cretaceous crustal thinning. This weak layer corresponds to the Upper Triassic Keuper
191 evaporites which contain clays and sands as well as minor carbonates and doleritic MORB
192 basalts (ophites). Its maximum thickness in the Pyrenean realm reached 2.7 km, as deduced

361
362
363 193 from field data in the southern Pyrenees coupled to well data in the Mauléon and Aquitaine
364
365 194 basins and the Bay of Biscay region (James & Canérot, 1988; McClay et al., 2004; Biteau et
366
367 195 al., 2006; Jammes et al., 2010a; 2010b; 2010c; Roca et al., 2011; Saura et al., 2016; Orti et
368
369 196 al., 2017; Saspiturry et al., 2019). In the décollement layer now exposed in the metamorphic
370
371 197 NPZ, the Triassic clays were transformed into talc and chlorite, and the carbonates most
372
373 198 often suffered intense tectonic brecciation with talc, tremolite and dolomite
374
375 199 recrystallizations (Thiébaud et al., 1992; Lagabrielle et al., 2019a, 2019b). Pre-rift to syn-rift
376
377 200 salt diapirism was also frequently observed in the non-metamorphic NPZ and in the
378
379 201 Southern Pyrenees (e.g. Canérot, 1988; 1989; Lenoble and Canérot, 1992; Canérot and
202
203 Lenoble, 1989; 1993; James and Canérot, 1999; Canérot et al., 2005; Jammes et al., 2009;
204
205 Jammes et al., 2010a; 2010b; Roca et al., 2011; Saura et al., 2016; Teixell et al., 2016).

204
205 As early stated by Clerc and Lagabrielle, (2014), the main consequence of the presence of
206
207 the low-strength Keuper layer along the north Iberia margin is that during the Cretaceous
208
209 rifting, the pre-rift Mesozoic cover was efficiently decoupled from the Paleozoic basement
210
211 along the evaporites and thus remained on top of the stretched continental lithosphere in
212
213 the center of the basin. It must be noted that in the external parts of the Pyrenean rift, the
214
215 borders of the subsiding Cretaceous flysch basins remain at low temperature and display
216
217 classical faulted and tilted blocks (e.g. half-grabens of Quillan basin, Camarade basin,
218
219 Gensac-Bonrepos basin, western border of the Mauléon basin, edges of the Gran Rieu high
220
221 and Lacq basin) (Debroas, 1978; 1990; Biteau et al., 2006; Lagabrielle et al., 2010; Masini et
222
223 al., 2014; Grool et al., 2018; Espurt et al., 2019).

215
216 The Cinco Villas Paleozoic massif and the Le Danois Bank (fig. 1) respectively form the
217
218 eastern and western boundary of the Basque-Cantabrian basin which develops to the west
219
220 of the NPZ towards the northern Iberia Peninsula. It is filled by an up to 12.5 km thick
221
222 succession of Upper Jurassic-Cretaceous sediments with interlayered Aptian to Santonian
223
224 basic volcanic rocks (Azambre and Rossy, 1976; Rat et al., 1983; Rat, 1988; Castañares et al.,
2001; García-Mondéjar et al., 1996; 2004; Floquet, 2004) (fig. 2f-h). This basin was floored by
an extremely thinned lithosphere in its central parts (Biscay Synclinorium and Nappes des
Marbres) and was also affected by a Late Cretaceous thermal metamorphism (Golberg and
Leyreloup, 1990; Cuevas and Tubía, 1999; Pedrera et al., 2017). A peridotite outcrop close to

421
422
423 225 the Leiza fault shows that crustal thinning led to the exhumation of the upper mantle close
424 226 to the floor of the basin (Mendia and Gil-Ibarguchi, 1991; deFelipe et al., 2017). The basin
425 227 architecture deduced from field investigations in the eastern part of the Basque-Cantabrian
426 228 basin (the “Nappe des Marbres” area) includes smooth-slopes margins with normal faults
427 229 and tilted blocks restricted to the external domains (deFelipe et al., 2017; Pedrera et al.,
430 230 2017; Ducoux et al., in review). These reconstructed geometries bear affinities with basin
431 231 architectures deduced from geological observations in the NPZ (fig. 2f-h). Indeed, such
432 232 architecture and the overall evolution deduced for this rift system implicate gliding of the pre-
433 233 rift sequence over its basement during crustal extension with ductile crustal thinning in its
434 234 central part in a way similar to models deduced from NPZ studies (e.g. Clerc and Lagabrielle,
435 235 2014; Corre et al., 2016; Teixell et al., 2016). The Leiza detachment system of deFelipe et al.
436 236 (2017) (fig. 2g) corresponds to the basal décollement allowing pre-rift sequence allochthony.
437 237 The presence of a high-density mantle body beneath the Basque-Cantabrian basin has been
438 238 established on the basis of lithospheric-scale gravity inversion (Pedrera et al., 2017). The
439 239 association of this exhumed mantle body with rift and post-rift structural geometries
440 240 suggests the activation of a major south-dipping ramp-flat-ramp extensional detachment
441 241 between Valanginian and early Cenomanian times with horizontal extension of ~48 km.
442 242 Interpretation of geophysical data shows that low-strength Triassic Keuper evaporites and
443 243 mudstones above the basement favor the decoupling of the cover with formation of
444 244 minibasins, expulsion rollovers, and diapirs (Pedrera et al., 2017).

445
446
447
448
449
450
451
452
453
454
455
456
457 245

458
459 246 Finally, the presence of a thick pre-rift salt layer underlying the Mesozoic carbonates
460 247 appears as an ubiquitous parameter to take into account when reconstructing the evolution
461 248 of the Cantabrian-Pyrenean range. Recent models of rift development at the northern Iberia
462 249 margin show that Triassic lithology controls the three intrinsic characteristics of the
463 250 Pyrenean rifting which can be summarized as follows:

- 464
465
466
467 251 i. Tectonic juxtaposition of exhumed peridotites and pre-rift sediments. This occurs
468 252 when the lateral extraction of the thinned continental crust is completed. In
469 253 response to plate separation, the stretched crust is removed horizontally from the
470 254 center of the rift and decoupling of the pre-rift cover from its basement occurs along
471 255 the Keuper décollement. As a consequence a tectonic contact is established between
472 256 the decoupled pre-rift sediments and the uplifted sub-continental mantle rocks

481
482
483
484
485
486
487
488
489
490
491
492
493
494
495
496
497
498
499
500
501
502
503
504
505
506
507
508
509
510
511
512
513
514
515
516
517
518
519
520
521
522
523
524
525
526
527
528
529
530
531
532
533
534
535
536
537
538
539
540

257 (Clerc and Lagabrielle, 2014) (fig. 2e). In some locations, due to subsequent complete
258 removal of the pre-rift cover, mantle rocks may be in turn exposed to the seafloor as
259 observed around the Lherz, Urdach and Bestiac Iherzolite bodies (Lagabrielle et al.
260 2010; 2016; de Saint Blanquat et al., 2016).

261 ii. Crustal stretching under dominantly-ductile conditions. The geometry of the thinned
262 crustal units in the distal domain of the rift margins does not correspond to a
263 succession of triangular-shaped isolated undeformed blocks (extensional
264 allochthons) as described along the Iberia-Newfoundland conjugate margins and
265 along the reconstructed alpine paleomargins (Manatschal, 2001; Manatschal et al.,
266 2001; 2006; Peron-Pinvidic and Manatschal, 2009; Mohn et al., 2010; 2012; 2015)
267 (fig. 3). By contrast, it appears as an assemblage of very thin lenses of ductilely
268 deformed pre-Mesozoic material, originating mainly from the middle crust,
269 separated by anastomosing shear zones that developed in greenschist facies
270 conditions at low pressure (e.g. Corre et al., 2016; Teixell et al., 2016; Asti et al.,
271 2019; Espurt et al., 2019) (fig. 2b-d). This important feature occurs because stretching
272 develops under the allochthonous pre-rift cover that maintains moderate
273 temperature in the upper and middle crust. Microscopic study of crustal material
274 welded on the Urdach Iherzolites demonstrates that the middle crust was extracted
275 laterally from the rift axis and deformed ductilely at temperatures between 450°C
276 and 350°C (Asti et al., 2019). Large strains in the greenschist facies are testified by
277 strongly elongate quartz ribbons in ortho- and para-derived mylonites with bulging
278 recrystallization and brittle fracturing of feldspar in cataclastic flows (fig. 4a-b).

279 iii. Dominantly ductile deformation of the pre-rift and syn-rift sediments under HT-LP
280 conditions. All along the rifting phase, the decoupled pre-rift cover remains in the
281 center of the rift where the rift-related rise of the isotherms is more pronounced and
282 where it is progressively buried under thick flysch sequence deposits. Sedimentary
283 burial first preserves heat acquired during early rifting stages and second trigger
284 temperature increase in the pre-rift cover. As a result, the detached pre-rift cover
285 locally undergoes drastic syn-metamorphic ductile thinning and boudinage during
286 continental breakup (fig. 5a-d). Such peculiar mechanical behaviour is outlined in all
287 published rifting models (i.e. base of Nappe des Marbres basins, Leiza detachment
288 system, base of Mauléon and Chaînons Béarnais basin infills, base of Baronnies and

541
542
543
544
545
546
547
548
549
550
551
552
553
554
555
556
557
558
559
560
561
562
563
564
565
566
567
568
569
570
571
572
573
574
575
576
577
578
579
580
581
582
583
584
585
586
587
588
589
590
591
592
593
594
595
596
597
598
599
600

289 Boucheville basins infill, fig. 2). Progressive rifting triggers the upward propagation of
290 the brittle-ductile transition which may reach syn-rift sediments deposited at the
291 early stage of the basin opening (Clerc et al., 2016). Brittle deformation dominated by
292 cataclastic brecciation follows ductile shearing and flattening in sedimentary units
293 accompanying final exposure of mantle rocks to the seafloor, as proposed from
294 studies in the Lherz area (Lagabrielle et al., 2016). The ductile-brittle transition is
295 frequently observed at the mesoscopic and microscopic scale with sets of normal
296 faults offsetting the extensional HT foliation (fig. 5e-f, 5h). Finally, at the scale of the
297 entire rift, extensional deformation in the lower margin is accompanied by tectonic
298 denudation of the cover in the upper margin (Lagabrielle et al., 2010; Teixell et al.,
299 2016, 2018).

300

301 To sum up, figure 6 presents the intrinsic characteristics of the Pyrenean rifting listed
302 above, compiled along an idealized column of the NPZ lithologies with photographs
303 illustrating the most emblematic deformed levels exposed along the NPZ.

304

305 **II. A review of smooth-slopes basins around the Pyrenees and Cantabrian ranges**

306

307 Seismic images of oceanic margins and intracontinental rifts in the close surroundings of the
308 Pyrenees and Cantabrian ranges bear crucial information on the mode of crustal thinning
309 along the northern Iberia margin and adjacent areas during the Cretaceous.

310

311 (1) Parentis basin (fig. 1 and 7a). First interpretations of the Parentis ECORS profile point to a
312 symmetrical, syncline-shaped basin, with only few normal faults in the stretched crust, even
313 in the proximal domain (Pinet et al., 1987; Bois et al., 1997). Beneath the Parentis basin fill,
314 the crust is less than 10 km thick and decreases westward from 7 km (along the ECORS Bay
315 of Biscay profile, fig. 1), to 6–5 km (along the MARCONI 3 profile, fig. 1) (Tomassino and
316 Marillier, 1997; Gallart et al., 2004; Ruiz, 2007). More recently, Jammes et al. (2010a),
317 proposed that the southern Parentis basin represents a lower plate sag basin floored by a
318 top-basement detachment system with an asymmetrical mode of opening. These authors
319 emphasize the presence of a thick pre-rift salt layer in the area undergoing extreme crustal
320 thinning, forcing sub- and suprasalt layers to deform differently. Whatever the processes of

601
602
603 321 crustal thinning are favoured, both older and recent models of Parentis basin evolution
604
605 322 highlight three major features: (1) the occurrence of symmetrical smooth-slopes gently
606
607 323 dipping basinward; (2) the presence of a crust which thins regularly towards basin axis,
608
609 324 without discrete steeply dipping faults, and (3) the presence of a thick pre-rift salt layer
610
611 325 allowing décollement of the pre-rift cover from its basement (Jammes et al., 2010b, 2010c).

612
613 326 (2) South Bay of Biscay margin (fig. 1, fig. 7b-c). Both the northern and southern margins of
614
615 327 the Bay of Biscay have been explored seismically. North-south transects of the Armorican
616
617 328 margin (Norgasis profiles, fig. 1: Thinon et al., 2003; Tugend et al., 2014) reveal a short
618
619 329 necking domain that concentrates most of the crustal deformation. Crustal thickness
620
621 330 decreases from 35 km at the shelf break to less than 10 km at the foot of the slope. Steep
622
623 331 rise of mantle implies the disappearance of the lower crust beneath the slope. Based on
624
625 332 results of gravity inversion combined with seismic interpretations, Tugend et al. (2014) map
626
627 333 a continuous domain of exhumed mantle from the Armorican basin toward the
628
629 334 hyperthinned Parentis basin where minimum crustal thickness occurs (fig. 7a) (Pinet et al.,
630
631 335 1987, Bois et al., 1996, Jammes et al., 2010a). According to Roca et al. (2011), the Bay of
632
633 336 Biscay Abyssal Plain itself consists of a transitional zone formed by a thin (4–9 km) crust with
634
635 337 riders of Mesozoic pre-rift and syn-rift sediments and continental crustal rocks that are
636
637 338 extensionally detached over an exhumed sub-continental mantle with seismic velocities
638
639 339 comprised between 7.2 and 8 km/s. The distal domain of the Bay of Biscay Abyssal Plain
640
641 340 bounds to the north the North Iberian margin, an extended continental margin with
642
643 341 Cretaceous basins (e.g. the Asturian basin, up to 10 km thick, fig. 1) and basement highs as
644
645 342 the Le Danois Bank (Cadenas and Fernández Viejo, 2016; Teixell et al., 2018), where
646
647 343 granulites have been dredged (Capdevila et al., 1980; Fügenschuh et al., 2003) (fig. 1).

648
649 344 (3) North-eastern Iberia intra-crustal basins (Iberian Chain and Valencia trough) (fig 1 and fig.
650
651 345 7b-d). Helpful additional information regarding the thinning modes of the northern Iberia
652
653 346 crust can be obtained from seismic images of the Los Cameros, Maestrat and Columbrets
654
655 347 basins now partly inverted in the Iberian Chain (fig. 1). These basins result from the
656
657 348 distributed extension of the northern Iberia plate synchronously with the opening of the Bay
658
659 349 of Biscay-Pyrenees in the mid-Cretaceous (Verges and Garcia-Senz, 2001; Mas et al., 2011).
660
661 350 They represent a well-developed Mesozoic rift having similarities with the North Atlantic
662
663 351 margins (Salas and Casas, 1993; Salas et al., 2001). In their internal parts, reconstructed

661
662
663 352 Iberian Chain basin geometries point to simple troughs exhibiting gentle slopes devoid of
664
665 353 marked fault stepping, suggesting the absence of tilted blocks and a smooth basement top
666
667 354 (e.g. Guimerà et al., 1995; Casas-Sainz and Gil-Imaz, 1998; Omodeo et al., 2014). The Moho
668
669 355 generally shows an arched outline with a regular shallowing toward the basin center where
670
671 356 the crust is reduced to some kilometers only. The Triassic evaporites play an important role
672
673 357 during the Albian rifting in the basins of northeast Iberia. This role was recently well
674
675 358 illustrated by interpretation of seismic reflection profiles in the Valencia trough (Etheve et
676
677 359 al., 2018) (fig. 7b). These profiles reveal the presence of a large Albian basin, the Columbrets
678
679 360 basin (fig. 1), filled with up to 10 km thick Mesozoic sediments over a highly extended
680
681 361 continental basement locally only 3.5 km thick. The pre-rift and syn-rift successions form a
682
683 362 large-scale synclinal with thinned borders, in relation with displacement along local
684
685 363 extensional detachments. Whole deformation results of interaction between the thick pre-
686
687 364 rift Triassic salt layer and dominantly ductile crustal thinning (Etheve et al. 2018) leading to
688
689 365 the development of an abnormally thin continental crust (Gallart et al., 1990; Dañobeitia et
690
691 366 al., 1992; Ayala et al., 2015). In the Cameros basin (fig. 7c-d), the pre-rift cover is decoupled
692
693 367 on Triassic evaporites and is smeared all over the stretched domain. No major offset of the
694
695 368 top basement is attested by the syn-rift record (Casas-Sainz and Gil-Imaz, 1998; Casas-Sainz
696
697 369 et al., 2000). A striking feature is that like in the NPZ, HT-LP metamorphism associated with
698
699 370 crustal thinning is reported in the Cameros basin fill (Guiraud and Séguret, 1985; Goldberg et
700
701 371 al., 1988; Rat et al., 2019).

702 **III. Discussion**

703

704 **A. Smooth-slopes basins: symmetrical geometries versus asymmetrical tectonic regime**

705

706 376 A common characteristic of the smooth-slopes basins described in this review is the lack of
707
708 377 tilted crustal blocks and related stepping fault scarps in their central part, thus defining a
709
710 378 dominant symmetrical smooth-slopes profile of the basement top (figs. 2 and 7). Based on
711
712 379 field data from the NPZ, we have shown that stretching of the crustal basement occurs in a
713
714 380 dominant ductile mode under greenschist facies conditions, since the central part of the
715
716 381 basin remains overlain by a permanent cover of detached pre- and syn-rift sediments . An
717
718 382 important question is now to determine whether such symmetrical shapes result from

721
722
723 383 symmetrical or asymmetrical stretching processes.
724

725 384

726
727 385 The symmetry or asymmetry of the processes of lithosphere stretching and continental
728
729 386 breakup has been largely debated over the last 30 years (i.e. Buck et al., 1988; Allemand et
730
731 387 al., 1989; Buck, 1991; Brun, 1999, with references therein). More recently, the symmetrical
732
733 388 character of the final architecture of passive margins has been discussed by many authors
734
735 389 (i.e. Michon and Merle, 2003; Huisman and Beaumont, 2007; Reston et al., 1995; Sutra et
736
737 390 al., 2013; Brune et al., 2014). Apparent symmetry does not imply dominant pure shear
738
739 391 thinning mechanisms but may result from asymmetrical tectonic processes involving large-
740
741 392 scale discrete extensional shear zones (simple shear) as discussed by Nagel and Buck (2004)
742
743 393 (fig. 8a).

744 394

745
746 395 It is well admitted that architecture of extended crustal systems depends on the geometrical
747
748 396 and temporal associations between simple shear and pure shear regimes. In the pure shear
749
750 397 model of McKenzie (1978), designed to explain the evolution of sedimentary basins, the
751
752 398 lithosphere is stretched uniformly resulting in a symmetrical basin with faulting in the brittle
753
754 399 crust. By contrast, the simple shear model (Wernicke, 1981, 1985) points to one or few
755
756 400 detachment faults that originate at low-angle with dips less than 30° and concentrate the
757
758 401 entire deformation, so that, apart from the fault zones, the lithosphere is not deformed. The
759
760 402 simple shear model has been complicated with the adjonction of sequential detachments
761
762 403 faults (Lister and Davis, 1989). Combination of pure and simple shear model was further
763
764 404 proposed (Lister et al., 1991). In this combination model, crustal deformation is controlled
765
766 405 by low angle detachment faulting but thinning of the mantle lithosphere results from pure
767
768 406 shear. By introducing time-dependant rheological changes at the lithospheric scale, Reston
769
770 407 and Perez-Gussinye (2007) report a complex evolution from symmetric to asymmetric
771
772 408 extension, and back to symmetric, at margins displaying exhumed mantle in the hyper-
773
774 409 extended domain.

775 410

776
777 411 A laboratory model combining simple and pure shear has been realized by Brun and Beslier
778
779 412 (1996) in order to account for the exhumation of mantle rocks at ocean-continent
780
413 boundaries (fig. 8b). This model applies easily to the case of rifts with exhumed mantle such
414 as the Pyrenean and peri-Pyrenean smooth-slopes basins. This four-layer model is composed

781
782
783 415 of sand and silicone putty layers, regarded as analogues of the brittle and ductile layers of
784 416 both crust and mantle. However, it does not discriminate a mid-crustal level. The lower crust
785 417 deforms ductilely and the upper mantle is strong. Necking of the whole lithosphere model is
786 418 nearly symmetrical (pure shear) but asymmetrical structures (simple shear) develop
787 419 internally, due to boudinage and/or faulting of brittle layers. This model explains the
788 420 occurrence of shear zones in the mantle lithosphere as described by Vissers et al. (1995) in
789 421 the Pyrenean mantle and accounts for the ductile deformation of the crust as demonstrated
790 422 by Asti et al. (2019).

796 423

797 424 In contrast with the Brun and Beslier (1996) symmetrical model, recent models of margin
798 425 evolution based on the Iberian or Alpine examples have put forward asymmetric
799 426 architectures resulting from the development of few major detachment faults, and
800 427 promoted the use of “lower-” and “upper-plate” terminology (Manatschal, 2004; Mohn et
801 428 al., 2010, 2012, 2015; Sutra et al., 2013). Mohn et al. (2012) propose a model of three-layer
802 429 continental crust where the brittle upper and lower crusts are strongly decoupled by a
803 430 ductile middle crust (fig. 3b). Crustal thinning, accommodated through a so-called necking
804 431 zone, is the result of interplay between detachment faulting in the brittle layers and
805 432 decoupling in ductile quartzo-feldspatic mid-crustal levels along localized ductile
806 433 décollements. The excision of ductile mid-crustal layers and the progressive embrittlement
807 434 of the crust by coupling the lower and upper crusts enable major detachment faults to cut
808 435 into the underlying mantle, exhuming it to the seafloor.

809 436 In the Iberian and Alpine examples, authors envision the presence of one or few large-scale
810 437 discrete detachment faults controlling the entire crustal thinning and the basin subsidence.
811 438 This is also applied by Masini et al. (2014) in their model for the western NPZ where a major
812 439 north-dipping detachment fault accomodates the denudation of the sub-Eurasian mantle to
813 440 form the basement of the Mauléon basin (fig. 9a). Interpretation involving single
814 441 detachment faults has also been retained in the preliminary reconstructions of the NPZ
815 442 basins by Lagabrielle and Bodinier (2008), Lagabrielle et al. (2010) and Vauchez et al. (2013)
816 443 (fig.9b, c), as well as in the reconstructed S-N transect from the Basque – Cantabrian to the
817 444 Armorican margin by Roca et al. (2011) (fig. 9d). Similarly, few detachment faults are used in
818 445 the Espurt et al. (2019), Saspiturry et al. (2019) and Ducoux et al. (in review) models for the
819 446 Barronies, Mauléon and “Nappe des Marbres” basins respectively (fig. 2). Others models

841
842
843 447 invoke deep-seated staircase extensional faults accounting for large-scale ramp-synclinal
844
845 448 folding as documented in the Cameros and Columbrets basins (Guimerà et al., 1995; Roma
846
847 449 et al., 2018). By contrast, models from the western NPZ by Corre et al. (2016) and Teixell et
848
849 450 al. (2016, 2018) (fig. 2) do not favor the activation of single detachment faults alone. Rather,
850
851 451 they involve symmetrical tectonic processes triggering a homogeneous thinning of the crust
852
853 452 during its lateral extraction from the rift axis.

854
855 453 In their study of the evolution of the western Betics including the exhumation of the Ronda
856
857 454 subcontinental mantle, Frasca et al. (2016) identify three successive steps: (i) ductile crust
858
859 455 thinning and ascent of subcontinental mantle thanks to mid-crustal shear zone and crust-
860
861 456 mantle shear zones acting synchronously; (ii) disappearance of the ductile crust bringing the
862
863 457 upper crust in contact with the subcontinental mantle, (iii) complete exhumation of the
864
865 458 mantle in the zone of localized stretching and high-angle normal faulting cutting through the
866
867 459 Moho, with related block tilting. These steps do not completely apply to the Pyrenean case,
868
869 460 notably because field and geophysical studies of the metamorphic NPZ never evidenced
870
871 461 brittle faulting of the Moho during the Cretaceous rifting.

872
873 462

874
875 463 Based on these examples of recent interpretations of rifting evolution, we stress that both
876
877 464 Alpine and Betic examples do not refer to a décollement level at the base of the pre-rift
878
879 465 cover. They promote evolutionary models lacking allochthony of the detached pre-rift
880
881 466 sediments, in contradiction with the examples detailed in section I and II. In addition, both
882
883 467 Alpine and Betic models refer to a progressive embrittlement in the rift axis resulting in the
884
885 468 complete elimination of ductile crustal layers. Again, this contrasts with the NPZ examples
886
887 469 where thin ductile crustal layers are extracted in the distal domain and remain welded on
888
889 470 the exhumed mantle.

890
891 471

892
893 472 **B. Smooth-slopes basins: crustal shear zones and lenticular fabrics at the mesoscale.**

894
895 473

896
897 474 Petrological studies of continental units exposed around the Urdach and Sarailé lherzolite
898
899 475 bodies (western NPZ) provide information on the deformation mode associated with crustal
900
476 thinning and mantle exhumation (Corre et al., 2016; Asti et al., 2019). Reconstruction of
477 sections across the NPZ Cretaceous basins by Clerc et al. (2015b), Teixell et al. (2016), Corre
478 et al. (2016) and Asti et al. (2019) use such ductile deformation mode having affinities with a

901
902
903 479 regional-scale, uniform pure shear mechanism. It is shown that extension in the Paleozoic
904
905 480 basement was achieved through lenticular deformation and pervasive ductile flattening with
906
907 481 anastomosing extensional mylonitic shear zones developing at temperatures of 350-450°C.
908
909 482 Here, during its lateral extraction from the rift axis, the crust thinned ductilely under
910
911 483 greenschist facies P-T conditions. Stretching occurred by the mean of undulating shear
912
913 484 contacts between tectonic lenses of flattened crustal material as described in figure 10. At
914
915 485 the final step of the continental breakup, very thin continental crustal lenses remained
916
917 486 welded on the exhumed mantle.

918
919 487 A very similar lenticular mode of deformation derives from investigations in the Basin and
920
921 488 Range province. Hamilton (1987) describes tectonic lenses of middle crustal rocks that
922
923 489 normally lie at separate levels in the crust with undulating shear contacts between them (fig.
924
925 490 8c). This deformation mode allows the juxtaposition of different lithologies by uplifting
926
927 491 deeper lenses during the extensional deformation. In a different way, Gartrell (1997)
928
929 492 propose a large scale crustal boudinage involving successive necking regions where the
930
931 493 ductile middle crust is extremely sheared (fig. 8d). The resulting architecture is a succession
932
933 494 of tectonic lenses that may evolve toward a large-scale lenticular geometry as proposed by
934
935 495 Espurt et al. (2019) for the evolution of the North Pyrenean massifs (fig. 2d).

936
937 496 In their recent detailed study of the tectonic and metamorphic evolution of the Urdach and
938
939 497 Sarailé mantle bodies and associated units, Lagabrielle et al. (2019a; 2019b) describe two
940
941 498 types of low-angle shear zones that accommodated part of extension of the distal domain of
942
943 499 the Iberia passive margin during the mid-Cretaceous (fig. 10a, b). The deepest shear zone is
944
945 500 the crust-mantle detachment. It separates the ultramafic mantle rocks from strongly thinned
946
947 501 continental Paleozoic rocks. It is composed of a basal 20-50 m thick lenticular layer of
948
949 502 sheared serpentinites followed by a 10 m thick damage zone. The lenticular layer consists of
950
951 503 ultramafic symmetrical tectonic lenses, a few meters long, separated by anastomosing
952
953 504 serpentine-rich shear zones. The damage zone consists of an assemblage of centimeter-sized
954
955 505 symmetrical lenses of a soft, talc-rich, sheared material, separated by conjugate shear zones.
956
957 506 The shallowest shear zone is the cover sole décollement. It corresponds to the tectonic
958
959 507 boundary separating the base of the detached pre-rift Mesozoic metasedimentary cover
960
961 508 from either mantle lherzolites or continental basement rocks. It consists of a thick
962
963 509 deformation zone (some meters to tens of meters thick) that was the locus of important
964
965 510 metasomatic crystallizations involving notably fluids of Triassic origin (Corre et al., 2016).

961
962
963 511 Detailed structural study of the basement and mantle rocks shows that it is not easy to
964
965 512 discriminate between dominant pure shear and dominant simple shear processes at the
966
967 513 outcrop and regional scales (Lagabrielle et al. 2019a; 2019b). Indeed, a major detachment
968
969 514 fault zone (typically related to regional simple shear) may contain abundant symmetrical
970
971 515 lenses suggesting locally dominant pure shear.

972 516 Finally, in the studied smooth-slopes basins, dominant pure shear mechanisms concentrate
973
974 517 into the strongly thinned continental tectonic lenses whereas simple shear mechanism
975
976 518 characterize the main detachments. Pure shear mechanisms associated with overall
977
978 519 flattening of the syn-rift and pre-rift sedimentary pile progressively develop into the basin
979
980 520 center as represented in figure 10a. Chronological constraints have to be integrated in order
981
982 521 to establish possible succession from simple shear-dominant toward pure shear-dominant
983
984 522 deformation mechanisms at the scale of the entire system.

985
986 523

987 **524 C. Smooth-slopes basins formation, insights for the evolution of passive, magma-poor**
988
989 **525 continental margins.**

990
991 526

992 527 We deduce from section B above that dominant pure shear deformation concentrates into
993
994 528 anastomosed tectonic lenses forming the strongly stretched continental in the central region
995
996 529 of smooth-slopes basins. In the following, we review examples of comparable uniform
997
998 530 modes of ductile deformation worldwide.

999 531 A lenticular mode of deformation devoid of any steep normal fault is proposed at the scale
1000
1001 532 of an entire passive margin by Gernigon et al., (2014) to account for the symmetrical
1002
1003 533 stretching of the continental crust during the formation of the Barents margin (fig. 11a). This
1004
1005 534 geometry recalls the structures proposed by Gartrell (1997) (fig. 8d). Lenticular fabric is also
1006
1007 535 suggested for deep crustal units connected to tilted blocks through listric faults along the
1008
1009 536 Norway margin (Osmundsen and Ebbing, 2008; fig. 11b). These structures accommodate
1010
1011 537 crustal thinning to only a few kilometer thicknesses through dominant ductile mode. The
1012
1013 538 symmetrical mode of stretching implying ductile thinning or boudinage of some crustal layer
1014
1015 539 can be compared to processes of depth-dependent stretching or thinning (DDT and DDS)
1016
1017 540 envisioned by Reston and McDermott (2014) in order to account for extensional
1018
1019 541 discrepancies at some passive margins. It must be noted that according to an interpretation
1020
542 of deep seismic reflection profiles by Reston (1988), lens-shaped low-strain lozenges

1021
1022
1023 543 separated by high strain shear zones form the structural pattern of the lower crust beneath
1024
1025 544 the United Kingdom. This overall pattern seems to be possibly applied to numerous units of
1026
1027 545 stretched crust at a large scale.

1028 546 Several distal domains of North Atlantic passive margins display geometries that suggest the
1029
1030 547 presence of lens-shaped units of thinned to hyper-thinned continental crust detached along
1031
1032 548 anastomosing shear zones and now separated by large zones exposing exhumed mantle (e.g.
1033
1034 549 Labrador and West Greenland margins; Reston and Perez-Gussinyé, 2007) (fig. 11c, d). These
1035
1036 550 units do not resemble extensional allochthons of the West Iberia-type margins (figs. 2 and
1037
1038 551 11e) and show geometrical affinities with crustal boudins extracted during the Pyrenean
1039
1040 552 extension in the center of the Cretaceous rift (e.g. the Baronnies and Agly crustal boudins;
1041
1042 553 Espurt et al., 2019; Clerc et al., 2016) (fig. 2). Such large areas of hyper-thinned continental
1043
1044 554 crust possibly composed of an assemblage of heterogeneous boudins, can be viewed as
1045
1046 555 sheets representing considerable volumes of sheared and flattened continental material
1047
1048 556 (thickness less than 10 km, width of 100 km and length more that few 1000 km, along the
1049
1050 557 margin), formed through processes of uniform pure shear at a crustal scale. We infer that
1051
1052 558 the modes of deformation exhibited by the Pyrenean crustal units welded on the exhumed
1053
1054 559 mantle (although at a much smaller scale) can apply to the formation of these crustal sheets,
1055
1056 560 suggesting predominance of greenschists facies mylonites. Similar crustal sheets underlying
1057
1058 561 sag basins are well imaged in recent numerical models of margin evolution (Brune et al.,
1059
1060 562 2014 ; Huisman and Beaumont, 2011; 2014) as shown in figure 12a, b. Crustal sheets are
1061
1062 563 present along the Angola margin (fig. 12d), they may be present in the very distal domain of
1063
1064 564 the Gulf of Lion margin where they may originate by extraction of lower crustal material
1065
1066 565 (Jolivet et al., 2017) (fig. 11f). Similar long and thin sheets are typically imaged by Wang et al.
1067
1068 566 (2016) at the base of the reconstructed Iberia margin of the Mauléon basin, and by Roca et
1069
1070 567 al. (2011) in their reconstruction of the north Iberia margin north of the Cantabrian coast
1071
1072 568 (fig. 9d).

1067 569 In their compilation of high-quality and deep penetration seismic profiles of several passive
1068
1069 570 margins (Uruguay, Southern Namibia, Gabon, South China Sea and Barents Sea), Clerc et al.
1070
1071 571 (2015a; 2018) suggest that the lower crust of some margins is weaker than assumed and
1072
1073 572 accommodates a large part of extension by ductile shearing (fig. 8e). Boudinage appears as a
1074
1075 573 recurrent deformation process accounting for the thinning of the continental crust at
1076
1077 574 variable scales. This leads authors to an unorthodox vision of some type of passive margins

1081
1082
1083 575 where: (i) the lower crust is weak, (ii) boudinage controls a large part of the deformation and
1084
1085 576 localization of low-angle normal faults, and (iii) these normal faults often dip toward the
1086
1087 577 continent. This study highlights a crustal behavior dominated by boudinage and
1088
1089 578 lenticulation, implying interplay between ductile shear zones (boudin edges) and more
1090
1091 579 resistant crustal volumes (boudin cores). As discussed above in section B, this deformation
1092
1093 580 mode may apply to the thinned crustal levels in the axis of the Cretaceous Pyrenean rifts
1094
1095 581 (Teixell et al. 2016, 2018; Asti et al., 2019) (fig. 10) and is supported by recent numerical
1096
1097 582 models of lithospheric rifting incorporating macroscale anisotropy (Duretz et al., 2016).
1098
1099 583 In their interpretation of deep seismic profiles of the Gulf of Lion margin, Jolivet et al. (2015)
1100
1101 584 point to an intense stretching of the distal margin and reveal a 80 km-wide ocean-continent
1102
1103 585 transition zone that may consist of thin lower continental crust (the “Gulf of Lion
1104
1105 586 metamorphic core complex”) and exhumed mantle (fig. 11f). They infer an overall hot
1106
1107 587 geodynamic environment with a shallow lithosphere-asthenosphere boundary able to
1108
1109 588 weaken the upper mantle and the lower crust enough to make them flow south-eastward. In
1110
1111 589 this example, the lower crust bears an important role, which is not fully documented by field
1112
1113 590 data in the NPZ since evidence of exposure of lower crustal levels during the Cretaceous
1114
1115 591 rifting event has not yet been reported with confidence. Moreover, in most of the sections
1116
1117 592 of figures 3 and 7, the lower crust is considered as a high-strength layer that does not
1118
1119 593 deform ductilely but tends to break into large scale boudins and to remain at depth during
1120
1121 594 the rifting processes (e.g. figs. 2a, e, f, h).

1117 595

1119 596 **D. Comparison with thermo-mechanical models of crustal hyper-extension.**

1120 597

1122 598 The examples discussed above lead us to emphasize the frequency of lenticular fabrics at
1123
1124 599 various scales reported from different studies in both the upper mantle and the crust. The
1125
1126 600 formation of lenticular fabrics, necking and lateral extraction during continental rifting have
1127
1128 601 been addressed in mechanical and thermo-mechanical numerical models (Duretz and
1129
1130 602 Schmalholz, 2015; Duretz et al., 2016). These models emphasize the role of a pre-existing
1131
1132 603 macroscopic mechanical anisotropy on the development of continental rifts. They illustrate
1133
1134 604 the interplay between necking and lateral extraction of strong layers along weak
1135
1136 605 décollements, thus defining a lenticular fabric and anastomosed shear zone networks at the
1137
1138 606 regional scale as envisioned in the NPZ case.

1141
1142
1143 607 Models of metamorphic core complexes (MCCs) formation generally involve a thick and hot
1144
1145 608 continental crust (Brun and van den Driessche, 1994). This does not apply to the Pyrenean
1146
1147 609 case but constructive inputs can be expected from a confrontation with the rheological
1148
1149 610 parameters used for MCCs modeling. For instance, Tirel et al. (2008) use initial Moho
1150
1151 611 temperatures of 800°C or higher, with crustal thicknesses of 45 km or greater. This is much
1152
1153 612 more than what can be retained for the post-Variscan crust in the Pyrenees (thicknesses
1154
1155 613 between 30 and 20 km) (Teixell et al., 2018, and references therein) and Moho
1156
1157 614 temperatures lower than 800°C. In the Tirel et al. (2008) experiment, the exhumation
1158
1159 615 process of the metamorphic dome results in the progressive development of a detachment
1160
1161 616 zone and the Moho remains flat because the lower crust has a low viscosity and the upper
1162
1163 617 mantle is weak enough. With Moho temperatures lower than 800°C, the sub-Moho mantle
1164
1165 618 has high strength and effective viscosity resulting in strong Moho deflection and crustal-
1166
1167 619 scale necking. These conditions (relatively cold mantle and thin crust) are reached in the
1168
1169 620 Pyrenean rift explaining why the Pyrenean mantle rapidly reached the surface when it was
1170
1171 621 passively mobilized in response to the drift of the Iberia plate.

1168
1169 622 A former numerical model that applies to the formation of passive continental margins
1170
1171 623 suggests that the crust may be thinned by permanent pure shear both at the proximal and
1172
1173 624 distal margin (Huisman and Beaumont, 2011) (fig. 12a). This scenario can apply easily to the
1174
1175 625 Pyrenean case where the ductile behaviour of the middle crust is demonstrated (Asti et al.,
1176
1177 626 2019). The Huisman and Beaumont (2011) model produces symmetric margins associated
1178
1179 627 with distal domain characterized by large sheets of thinned crustal material, as discussed
1180
1181 628 above. The symmetrical outline is well imaged by current reconstructions of the Pyrenean
1182
1183 629 basins from the North Pyrenean Zone and associated examples (Parentis, Cameros and
1184
1185 630 Columbrets basins, fig. 1, 2 and 7).

1184
1185 631 Brune et al. (2014) produce a different numerical model that emphasizes a rift migration
1186
1187 632 accomplished by sequential upper crustal faults balanced through lower crustal flow (fig.
1188
1189 633 12b). An interesting concept is that of 'exhumation channel', a weak locus of deformation
1190
1191 634 where the crust and part of the uppermost mantle are actively deformed and extremely
1192
1193 635 thinned during their transfer from lower to shallower levels, over a dome of upwelling
1194
1195 636 lithospheric mantle. This high strain volume is not a detachment fault and thus may bear
1196
1197 637 some affinity with the lenses of crustal material exhumed with NPZ mantle and described by
1198
1199 638 Asti et al. (2019). As discussed in section C above, the resulting geometry is that of areas of

1201
1202
1203 639 drastically thinned crust (named *crustal sheets* in the following) forming the distal margin
1204
1205 640 domain lying over a cooled and strengthened mantle. This mantle is exposed locally at the
1206
1207 641 rift axis depending on the extension rate. The final sketch derived from this model, including
1208
1209 642 a dome of strong mantle rimmed in its upper part by a thin layer of mylonitic crust, is a
1210
1211 643 reliable image for the geometry resulting from the Pyrenean rifting and associated basins at
1212
1213 644 a lithospheric scale.

1214
1215 645 Jammes et al. (2015) and Jammes and Lavier (2016), introduced compositional complexities
1216
1217 646 in the lithosphere by using an explicit biminerale assemblage which results in the
1218
1219 647 development of anastomosing shear zone. In their models, the deformation appears
1220
1221 648 localized in the middle/lower crust and the upper lithospheric mantle and leads to the
1222
1223 649 preservation of almost undeformed lenses of material surrounded by localized shear zones
1224
1225 650 concentrating most of the deformation. Such a lenticular final geometry is also evocative of
1226
1227 651 the one observed in the North Pyrenean Zone as discussed in detail by Asti et al. (2019) and
1228
1229 652 illustrated in fig. 10.

1230
1231 653 To unravel the dynamic evolution of the Cretaceous Pyrenean rift, Duretz et al. (2019)
1232
1233 654 carried out a set of thermo-mechanical numerical models of lithosphere-scale extension
1234
1235 655 based on the available geological constraints listed above in section I. The models were used
1236
1237 656 to explore the role of a km-thick basement-cover décollement layer at the base of the pre-
1238
1239 657 rift sediments. These numerical experiments highlight the key-role of the décollement layer
1240
1241 658 that can alone explain collectively: (i) salt tectonics deformation style and cover
1242
1243 659 décollement, (ii) high temperature metamorphism of the pre-rift cover, and (iii) ductile
1244
1245 660 mode of crustal thinning in the inner domain of the models. In the axis of the synclinal-
1246
1247 661 shaped basin (“sag” basin in the margin literature), extreme pure shear leads to the
1248
1249 662 development of a very thin basement layer, overlain by poorly-thinned pre-rift and syn-rift
1250
1251 663 sediments and underlain by exhuming mantle. These models are in good agreement with the
1252
1253 664 current knowledge of the architecture of the Cretaceous Pyrenean basins as exemplified by
1254
1255 665 reconstructions of figs. 2 and 7, as well as with the presence of large sheets of hyper thinned
1256
1257 666 crustal material (crustal sheets) in the distal part of numerous magma poor passive margins.

1258
1259
1260 667

1261
1262
1263 **668 E. The pre-rift salt décollement layer: a mechanical key-factor in the evolution of smooth-**
1264 **669 slopes basins. Establishing a new link between Triassic paleogeography and rifting**
1265 **670 mechanisms.**
1266
1267
1268
1269

1270 671
1271 672 As reported in section I and II, the common character between all pre-rift sequences of the
1272 673 aforementioned smooth-slopes basins is the presence of the thick low-strength Late Triassic
1273 674 evaporitic layer (Keuper). All related geological and geophysical studies highlight the
1274 675 importance of this décollement layer in the evolution of the rift basins under study. As
1275 676 detailed above, efficient décollement along the Keuper evaporites and clays triggers
1276 677 mechanical decoupling and gliding of the pre-rift cover that remains in the center of the
1277 678 basin as the crust is laterally extracted. In response to crustal hyper-thinning and horizontal
1278 679 crustal extraction, hot mantle material approaches the detached pre-rift cover. As a
1279 680 consequence, HT-LP metamorphism develops in the pre-rift sediments and at the base of
1280 681 the syn-rift flysch levels as recorded in the NPZ and in the pre-rift sediments of the Cameros
1281 682 basin. Subsequent deposition of syn-rift sediments allows preservation of the initial thermal
1282 683 anomaly with a major consequence on the deformation regime in the pre-rift sediments and
1283 684 crustal basement. Temperature increase in the NPZ basins center progressively leads to the
1284 685 uprising of the brittle/ductile transition avoiding the development of prominent crustal normal
1285 686 faults and leading to the dominantly ductile thinning of the Paleozoic basement and parts of
1286 687 the pre-rift and syn-rift sediments (Clerc and Lagabrielle, 2014; Clerc et al., 2015b; Asti et al.,
1287 688 2019; Duretz et al., 2019). We may now question the paleogeographic distribution of the
1288 689 Keuper group sediments at the Europa-Iberia scale in order to evaluate a possible link
1289 690 between modes of rift development and the occurrence of a thick Keuper layer at the base
1290 691 of the pre-rift sequence.
1291
1292
1293
1294
1295
1296
1297
1298
1299
1300
1301
1302
1303

1304 692 Several extensional systems interacted in the Iberia platform during the Trias, resulting in
1305 693 the creation of intraplate basins or troughs including the Valencian, Basque-Cantabrian, and
1306 694 Pyrenean basins (figs. 1 and 13). The sedimentary infill of these platform basins continued
1307 695 throughout the Mesozoic. Seismic, well and field data from the Bay of Biscay region, the
1308 696 Pyrenees and the Aquitanian Basin, suggest initial thickness of Upper Triassic formations
1309 697 ranging from 1000 to 2700 m (James and Canérot, 1999; Biteau et al., 2006; Jammes et al.,
1310 698 2010a; Roca et al., 2011; Rowan, 2014; Lopez-Mir et al., 2014; Saura et al., 2016; Soto et al.,
1311 699 2017; Zamora et al., 2017). The salt-rich layers generally consist of shales and evaporites
1312
1313
1314
1315
1316
1317
1318
1319
1320

1321
1322
1323 700 including dominant gypsum and minor halite and anhydrite (figs. 13 and 14).
1324
1325 701 Paleogeographic reconstructions are available for the Triassic period at the scale of the
1326
1327 702 Iberia-western Europa region (Dercourt et al., 1986; 1993; Ziegler, 1988; Ortí et al., 2017;
1328
1329 703 Soto et al., 2017). The distribution of Triassic shales and evaporites is contrasted around the
1330
1331 704 future Iberia plate margins. This paleogeography is confirmed by a compilation of data
1332
1333 705 collected independantly by D. Frizon de Lamotte (fig. 13c). Evaporites are well developed
1334
1335 706 along the eastern edge of Iberia (Tethys side) and in the rift opened at the place of the
1336
1337 707 future NPZ, the Basque-Cantabrian basin, the Bay of Biscaye basin and the southern part of
1338
1339 708 the Armorican margin. In the place of the future North Atlantic rift system, evaporites are
1340
1341 709 restricted to the Peniche, Lusitanian, Alentejo and Algarve basins along the southern half of
1342
1343 710 the Portugal margin and are lacking along the northern half of the Iberia Atlantic margin.
1344
1345 711 Along the conjugate north American margin, evaporites are known at the base of the
1346
1347 712 Jeanne-d'Arc basin and are of restricted extension compared to the Keuper group exposed in
1348
1349 713 Central Europe (fig. 13b, c).
1350
1351 714 Finally, along the western half of the Iberia-Newfoundland transect, evaporitic formation are
1352
1353 715 not reported, whereas thick evaporites are reported from areas characterized by Parentis-
1354
1355 716 type basins. As outlined in figures 13 and 14, this paleogeography matches the distribution
1356
1357 717 of the two opposite types of basins discussed in this article (Parentis type vs. Iberia-
1358
1359 718 Newfoundland type). Thus, we establish a link between the presence of a pre-rift salt layer
1360
1361 719 and the deep mechanisms of crustal stretching. Because they remain in the center of the
1362
1363 720 basin, evaporites contribute to the preservation of a rather high thermal gradient in the axial
1364
1365 721 rift allowing a dominant-ductile deformation of the basement. The lack of a major
1366
1367 722 décollement level at the base of the pre-rift sequence may explain by itself why pre-rift
1368
1369 723 sediments remain welded and coupled to the basement on the top of tilted blocks in the
1370
1371 724 Iberia-Newfoundland-type margins as illustrated in figure 3a, b. Indeed, in the Iberia as well as
1372
1373 725 in Alpine margin-types, only syn-rift sediments are deposited over the exhumed lower
1374
1375 726 crustal levels and subcontinental mantle (Péron-Pinvidic et al., 2007; Péron-Pinvidic and
1376
1377 727 Manatschal, 2009; Mohn et al., 2012), which contrasts with the evolution of the Parentis-
1378
1379 728 type basins.
1380
729
730 In this review, on the basis of examples clustering along the Iberia-Eurasia plates boudaries,
731 we emphasize the major role played by the Upper Triassic evaporitic layer during extensional

1381
1382
1383 732 processes. In the reported smooth-slopes basin examples, cover gliding occurred on a pre-
1384
1385 733 rift layer and thus contrasts with cases involving syn- to post-rift weak layers. The latter
1386
1387 734 cases have been largely documented by studies of passive margins displaying thick syn-rift
1388
1389 735 salt formations such as the Angola margin where the post-salt sedimentary units have glided
1390
1391 736 gravitationally after the margin formation (e.g. Brun and Fort, 2011, and references therein,
1392
1393 737 see also additional discussion relative to the pre-rift/post-rift salt effects during rifting in
1394
1395 738 Jammes et al., 2010c). To sum up, the specific characters emphasized in this review are
1396
1397 739 twofold : (i) the peri-Pyrenean salt is pre-rift allowing conservation of the pre-rift cover over
1400
1401 740 the high-strain axial rift. Crustal faulting has not disrupted the continuity of the Triassic
1398
1399 741 evaporite formation, allowing for décollement of the pre-rift sequence basinward, down to
1402
1403 742 the distal margin. (ii) Consequently, the axial thermal anomaly is preserved and the
1404
1405 743 dominant ductile mode of crustal deformation prevented the formation of faulting-related
1406
1407 744 steps leading to smooth-slopes basin edges.

1405
1406 745

1407 746 **F. Time-dependent rheology during the evolution of smooth-slopes basins**

1408
1409 747

1410 748 From the statements listed at the end of section I as well as from the discussion above, we
1411
1412 749 first stress that the models of Pyrenean Cretaceous rifting established on the basis of
1413
1414 750 geological constraints from the NPZ differ significantly from the classical models of passive
1415
1416 751 margin formation based on the Iberia-Newfoundland margins example (Peron-Pinvidic and
1417
1418 752 Manatschal, 2009; Sutra et al., 2013; Osmundsen and Peron-Pinvidic, 2018, and references
1419
1420 753 therein). The latter models involve a dominantly brittle behavior of the crust and the
1421
1422 754 individualization of tilted faulted blocks bearing a concordant pre-rift cover permanently
1423
1424 755 welded on their back (fig. 3). In the models based on the geology of the NPZ (e.g. models of
1425
1426 756 Clerc et al., 2016; Teixell et al., 2016; Espurt et al., 2019), the external borders of the
1427
1428 757 subsiding Cretaceous flysch basins remain at low temperature and display classical faulted
1429
1430 758 and tilted blocks (e.g. half-grabens of Quillan basin, Camarade basin, Gensac-Bonrepos
1431
1432 759 basin, western border of the Mauléon basin, Arbailles basin, edges of the Gran Rieu high and
1433
1434 760 Lacq basin). By contrast, in the internal regions of the rift system (corresponding to the
1435
1436 761 future metamorphic NPZ), the basement thinned in a dominant-ductile mode because
1437
1438 762 temperature conditions reached 350°C to 450°C beneath the detached pre-rift cover and the
1439
1440 763 syn-rift flysch.

1441
1442
1443 764 The peculiar evolution of the NPZ basins is depicted on figure 15 based on an original model
1444
1445 765 by Clerc et al., (2016). This model is strictly conceptual and was designed to account for
1446
1447 766 geological constraints gathered from various sites along the NPZ. The simplified system
1448
1449 767 includes the subcontinental mantle, a continental basement, a first decollement level in
1450
1451 768 Triassic evaporites, a level of layered pre-rift carbonates and a cover of syn-rift flysch. The
1452
1453 769 carbonates are able to deform by crystalline plasticity of calcite under HT conditions. The
1454
1455 770 corresponding lithologies are illustrated and briefly described in the NPZ lithostratigraphical
1456
1457 771 column of figure 5.

1458
1459 772 In order to better assess the time-dependent rheological changes that necessarily affect
1460
1461 773 each geological layer involved during this three steps evolution, we provide synthetic
1462
1463 774 rheological profiles and geotherms for selected parts of the basin: in the external portion
1464
1465 775 representing the initial pre-extension model (fig. 15a) and in the center of the basin for the
1466
1467 776 following two steps (fig. 15b and c). The data used to construct these profiles derived from
1468
1469 777 the Duretz et al. (2019) model discussed in section D above.

1470
1471 778 The three steps of this conceptual evolutionary model can be described as follows:

1472
1473 779 (1) At an early rifting stage (fig. 15a) moderate extension leads to crustal thinning
1474
1475 780 accommodated through normal faults in the upper crust. The rheological profile consists of a
1476
1477 781 15 km thick, cold and brittle upper crust ($T > 300^{\circ}\text{C}$) overlying a 15 km thick ductile lower
1478
1479 782 crust with Moho temperature around 550°C . The uppermost mantle is a strong 15 km thick
1480
1481 783 layer. In the inner part of the system, normal faults may pass downward to ductile shear
1482
1483 784 zones dipping toward the external side thus delineating a small central horst. The Triassic
1484
1485 785 evaporitic layers act as a décollement layer that allows the pre-rift carbonates to remain in
1486
1487 786 the most thinned and subsiding domains on both sides of the central horst while the syn-rift
1488
1489 787 flysch is being deposited above. Sliding of the pre-rift carbonates in the deep domain results
1490
1491 788 in the local tectonic denudation of the margins where carbonates remnants form isolated
1492
1493 789 rafts tilted on listric faults.

1494
1495 790 (2) At the mid-rifting stage (fig. 15b), ductile thinning of the crust occurs in response to
1496
1497 791 heating due to rapid mantle uplift. The central crustal horst starts to deform ductilely and
1498
1499 792 progressively acquires a lens shape. Due to blanketing effect under the syn-rift sediments,
1500
793 the HT pre-rift carbonates suffer syn-metamorphic ductile deformation. Rheological profile

1501
1502
1503 794 in the center of the basin shows the Keuper weak zone at the base of the pre-rift cover and a
1504
1505 795 newly formed weak zone corresponding to the thinned crust which deforms at temperatures
1506
1507 796 between 300°C and 500°C. The lower crust has been extracted laterally and the brittle
1508
1509 797 mantle layer shows a decreasing thickness due to temperature increase from 400°C (step 1)
1510
1511 798 to 1000°C at only 20 km depth.

1512
1513 799 (3) At the final rifting stage (fig. 15c), extreme thinning and boudinage of the crust leads to
1514
1515 800 local denudation of the sub-continental mantle, which is by place in tectonic contact with
1516
1517 801 the pre- or syn-rift sediments. The crust in the center of the basin has been cut into few
1518
1519 802 lenses that move independently. The crust at both edges of the proximal domain thins and
1520
1521 803 moves horizontally (*lateral extraction* concept of Clerc and Lagabrielle, 2014). The Triassic
1522
1523 804 décollement layer undergoes drastic thickness reduction leading to boudinage in response
1524
1525 805 to fluid-assisted tectonic brecciation and to metasomatic dissolution as observed in the
1526
1527 806 Urdach and Sarailé massifs in the western NPZ (Lagabrielle et al., 2019a, 2019b in press).
1528
1529 807 Due to their increasing plasticity, the HT marbles of the pre-rift cover progressively
1530
1531 808 accommodate a large part of the deformation at the base of the basin, involving calcite
1532
1533 809 plasticity and recrystallization, boudinage, drag folding and low angle normal shear bands. In
1534
1535 810 turn, the lower levels of the syn-rift flysch sequence are progressively affected by HT
1536
1537 811 metamorphism and ductile deformation with bedding-parallel foliation and boudinage.
1538
1539 812 Continuous extension of the basin floor leads also to the progressive exhumation of the
1540
1541 813 metamorphic pre-rift sediments, which are progressively extracted from below the syn-rift
1542
1543 814 cover (see complete description of this process in Clerc et al., 2016). In the thinnest crustal
1544
1545 815 portion, the rheological profile bears similarities with that of step 2. The crustal thickness
1546
1547 816 has now reduced to less than one km and the brittle/ductile transition has moved upward.
1548
1549 817 The pre-rift cover, salt décollement as well as the thinned basement thus deform under
1550
1551 818 dominant ductile deformation.

1547 819 **IV. Conclusions**

1548
1549 820

1550
1551 821 Almost fourty years after the discovery of mantle exhumed at the foot of the north Iberia
1552
1553 822 passive margin (Boillot et al. 1980), this review highlights the affinities between the
1554
1555 823 architecture of two types of extensional basins now variously inverted in the Pyrenean
1556
1557 824 orogeny. These are : (i) the extensional basins that opened during the mid-Cretaceous times

1561
1562
1563 825 along the Iberia-Eurasia plate boundary and, (ii) the intraplate basins of northern Iberia
1564
1565 826 (Cameros to Columbrets basins). Taking as a reference the Parentis basin profile and on the
1566
1567 827 basis of geological reconstructions of NPZ rift architecture, we have designed an idealized
1568
1569 828 cross-section of a smooth-slopes basin shown in figure 16. The dominant features put
1570
1571 829 forward in this cross-section relate to the basin central region which lacks stepping normal
1572
1573 830 faults and large-scale tilted crustal blocks. The section shows a dominant symmetrical shape
1574
1575 831 with smooth-slopes that relates to a new mode of crustal stretching during continental
1576
1577 832 rifting characterized by a ductilely thinned crust in the central rift domain. This deformation
1578
1579 833 mode is typically symmetrical and contrasts drastically with stretching processes described
1580
1581 834 from the Iberia-Newfoundland and Alpine Tethys margins implying asymmetrical
1582
1583 835 architecture and extensional detachment separating upper and lower plates having
1584
1585 836 differential evolution.

1584 837

1586 838 The common character between all pre-rift sequences of the studied basins is the presence
1587
1588 839 of the thick low-strength Late Triassic evaporitic layer (Keuper facies). Geological and
1589
1590 840 geophysical studies point to the importance of this décollement layer in the evolution of
1591
1592 841 these rift basins. As established by geological studies in the NPZ, efficient décollement along
1593
1594 842 the Keuper evaporites and clays triggers mechanical decoupling and gliding of the pre-rift
1595
1596 843 cover that remains in the center of the basin as the crust is laterally extracted. Subsequent
1597
1598 844 deposition of syn-rift sediments allows preservation of the initial thermal anomaly with a
1599
1600 845 major consequence on the deformation regime in the pre-rift sediments and crustal
1601
1602 846 basement. The ubiquitous character of the ductilely deformed marbles in the metamorphic
1603
1604 847 NPZ relates to a dominant-ductile deformation regime in the pre-rift cover during the
1605
1606 848 Cretaceous extension. In these smooth-slopes basins, the ductilely stretched crust behaves
1607
1608 849 homogeneously at the regional scale and extensional allochthons are not individualized. A
1609
1610 850 lenticular mode of homogeneous deformation is thus defined implying interplay between
1611
1612 851 hectometric lenses of ductile crustal material separated by anastomosing shear zones.

1610 852

1611 853 Both laboratory and thermo-mechanical numerical models reproduce remarkably the mode
1612
1613 854 of deformation deduced from geophysical and geological constraints compiled in the studied
1614
1615 855 basins. Thus it appears that the pre-rift character of the salt layer is the key-factor of the

1621
1622
1623 856 rifting style in controlling the very early decoupling between the basement and the pre-rift
1624
1625 857 cover. This strongly contrasts with the evolution of Atlantic margins where the salt is either
1626
1627 858 syn-rift or post-rift. For the first time, we evidence a strong link between the occurrence of a
1628
1629 859 sedimentary layer covering the future rifted region (here Keuper salt and clays deposits) and
1630
1631 860 a mode of crustal thinning (here homogeneous bulk ductile deformation). Décollement
1632
1633 861 along the evaporites and clays level finally favors the formation of symmetrical basins
1634
1635 862 lacking numerous normal faults and related tilted blocks. This new mode of crustal
1636
1637 863 deformation might not be restricted to the Pyrenean region, but may apply to all regions
1638
1639 864 hosting thick pre-rift décollement series. It may have been active worldwide, in the distal
1640
1641 865 portion of continental margins devoid of typical tilted blocks and extensional allochthons
1642
1643 866 and where large units of extremely thinned continental crust are present.

1642 867

1643
1644 868 To sum up, the specific characters of the smooth-slopes basins emphasized in this review are
1645
1646 869 twofold: (i) the peri-Pyrenean salt is pre-rift allowing conservation of the pre-rift cover over
1647
1648 870 the high-strain axial central region. The continuity of the Triassic evaporite formation is
1649
1650 871 preserved allowing for décollement of the pre-rift sequence which remain in the basin
1651
1652 872 center. (ii) Consequently, the axial thermal anomaly is preserved and the dominant ductile
1653
1654 873 mode of crustal deformation prevents the formation of faulting-related steps, thus leading
1655
1656 874 to smooth-slopes basin edges. Continuous sedimentation in the subsiding basin leads to
1657
1658 875 progressive sedimentary burial of the prerift sequence. This in turn allows the preservation
1659
1660 876 of the initial thermal anomaly that may grow during the rifting evolution.

1659 877

1660 878 **Acknowledgements**

1661
1662 879 This work is the result of a 10 years field and laboratory research conducted in the Pyrenean
1663
1664 880 range with funding from various programs and institutions. We benefited of grants from the
1665
1666 881 French ANR Pyramid program, the Bureau de Recherche Géologique et Minière (BRGM),
1667
1668 882 Référentiel Géologique de la France (RGF) program and the Total/INSU/BRGM OROGEN
1669
1670 883 program with contributions from the CNRS and from Géosciences Montpellier and Rennes
1671
1672 884 research units. We thank Thierry Baudin (BRGM) and Sylvain Calassou (Total) for program
1673
1674 885 management and encouraging discussions. We also thank B. Azambre, P. Boulvais, M. Pujol,
1675
1676 886 and many others for stimulating exchanges that helped improve our ideas.

1681
1682
1683
1684
1685
1686
1687
1688
1689
1690
1691
1692
1693
1694
1695
1696
1697
1698
1699
1700
1701
1702
1703
1704
1705
1706
1707
1708
1709
1710
1711
1712
1713
1714
1715
1716
1717
1718
1719
1720
1721
1722
1723
1724
1725
1726
1727
1728
1729
1730
1731
1732
1733
1734
1735
1736
1737
1738
1739
1740

1741
1742
1743
1744
1745
1746
1747
1748
1749
1750
1751
1752
1753
1754
1755
1756
1757
1758
1759
1760
1761
1762
1763
1764
1765
1766
1767
1768
1769
1770
1771
1772
1773
1774
1775
1776
1777
1778
1779
1780
1781
1782
1783
1784
1785
1786
1787
1788
1789
1790
1791
1792
1793
1794
1795
1796
1797
1798
1799
1800

889 References

890

891 Allemand, P., Brun J.-P., Davy P., and Van Den Driessche J., 1989. Symétrie et asymétrie des
892 rifts et mécanismes d'amincissement de la lithosphère, *Bull. Soc. Géol. Fr.*, 5, 445–451.

893

894 Asti, R., Lagabrielle, Y., Fourcade, S., Corre, B., Monié, P., 2019. How do continents deform
895 during mantle exhumation? Insights from the northern Iberia inverted paleopassive margin,
896 western Pyrenees (France). *Tectonics*, 38, 1666–1693.

897 <https://doi.org/10.1029/2018TC005428>

898

899 Ayala, C., Torne, M., Roca, R., 2015. A review of the current knowledge of the crustal and
900 lithospheric structure of the Valencia Trough Basin. *Bol. Geológico Min.* 126, 533–552.

901

902 Azambre, B., Rossy, M., 1976. Le magmatisme alcalin d'âge crétacé, dans les Pyrénées
903 occidentales et l'Arc basque; ses relations avec le métamorphisme et la tectonique. *Bull.*
904 *Société Géologique Fr.* 7, 1725–1728.

905

906 Bernus-Maury, C., 1984. Etude des paragéneses caractéristiques du métamorphisme
907 mésozoïque dans la partie orientale des Pyrénées. Thèse, Pierre et Marie Curie, Paris.

908

909 Biteau, J.-J., Le Marrec, A., Le Vot, M., Masset, J.-M., 2006. The Aquitaine Basin. *Pet. Geosci.*
910 12, 247–273.

911

912 Boillot, G., S. Grimaud, A. Mauffret, D. Mougénot, J. Kornprobst, J. Mergoïl-Daniel, and G.
913 Torrent, 1980. Ocean-continent boundary off the Iberian margin: A serpentinite diapir west
914 of the Galicia bank, *Earth Planet. Sci. Lett.*, 48, 23–34.

915

916 Bois, C., Gabriel, O., Lefort, J.-P., Rolet, J., Brunet, M.-F., Masse, P., Olivet, J.-L., 1997.
917 Geologic contribution of the Bay of Biscay deep seismic survey: a summary of the main
918 scientific results, a discussion of the open questions and suggestions for further
919 investigation. *Mém Soc Géol Fr.* 193–309.

920

921 Brun, J. P., 1999. Narrow rifts versus wide rifts: Inferences for the mechanics of rifting from
922 laboratory experiments, *Philos. Trans. R. Soc. London, Ser. A*, 357, 695–712.

923

924 Brun, J. P., Beslier M.O., 1996. Mantle exhumation at passive margin, *Earth Planet. Sci. Lett.*,
925 142, 161– 173.

926

927 Brun, J.-P., and van den Driessche, J., 1994. Extensional gneiss domes and detachment fault
928 systems; structure and kinematics. *Bull. Société Géologique Fr.* 165, 519–530.

929

930 Brun, J.P., Wenzel, F. and ECORS-DEKORP team, 1991. Crustal structure of the southern
931 Rhine Graben from ECORS-DEKORP seismic reflection data, *Geology*, 19, 758-762. DOI:
932 10.1130/0091-7613(1991)019<0758:CSSOTS>2.3.CO

933

934 Brun, J.-P., Fort, X., 2011. Salt tectonics at passive margins: Geology versus models. *Mar. Pet.*
935 *Geol.* 28, 1123–1145. <https://doi.org/10.1016/j.marpetgeo.2011.03.004>

1801
1802
1803 936
1804 937 Brune, S., Heine, C., Pérez-Gussinyé, M., Sobolev, S.V., 2014. Rift migration explains
1805 938 continental margin asymmetry and crustal hyper-extension. *Nat. Commun.* 5.
1806 939 <https://doi.org/10.1038/ncomms5014>
1807 940
1808 941 Buck, W. R., 1991. Modes of continental lithospheric extension, *J. Geophys. Res.*, 96, 20,161-
1809 942 20,178.
1810 943
1811 944 Buck, W. R., F. Martinez, M. S. Steckler, and J. R. Cochran, 1988. Thermal consequences of
1812 945 lithospheric extension: Pure and simple, *Tectonics*, 7, 213 - 234.
1813 946
1814 947 Cadenas, P., Fernández-Viejo, G., 2017. The Asturian Basin within the North Iberian margin
1815 948 (Bay of Biscay): seismic characterisation of its geometry and its Mesozoic and Cenozoic
1816 949 cover. *Basin Res.* 29, 521-541. <https://doi.org/10.1111/bre.12187>
1817 950
1818 951 Canérot, J., 1988. Manifestations de l'halocinèse dans les Chaînons Béarnais (Zone Nord-
1819 952 Pyrénéenne) au Crétacé inférieur. *Comptes Rendus de l'Académie des Sciences de Paris* 306,
1820 953 1099-1102.
1821 954
1822 955 Canérot, J., 1989. Rifting éocrétacé et halocinèse sur la marge ibérique des Pyrénées
1823 956 Occidentales (France). Conséquences structurales. *Bull. Cent. Rech. Explor.-Prod. Elf-*
1824 957 *Aquitaine* 13, 87-99.
1825 958
1826 959 Canérot, J., 2017. The pull apart-type Tardets-Mauléon Basin, a key to understand the
1827 960 formation of the Pyrenees. *Bull. Société Géologique Fr.* 188, 35.
1828 961 <https://doi.org/10.1051/bsgf/2017198>
1829 962
1830 963 Canérot, J., Hudec, M.R., Rockenbauch, K., 2005. Mesozoic diapirism in the Pyrenean orogen:
1831 964 Salt tectonics on a transform plate boundary. *AAPG Bull.* 89, 211-229.
1832 965 <https://doi.org/10.1306/09170404007>
1833 966
1834 967 Canérot, J., Lenoble, J.-L., 1989. Le diapir du Lichançumendy (Pyrénées-Atlantiques), nouvel
1835 968 élément de la marge ibérique des Pyrénées occidentales. *Comptes Rendus Académie Sci.*
1836 969 *Sér. 2 Mécanique Phys. Chim. Sci. Univers Sci. Terre* 308, 1467-1472.
1837 970
1838 971 Canérot, J., Lenoble, J.-L., 1993. Diapirisme crétacé sur la marge ibérique des Pyrénées
1839 972 occidentales; exemple du pic de Lauriolle; comparaisons avec l'Aquitaine, les Pyrénées
1840 973 centrales et orientales. *Bull. Société Géologique Fr.* 164, 719-726.
1841 974
1842 975 Capdevila, R., Boillot, G., Lepvrier, C., Malod, J.-A., Mascle, G., 1980. Les formations
1843 976 cristallines du Banc Le Danois (marge nord ibérique). *Comptes Rendus Académie des*
1844 977 *Sciences de Paris* 291, 317-320.
1845 978
1846 979 Casas-Sainz, A.M., Gil-Imaz, A., 1998. Extensional subsidence, contractional folding and
1847 980 thrust inversion of the eastern Cameros basin, northern Spain. *Geol Rundsch* 86(4):802-818
1848 981
1849 982 Castanares, L.M., Robles, S., Gimeno, D. and Vicente Bravo, J.C., 2001. The Submarine
1850
1851
1852
1853
1854
1855
1856
1857
1858
1859
1860

1861
1862
1863 983 Volcanic System of the Errigoiti Formation (Albian-Santonian of the Basque-Cantabrian
1864 984 Basin, Northern Spain): Stratigraphic Framework, Facies, and Sequences. *Journ. Sedim.*
1865 985 *Research.* 71 , 2, 318-333.
1866 986
1867 987 Chevrot, S., Sylvander, M., Díaz, J., Ruiz, M., Paul, A., PYROPE Working Group, 2015. The
1868 988 Pyrenean architecture as revealed by teleseismic P-to-S converted waves recorded along
1870 989 two dense transects. *Geophysical Journal International* 200, 1094-1105.
1871 990
1872 991 Chevrot, S., Sylvander, M., Diaz, J., Martin, R., Mouthereau, F., Manatschal, G., Masini, E.,
1873 992 Calassou, S., Grimaud, F., Pauchet, H., Ruiz, M., 2018. The non-cylindrical crustal architecture
1874 993 of the Pyrenees. *Sci. Rep.* 8. <https://doi.org/10.1038/s41598-018-27889-x>
1875 994
1876 995 Choukroune, P., 1976a. Strain patterns in the Pyrenean chain: *Philosophical Transactions of*
1878 996 *the Royal Society of London A: Mathematical, Physical and Engineering Sciences*, v. 283, no.
1879 997 1312, p. 271-280.
1880 998
1881 999 Choukroune, P., 1976b. Structure et évolution tectonique de la zone nord pyrénéenne,
1882 1000 *Mem. Soc. Geol. Fr.*, 127, 1-116.
1883 1001
1884 1002 Choukroune, P., ECORS Team, 1989. The ECORS Pyrenean deep seismic profile reflection
1886 1003 data and the overall structure of an orogenic belt. *Tectonics* 8, 23-39.
1887 1004
1888 1005 Choukroune, P., Mattauer, M., 1978. Tectonique des plaques et Pyrenees; sur le
1889 1006 fonctionnement de la faille transformante nord-pyreneenne; comparaisons avec des
1890 1007 modeles actuels. *Bull. Société Géologique Fr.* 7, 689-700.
1891 1008
1892 1009 Clerc, C., Lagabrielle, Y., 2014. Thermal control on the modes of crustal thinning leading to
1894 1010 mantle exhumation: Insights from the Cretaceous Pyrenean hot paleomargins. *Tectonics* 33,
1895 1011 1340-1359. <https://doi.org/10.1002/2013TC003471>
1896 1012
1897 1013 Clerc, C., Jolivet, L., Ringenbach, J.-C., 2015a. Ductile extensional shear zones in the lower
1898 1014 crust of a passive margin. *Earth Planet. Sci. Lett.* 431, 1-7.
1899 1015 <https://doi.org/10.1016/j.epsl.2015.08.038>
1900 1016
1901 1017 Clerc, C., Lahfid, A., Monié, P., Lagabrielle, Y., Chopin, C., Poujol, M., Boulvais, P.,
1903 1018 Ringenbach, J.C., Masini, E., de St Blanquat, M., 2015b. High-temperature metamorphism
1904 1019 during extreme thinning of the continental crust: a reappraisal of the North Pyrenean
1905 1020 passive paleomargin. *Solid Earth* 6, 643-668.
1906 1021
1907 1022 Clerc, C., Lagabrielle, Y., Labaume, P., Ringenbach, J.-C., Vauchez, A., Nalpas, T., Bousquet, R.,
1908 1023 Ballard, J.-F., Lahfid, A., Fourcade, S., 2016. Basement - Cover decoupling and progressive
1909 1024 exhumation of metamorphic sediments at hot rifted margin. Insights from the Northeastern
1910 1025 Pyrenean analog. *Tectonophysics* 686, 82-97. <https://doi.org/10.1016/j.tecto.2016.07.022>
1912 1026
1913 1027 Clerc, C., Ringenbach, J.-C., Jolivet, L., Ballard, J.-F., 2018. Rifted margins: Ductile
1914 1028 deformation, boudinage, continentward-dipping normal faults and the role of the weak
1915 1029 lower crust. *Gondwana Res.* 53, 20-40. <https://doi.org/10.1016/j.gr.2017.04.030>
1916
1917
1918
1919
1920

1921
1922
1923 1030
1924 1031 Corre, B., Lagabrielle, Y., Labaume, P., Fourcade, S., Clerc, C., Ballèvre, M., 2016.
1925 1032 Deformation associated with mantle exhumation in a distal, hot passive margin
1926 1033 environment: New constraints from the Sarailé Massif (Chaînons Béarnais, North-Pyrenean
1928 1034 Zone). *Comptes Rendus Geosci.* 348, 279–289. <https://doi.org/10.1016/j.crte.2015.11.007>
1929 1035
1930 1036 Cuevas, J., Tubia, J.M., 1999. The discovery of scapolite marbles in the Biscay Synclinorium
1931 1037 (Basque-Cantabrian basin, Western Pyrenees): geodynamic implications. *Terra Nova* 11,
1932 1038 259–265. <https://doi.org/10.1046/j.1365-3121.1999.00255.x>
1933 1039
1934 1040 Damotte, B., 1998. The ECORS Pyrenean Deep Seismic Surveys, 1985–1994, *Mémoires de la*
1935 1041 *Société géologique de France*, 173, 104 p., 8 pl.
1936 1042
1937 1043 Dañobeitia, J.J., Arguedas, M., Gallart, J., Banda, E., Makris, J., 1992. Deep crustal
1939 1044 configuration of the Valencia trough and its Iberian and Balearic borders from extensive
1940 1045 refraction and wide-angle reflection seismic profiling. *Tectonophysics* 203, 37–55.
1941 1046
1942 1047 Dauteuil, O., and Ricou, L.-E., 1989. Une circulation de fluides de haute-température à
1943 1048 l’origine du métamorphisme crétacé nord-pyrénéen. *Geodin. Acta* 3, 237–249.
1944 1049 <https://doi.org/10.1080/09853111.1989.11105190>
1945 1050
1946 1051 de Saint Blanquat, M., Bajolet, F., Grand’Homme, A., Proietti, A., Zanti, M., Boutin, A., Clerc,
1948 1052 C., Lagabrielle, Y., Labaume, P., 2016. Cretaceous mantle exhumation in the central
1949 1053 Pyrenees: New constraints from the peridotites in eastern Ariège (North Pyrenean zone,
1950 1054 France). *Comptes Rendus Geosci.* 348, 268–278. <https://doi.org/10.1016/j.crte.2015.12.003>
1951 1055
1952 1056 Debroas E.-J., 1978. Evolution de la fosse du flysch ardoisier de l’Albien supérieur au
1953 1057 Sénonien inférieur (zone interne métamorphique des Pyrénées navarro-languedociennes),
1954 1058 *Bull. Soc. Géol. Fr.* (7), XX, p. 639-648.
1955 1059
1956 1060 Debroas, E.J., 1990. Le flysch noir albo-cénomanié témoin de la structuration albienne à
1958 1061 sénonienne de la Zone nord-pyrénéenne en Bigorre (Hautes-Pyrénées, France). *Bull. Soc.*
1959 1062 *Geol. Fr.* VI, 273–285. <https://doi.org/10.2113/gssgfbull.VI.2.273>
1960 1063
1961 1064 DeFelipe, I., Pedreira, D., Pulgar, J.A., Iriarte, E., Mendia, M., 2017. Mantle exhumation and
1962 1065 metamorphism in the Basque-Cantabrian Basin (N Spain): Stable and clumped isotope
1963 1066 analysis in carbonates and comparison with ophicalcites in the North-Pyrenean Zone
1964 1067 (Urdach and Lherz). *Geochem. Geophys. Geosystems* 18, 631–652.
1965 1068 <https://doi.org/10.1002/2016GC006690>
1966 1069
1967 1070 Deramond, J., Souquet, P., Fondécave-Wallez, M.-J., Specht, M., 1993. Relationships
1968 1071 between thrust tectonics and sequence stratigraphy surfaces in foredeeps: model and
1969 1072 examples from the Pyrenees (Cretaceous-Eocene, France, Spain). *Geol. Soc. Lond. Spec.*
1970 1073 *Publ.* 71, 193–219.
1971 1074
1972 1075 Dercourt, J., Ricou, L. E., Vrielynck, B., 1993. Atlas Tethys Palaeoenvironmental maps Atlas
1973 1076 and Explanatory Notes, Gauthier Villars Ed. diffusion CGMW Paris, 307 p., 14 maps
1974
1975
1976
1977
1978
1979
1980

1981
1982
1983 1077
1984 1078 Dercourt, J., Zonenshain, L.P., Ricou, L.E. et al., 1986. Geological evolution of the Tethys belt
1985 1079 from the Atlantic to the Pamirs since the Lias. *Tectonophysics*, 123, 1, 241-315.
1986 1080
1987 1081 Ducoux, M., Jolivet, L., Cagnard, F., Gumiaux, C., Baudin, T., Masini, E., Callot, J.P., Aubourg,
1988 1082 C., Lahfid, A., Homonnay, E., 2019. The Nappe des Marbres unit of the Basque-Cantabrian
1989 1083 basin: the tectono-thermal evolution of a fossil hyperextended rift basin. *Tectonics*
1990 1084 submitted.
1991 1085
1992 1086 Duret, T., Schmalholz, S.M., 2015. From symmetric necking to localized asymmetric
1993 1087 shearing: the role of mechanical layering. *Geology*, 43, 8, 711-714.
1994 1088
1995 1089 Duret, T., Petri, B., Mohn, G., Schmalholz, S.M., Schenker, F.L., Müntener, O., 2016. The
1996 1090 importance of structural softening for the evolution and architecture of passive margins. *Sci.*
1997 1091 *Rep.* 6, 38704. <https://doi.org/10.1038/srep38704>
1998 1092
1999 1093 Duret, T., Asti, R., Lagabriele, Y., Brun, J.P., Jourdon, A., Clerc, C., Corre, B., 2019. Numerical
2000 1094 modelling of syn-rift salt tectonics during Cretaceous Pyrenean Rifting. *Basin Research*, in
2001 1095 press.
2002 1096
2003 1097 Espurt, N., Angrand, P., Teixell, A., Labaume, P., Ford, M., de Saint Blanquat, M, and Chevrot,
2004 1098 S., 2019. Crustal-scale balanced cross-section and restorations of the Central Pyrenean belt
2005 1099 (Nest- Cinca transect): superimposed orogenesis and Pyrenean rift system evolution.
2006 1100 *Tectonophysics*, (to be completed)
2007 1101
2008 1102 Ethève, N., Mohn, G., Frizon de Lamotte, D., Roca, E., Tugend, J., Gómez-Romeu, J., 2018.
2009 1103 Extreme Mesozoic Crustal Thinning in the Eastern Iberia Margin: The Example of the
2010 1104 Columbrets Basin (Valencia Trough). *Tectonics* 37, 636–662.
2011 1105
2012 1106 Fabriès, J., Lorand, J.-P., Bodinier, J.-L., Dupuy, C., 1991. Evolution of the Upper Mantle
2013 1107 beneath the Pyrenees: Evidence from Orogenic Spinel Lherzolite Massifs. *J. Petrol.*
2014 1108 *Special_Volume*, 55–76. https://doi.org/10.1093/petrology/Special_Volume.2.55
2015 1109
2016 1110 Fabriès, J., Lorand, J.-P., Bodinier, J.-L., 1998. Petrogenetic evolution of orogenic lherzolite
2017 1111 massifs in the central and western Pyrenees. *Tectonophysics* 292, 145–167.
2018 1112
2019 1113 Floquet, M., 1992. Outcrop sequence stratigraphy in a ramp setting: the Late Cretaceous
2020 1114 Early Palaeogene deposits of the Castilian Ramp (Spain), *Field Trip Guide Book in conjunction*
2021 1115 *with the international symposium Sequence Stratigraphy of Mesozoic- Cenozoic European*
2022 1116 *Basins: CNRS, Institut Français du Pétrole, Dijon. 130 p.*
2023 1117
2024 1118 Frasca, G., Gueydan, F., Brun, J.-P., Monié, P., 2016. Deformation mechanisms in a
2025 1119 continental rift up to mantle exhumation. Field evidence from the western Betics, Spain.
2026 1120 *Mar. Pet. Geol.* 76, 310–328. <https://doi.org/10.1016/j.marpetgeo.2016.04.020>
2027 1121
2028 1122 Fügenschuh, B., Froitzheim, N., Capdevila, R., & Boillot, G. (2003). Offshore granulites from
2029 1123 the Bay of Biscay margins: Fission tracks constrain a Proterozoic to Tertiary thermal history.

2041
2042
2043 1124 Terra Nova, 15, 337–342, doi:10.1046/j.1365-3121.2003.00502.x.
2044 1125
2045 1126 Gallart, J., Rojas, H., Diaz, J., Dañobeitia, J.J., 1990. Features of deep crustal structure and the
2046 1127 onshore-offshore transition at the Iberian flank of the Valencia Trough (Western
2047 1128 Mediterranean). *J. Geodyn.* 12, 233–252.
2049 1129
2050 1130 García-Mondéjar J, Agirrezabala LM, Aranburu A, Fernández-Mendiola PA, Gómez-Pérez I,
2051 1131 López-Horgue M, Rosales I., 1996. Aptian–Albian tectonic pattern of the Basque–Cantabrian
2052 1132 Basin (Northern Spain). *Geol J* 31(1):13–45
2053 1133
2054 1134 García-Mondéjar J, Fernández-Mendiola PA, Agirrezabala LM, Aranburu A, López-Horgue
2055 1135 MA, Iriarte E, Martínez de Rituerto S., 2004. Extensión del Aptiense-Albiense en la Cuenca
2056 1136 Vasco-Cantábrica. SGEIGME, Madrid. Geological Society, London, Special Publications, 282,
2057 1137 111-138, 1 January, <https://doi.org/10.1144/SP282.6>
2059 1138
2060 1139 Gartrell, A.P., 1997. Evolution of rift basins and low-angle detachments in multilayer analog
2061 1140 models. *Geology* 25, 615–618. doi:10.1130/0091 7613(1997)025<0615:EORBAL>2.3.CO;2
2062 1141
2063 1142 Gernigon, L., Brönnner, M., Roberts, D., Olesen, O., Nasuti, A., Yamasaki, T., 2014. Crustal and
2064 1143 basin evolution of the southwestern Barents Sea: From Caledonian orogeny to continental
2065 1144 breakup: Evolution of the Barents Sea. *Tectonics* 33, 347–373.
2066 1145 <https://doi.org/10.1002/2013TC003439>
2068 1146
2069 1147 Golberg, J.-M., Guiraud, M., Maluski, H., Séguret, M., 1988. Caractères pétrologiques et âge
2070 1148 du métamorphisme en contexte distensif du bassin sur décrochement de Soria (Crétacé
2071 1149 inférieur, Nord Espagne). *Comptes Rendus de l'Académie des Sciences Paris, Série* 11,307,
2072 1150 521-527.
2073 1151
2074 1152 Golberg, J.M., Leyreloup, A.F., 1990. High temperature-low pressure Cretaceous
2075 1153 metamorphism related to crustal thinning (Eastern North Pyrenean Zone, France). *Contrib.*
2076 1154 *Mineral. Petrol.* 104, 194–207. <https://doi.org/10.1007/BF00306443>
2077 1155
2078 1156 Gong, Z., Langereis, C.G., Mullender, T.A.T., 2008. The rotation of Iberia during the Aptian
2079 1157 and the opening of the Bay of Biscay. *Earth Planet. Sci. Lett.* 273, 80–93.
2080 1158 <https://doi.org/10.1016/j.epsl.2008.06.016>
2081 1159
2082 1160 Grool, A. R., Ford, M., Vergés, J., Huisman, R. S., Christophoul, F., & Dielforder, A. (2018).
2083 1161 Insights into the crustal-scale dynamics of a doubly vergent orogen from a quantitative
2084 1162 analysis of its forelands: A case study of the Eastern Pyrenees. *Tectonics*, 37.
2085 1163 <https://doi.org/10.1002/2017TC004731>
2086 1164
2087 1165 Guimerà, J., Alonso, Á., Mas, J.R., 1995. Inversion of an extensional-ramp basin by a newly
2088 1166 formed thrust: the Cameros basin (N. Spain).). in: *Basin Inversion* (J.G. Buchanan, P.G.
2089 1167 Buchanan, Eds). Geological Society, Special Publication, 88, 433-453.
2090 1168 <https://doi.org/10.1144/GSL.SP.1995.088.01.23>
2091 1169
2092 1170 Guiraud, M., Séguret, M., 1985. A releasing solitary overstep model for the late Jurassic–

2101
2102
2103 1171 early Cretaceous (Wealdian) Soria strike-slip basin (Northern Spain). In: Biddle KT, Christie-
2104 1172 Blick N (eds) Strike slip deformation, basin formation and sedimentation, vol 37., SEPM
2105 1173 Special Publication Society of Economic Paleontologists and Mineralogists, Tulsa, pp 159-
2106 1174 175.
2107
2108 1175
2109 1176 Hamilton, W., 1987. Crustal extension in the Basin and Range Province, southwestern United
2110 1177 States. Geol. Soc. Lond. Spec. Publ. 28, 155-176.
2111 1178 <https://doi.org/10.1144/GSL.SP.1987.028.01.12>
2112 1179
2113 1180 Huismans, R. S., Beaumont, C., 2007. Roles of lithospheric strain softening and heterogeneity
2114 1181 in determining the geometry of rifts and continental margins
2115
2116 1182
2117 1183 Huismans, R.S., Beaumont, C., 2011. Depth-dependent extension, two-stage breakup and
2118 1184 cratonic underplating at rifted margins. Nature 473, 74-78.
2119 1185 <https://doi.org/10.1038/nature09988>
2120 1186
2121 1187 Huismans, R.S., Beaumont, C., 2014. Rifted continental margins: The case for depth-
2122 1188 dependent extension. Earth Planet. Sci. Lett. 407, 148-162. doi:10.1016/j.epsl.2014.09.032
2123 1189
2124 1190 James, V., Canérot, J., 1988. Diapirisme et structuration post-triasique des Pyrénées
2125 1191 occidentales et de l'Aquitaine méridionale (France). Eclogae Geol. Helveticae 92, 63-72.
2126 1192
2127 1193 Jammes, S., Lavier, L., Manatschal, G., 2010a. Extreme crustal thinning in the Bay of Biscay
2128 1194 and the Western Pyrenees: From observations to modeling. Geochem. Geophys.
2129 1195 Geosystems 11. <https://doi.org/10.1029/2010GC003218>
2130 1196
2131 1197 Jammes, S., Tiberi, C., Manatschal, G., 2010b. 3D architecture of a complex transcurrent rift
2132 1198 system: The example of the Bay of Biscay-Western Pyrenees. Tectonophysics 489, 210-226.
2133 1199 <https://doi.org/10.1016/j.tecto.2010.04.023>
2134 1200
2135 1201 Jammes, S., Manatschal, G., Lavier, L., 2010c. Interaction between prerift salt and
2136 1202 detachment faulting in hyperextended rift systems: The example of the Parentis and
2137 1203 Mauléon basins (Bay of Biscay and western Pyrenees). AAPG Bull. 94, 957-975.
2138 1204 <https://doi.org/10.1306/12090909116>
2139 1205
2140 1206 Jammes, S., Lavier, L.L., Reber, J.E., 2015. Localization and delocalization of deformation in a
2141 1207 biminerale material. J. Geophys. Res. Solid Earth 120, 3649-3663.
2142 1208 <https://doi.org/10.1002/2015JB011890>
2143 1209
2144 1210 Jammes, S., Lavier, L.L., 2016. The effect of biminerale composition on extensional processes
2145 1211 at lithospheric scale. Geochem. Geophys. Geosystems 17, 3375-3392.
2146 1212 <https://doi.org/10.1002/2016GC006399>
2147 1213
2148 1214 Jammes, S., Manatschal, G., Lavier, L., Masini, E., 2009. Tectono-sedimentary evolution
2149 1215 related to extreme crustal thinning ahead of a propagating ocean: Example of the western
2150 1216 Pyrenees. Tectonics 28. <https://doi.org/10.1029/2008TC002406>
2151 1217
2152
2153
2154
2155
2156
2157
2158
2159
2160

2161
2162
2163 1218 Jolivet, L., Gorini, C., Smit, J., Leroy, S., 2015. Continental breakup and the dynamics of rifting
2164 1219 in back-arc basins: The Gulf of Lion margin: Backarc rift and lower crust extraction. *Tectonics*
2165 1220 34, 662–679. <https://doi.org/10.1002/2014TC003570>
2166 1221
2167 1222 Lagabrielle, Y., Bodinier, J.-L., 2008. Submarine reworking of exhumed sub-continental
2168 1223 mantle rocks: field evidence from the Lherz peridotites, French Pyrenees: Cretaceous
2169 1224 exhumation of pyrenean mantle. *Terra Nova* 20, 11–21. [https://doi.org/10.1111/j.1365-](https://doi.org/10.1111/j.1365-3121.2007.00781.x)
2170 1225 3121.2007.00781.x
2171 1226
2172 1227 Lagabrielle, Y., Labaume, P., de Saint Blanquat, M., 2010. Mantle exhumation, crustal
2173 1228 denudation, and gravity tectonics during Cretaceous rifting in the Pyrenean realm (SW
2174 1229 Europe): Insights from the geological setting of the Iherzolite bodies. *Tectonics* 29.
2175 1230 <https://doi.org/10.1029/2009TC002588>
2176 1231
2177 1232 Lagabrielle, Y., Clerc, C., Vauchez, A., Lahfid, A., Labaume, P., Azambre, B., Fourcade, S.,
2178 1233 Dautria, J.-M., 2016. Very high geothermal gradient during mantle exhumation recorded in
2179 1234 mylonitic marbles and carbonate breccias from a Mesozoic Pyrenean palaeomargin (Lherz
2180 1235 area, North Pyrenean Zone, France). *Comptes Rendus Geosci.* 348, 290–300.
2181 1236 <https://doi.org/10.1016/j.crte.2015.11.004>
2182 1237
2183 1238 Lagabrielle Y, Asti R, Fourcade S, Corre B, Pujol M, Uzel J, Labaume P, Clerc C, Lafay R,
2184 1239 Picazo S, Maury R. 2019. Mantle exhumation at magma-poor passive continental margins.
2185 1240 Part I. 3D architecture and metasomatic evolution of a fossil exhumed mantle domain
2186 1241 (Urdach Iherzolite, north-western Pyrenees, France), *BSGF - Earth Sciences Bulletin* 190: 8.
2187 1242 <https://doi.org/10.1051/bsgf/2019007>
2188 1243
2189 1244
2190 1245 Lagabrielle, Y., Asti, R., Fourcade, S., Corre, B., Uzel, J., Labaume, P., Clerc, C., Lafay, R.,
2191 1246 Picazo, S., 2019b. The mechanisms of mantle exhumation at magma-poor passive
2192 1247 continental margins. Part II. Insights from high-displacement, low-angle faults preserved in a
2193 1248 fossil distal margin domain (Sarailié Iherzolites, north-western Pyrenees, France). *BSGF Earth*
2194 1249 *Science Bull.*, in press.
2195 1250
2196 1251 Le Pichon, X., Bonnin, J., Francheteau, J., Sibuet, J.C., 1971. Une hypothèse d'évolution
2197 1252 tectonique du Golfe de Gascogne. *Hist. Struct. Golfe Gasc.* 2, 11–44.
2198 1253
2199 1254 Lenoble, J.-L., Canérot, J., 1992. La lame extrusive de Pont Suzon (Zone Nord-Pyrénéenne en
2200 1255 Vallée d'Aspe): reprise pyrénéenne d'une ride diapirique transverse d'âge créacé. *Comptes*
2201 1256 *Rendus Académie Sci. Sér. 2 Mécanique Phys. Chim. Sci. Univers Sci. Terre* 314, 387–391.
2202 1257
2203 1258 Lister, G.S. and Davis, G.A. 1989. The origin of metamorphic core complexes and detachment
2204 1259 faults formed during Tertiary continental extension in the northern Colorado River region,
2205 1260 U.S.A. *Journal of Structural Geology*, Vol. 11, No. 112, pp. 65 to 94,
2206 1261
2207 1262 Lister, G.S., Etheridge, M.A., Symonds, P.A., 1991. Detachment models for the formation of
2208 1263 passive continental margins. *Tectonics* 10, 1038–1064.
2209 1264
2210
2211
2212
2213
2214
2215
2216
2217
2218
2219
2220

2221
2222
2223 1265 Lopez-Mir, B., Muñoz, J.A., García Senz, J., 2014. Restoration of basins driven by extension
2224 1266 and salt tectonics: Example from the Cotiella Basin in the central Pyrenees. *J. Struct. Geol.*
2225 1267 69, Part A, 147–162. <https://doi.org/10.1016/j.jsg.2014.09.022>
2226 1268
2227
2228 1269 Manatschal, G., 2004. New models for evolution of magma-poor rifted margins based on a
2229 1270 review of data and concepts from West Iberia and the Alps. *Int. J. Earth Sci.* 93.
2230 1271 <https://doi.org/10.1007/s00531-004-0394-7>
2231 1272
2232 1273 Manatschal, G., Froitzheim, N., Rubenach, M., Turrin, B.D., 2001. The role of detachment
2233 1274 faulting in the formation of an ocean-continent transition: insights from the Iberia Abyssal
2234 1275 Plain. *Geol. Soc. Lond. Spec. Publ.* 187, 405–428.
2235 1276 <https://doi.org/10.1144/GSL.SP.2001.187.01.20>
2236 1277
2237
2238 1278 Manatschal, G., Engström, A., Desmurs, L., Schaltegger, U., Cosca, M., Müntener, O.,
2239 1279 Bernoulli, D., 2006. What is the tectono-metamorphic evolution of continental break-up: The
2240 1280 example of the Tasna Ocean–Continent Transition. *J. Struct. Geol.* 28, 1849–1869.
2241 1281 <https://doi.org/10.1016/j.jsg.2006.07.014>
2242 1282
2243 1283 Mas. R., Benito MI, Arribas J, Alonso A, Arribas ME, González-Acebrón L, Hernán J, Quijada E,
2244 1284 Suárez-González P, Omodeo Salè S (2011) Evolution of an intra-plate rift basin: the Latest
2245 1285 Jurassic-Early Cretaceous Cameros Basin (Northwest Iberian Ranges, North Spain). In: Post-
2246 1286 Meeting field trips 28th IAS Meeting, vol Geoguías 8. Zaragoza (Spain)
2247 1287
2248
2249 1288 Masini, E., Manatschal, G., Tugend, J., Mohn, G., Flament, J.-M., 2014. The tectono-
2250 1289 sedimentary evolution of a hyper-extended rift basin: the example of the Arzacq–Mauléon
2251 1290 rift system (Western Pyrenees, SW France). *Int. J. Earth Sci.* 103, 1569–1596.
2252 1291 <https://doi.org/10.1007/s00531-014-1023-8>
2253 1292
2254 1293 McClay, K., Muñoz, J.-A., García-Senz, J., 2004. Extensional salt tectonics in a contractional
2255 1294 orogen: A newly identified tectonic event in the Spanish Pyrenees. *Geology* 32, 737–740.
2256 1295 <https://doi.org/10.1130/G20565.1>
2257 1296
2258 1297 McKenzie, D., 1978. Some remarks on the development of sedimentary basins. *Earth Planet.*
2259 1298 *Sci. Lett.* 40, 25–32. [https://doi.org/10.1016/0012-821X\(78\)90071-7](https://doi.org/10.1016/0012-821X(78)90071-7)
2260 1299
2261 1300 Mendia, M., and Gil Iburguchi, J. I. 1991. High-grade metamorphic rocks and peridotites
2262 1301 along the Leiza Fault (Western Pyrenees, Spain), *Geologische Rundschau* 80/1.
2263 1302
2264 1303 Michon, L. and Merle, O. 2003. Mode of lithospheric extension: Conceptual models from
2265 1304 analogue modeling. *Tectonics*, 22 (4), pp.1028. <https://doi.org/10.1029/2002TC001435>
2266 1305
2267 1306 Mohn, G., Karner, G.D., Manatschal, G., Johnson, C.A., 2015. Structural and stratigraphic
2268 1307 evolution of the Iberia–Newfoundland hyper-extended rifted margin: a quantitative
2269 1308 modelling approach. *Geol. Soc. Lond. Spec. Publ.* 413, 53–89.
2270 1309 <https://doi.org/10.1144/SP413.9>
2271 1310
2272
2273
2274
2275
2276
2277
2278
2279
2280

2281
2282
2283
2284
2285
2286
2287
2288
2289
2290
2291
2292
2293
2294
2295
2296
2297
2298
2299
2300
2301
2302
2303
2304
2305
2306
2307
2308
2309
2310
2311
2312
2313
2314
2315
2316
2317
2318
2319
2320
2321
2322
2323
2324
2325
2326
2327
2328
2329
2330
2331
2332
2333
2334
2335
2336
2337
2338
2339
2340

1311 Mohn, G., Manatschal, G., Beltrando, M., Masini, E., Kuznir, N., 2012. Necking of continental
1312 crust in magma-poor rifted margins: Evidence from the fossil Alpine Tethys margins: Necking
1313 of continental crust. *Tectonics* 31, n/a-n/a. <https://doi.org/10.1029/2011TC002961>
1314
1315 Mohn, G., Manatschal, G., Müntener, O., Beltrando, M., Masini, E., 2010. Unravelling the
1316 interaction between tectonic and sedimentary processes during lithospheric thinning in the
1317 Alpine Tethys margins. *Int. J. Earth Sci.* 99, 75–101. [https://doi.org/10.1007/s00531-010-](https://doi.org/10.1007/s00531-010-0566-6)
1318 0566-6
1319
1320 Monchoux, P., 1970. Les lherzolites pyrénéennes: contribution à l'étude de leur minéralogie,
1321 de leur genèse et de leurs transformations. Université Paul Sabatier de Toulouse (Sciences).
1322
1323 Muñoz, J.A., 1992. Evolution of a continental collision belt: ECORS-Pyrenees crustal balanced
1324 cross-section, in: *Thrust Tectonics*. Springer, pp. 235–246.
1325
1326 Nagel, T. J. and Buck, W. R., 2004. Symmetric alternative to asymmetric rifting models.
1327 *Geology*, 32, 11. pp 937-940 Doi 10.1130/G20785.1
1328
1329 Olivet, J.L., 1996. La cinématique de la plaque ibérique. *Bull Cent Rech Explor Prod Elf*
1330 *Aquitaine* 20, 131–195.
1331
1332 Omodeo Salè, S., Guimerà, J., Mas, R., & Arribas, J. (2014). Tectono-stratigraphic evolution of
1333 an inverted extensional basin: The Cameros Basin (north of Spain). *International Journal of*
1334 *Earth Sciences*, 103(6), 1597–1620. <https://doi.org/10.1007/s00531-014-1026-5>
1335
1336 Ortí, F., Pérez-López, A., Salvany, J.M., 2017. Triassic evaporites of Iberia: Sedimentological
1337 and palaeogeographical implications for the western Neotethys evolution during the Middle
1338 Triassic–Earliest Jurassic. *Palaeogeogr. Palaeoclimatol. Palaeoecol.* 471, 157–180.
1339 <https://doi.org/10.1016/j.palaeo.2017.01.025>
1340
1341 Osmundsen, P.T., Ebbing, J., 2008. Styles of extension offshore mid-Norway and implications
1342 for mechanisms of crustal thinning at passive margins: STYLES OF EXTENSION OFFSHORE
1343 NORWAY. *Tectonics* 27, n/a-n/a. <https://doi.org/10.1029/2007TC002242>
1344
1345 Osmundsen, P.T., Péron-Pinvidic, G., 2018. Crustal-Scale Fault Interaction at Rifted Margins
1346 and the Formation of Domain-Bounding Breakaway Complexes: Insights From Offshore
1347 Norway. *Tectonics* 37, 935–964. <https://doi.org/10.1002/2017TC004792>
1348
1349 Pedrera, A., García-Senz, J., Ayala, C., Ruiz-Constán, A., Rodríguez-Fernández, L. R., Robador,
1350 A., & GonzálezMenéndez, L. (2017). Reconstruction of the exhumed mantle across the North
1351 Iberian Margin by crustal-scale 3-D gravity inversion and geological cross section. *Tectonics*,
1352 36. <https://doi.org/10.1002/2017TC004716>
1353
1354 Péron-Pinvidic, G., Manatschal, G., Minshull, T.A., Sawyer, D.S., 2007. Tectonosedimentary
1355 evolution of the deep Iberia-Newfoundland margins: Evidence for a complex breakup
1356 history. *Tectonics* 26, 1–19. <https://doi.org/10.1029/2006TC001970>
1357

2341
2342
2343 1358 Péron-Pinvidic, G., Manatschal, G., 2009. The final rifting evolution at deep magma-poor
2344 1359 passive margins from Iberia-Newfoundland: a new point of view. *Int. J. Earth Sci.* 98, 1581–
2345 1360 1597. <https://doi.org/10.1007/s00531-008-0337-9>
2346 1361
2347
2348 1362 Pinet, B., Montadert, L., ECORS Scientific Party, 1987. Deep seismic reflection and refraction
2349 1363 profiling along the Aquitaine shelf (Bay of Biscay). *Geophys. J. Int.* 89, 305–312.
2350 1364 <https://doi.org/10.1111/j.1365-246X.1987.tb04423.x>
2351 1365
2352 1366 Puigdefàbregas, C., Souquet, P., 1986. Tecto-sedimentary cycles and depositional sequences
2353 1367 of the Mesozoic and Tertiary from the Pyrenees. *Tectonophysics* 129, 173–203.
2354 1368
2355 1369 Rat, P., 1988. The Basque–Cantabrian basin between the Iberian and European plates: some
2356 1370 facts but still many problems. *Rev Soc Geol Esp* 1(3–4):327–348
2357 1371
2358
2359 1372 Rat, P., Amiot, M., Feuillée, P., Floquet, M., Mathey, B., Pascal, A., Salomon, J., García
2360 1373 Mondéjar, J., Pujalte, J., Lamolda, M., et al., 1983. Vue sur le Cretacé basco-cantabrique et
2361 1374 nord-ibérique. Une marge, son arrière-pays, ses environ. sédimentaires. *Mémoires Géol.*
2362 1375 *Univ. Dijon* 9, 191.
2363 1376
2364 1377 Rat, J., Mouthereau, F., Brichau, S., Crémadès, A., Bernet, M., Balvay, M., Ganne, J., Lahfid,
2365 1378 A., Gautheron, C., 2019. Tectonothermal Evolution of the Cameros Basin: Implications for
2366 1379 Tectonics of North Iberia. *Tectonics* 38, 440–469. <https://doi.org/10.1029/2018TC005294>
2367 1380
2368 1381 Ravier, J., 1959. Le métamorphisme des terrains secondaires des Pyrénées. *Mémoires de la*
2370 1382 *Société Géologique de France*, N° 86, 250 p., 19 flg., 9 pl. phot.
2371 1383
2372 1384 Reston, T., McDermott, K., 2014. An assessment of the cause of the ‘extension discrepancy’
2373 1385 with reference to the west Galicia margin. *Basin Res.* 26, 135–153.
2374 1386 <https://doi.org/10.1111/bre.12042>
2375 1387
2376 1388 Reston, T.J., 1988. Evidence for shear zones in the lower crust offshore Britain. *Tectonics* 7,
2378 1389 929–945. <https://doi.org/10.1029/TC007i005p00929>
2379 1390
2380 1391 Reston, T.J., Krawczyk, C.M., Hoffmann, H.-J., 1995. Detachment tectonics during Atlantic
2381 1392 rifting: analysis and interpretation of the S reflection, the west Galicia margin. *Geol. Soc.*
2382 1393 *Lond. Spec. Publ.* 90, 93–109. <https://doi.org/10.1144/GSL.SP.1995.090.01.05>
2383 1394
2384 1395 Reston, T.J., Pérez-Gussinyé, M., 2007. Lithospheric extension from rifting to continental
2385 1396 breakup at magma-poor margins: rheology, serpentinitisation and symmetry. *Int. J. Earth Sci.*
2387 1397 96, 1033–1046. <https://doi.org/10.1007/s00531-006-0161-z>
2388 1398
2389 1399 Roca, E., Muñoz, J.A., Ferrer, O., Ellouz, N., 2011. The role of the Bay of Biscay Mesozoic
2390 1400 extensional structure in the configuration of the Pyrenean orogen: Constraints from the
2391 1401 MARCONI deep seismic reflection survey. *Tectonics* 30.
2392 1402 <https://doi.org/10.1029/2010TC002735>
2393 1403
2394
2395
2396
2397
2398
2399
2400

2401
2402
2403
2404
2405
2406
2407
2408
2409
2410
2411
2412
2413
2414
2415
2416
2417
2418
2419
2420
2421
2422
2423
2424
2425
2426
2427
2428
2429
2430
2431
2432
2433
2434
2435
2436
2437
2438
2439
2440
2441
2442
2443
2444
2445
2446
2447
2448
2449
2450
2451
2452
2453
2454
2455
2456
2457
2458
2459
2460

1404 Roma, M., Ferrer, O., Roca, E., Pla, O., Escosa, F., Butillé, M., 2018. Formation and inversion
1405 of salt-detached ramp-syncline basins. Results from analog modeling and application to the
1406 Columbrets Basin (Western Mediterranean), *Tectonophysics* 10.1016/j.tecto.2018.08.012
1407

1408 Roure, F., Choukroune, P., 1998. Contribution of the ECORS seismic data to the Pyrenean
1409 geology: Crustal architecture and geodynamic evolution of the Pyrenees. *Mém. Société*
1410 *Géologique Fr.* 173, 37–52.
1411

1412 Rowan, M.G., 2014. Passive-margin salt basins: hyperextension, evaporite deposition, and
1413 salt tectonics. *Basin Res.* 26, 154–182. <https://doi.org/10.1111/bre.12043>
1414

1415 Ruiz, M., 2007. Caracterització estructural i sismotectònica de la litosfera en el Domini
1416 Pirenaico-Cantàbric a partir de mètodes de sísmica activa i passiva, Ph.D. thesis, Univ. of
1417 Barcelona, Barcelona, Spain.
1418

1419 Salas, R., Casas, A., 1993. Mesozoic extensional tectonics, stratigraphy and crustal evolution
1420 during the Alpine cycle of the eastern Iberian basin. *Tectonophysics* 228, 33–55.
1421 [https://doi.org/10.1016/0040-1951\(93\)90213-4](https://doi.org/10.1016/0040-1951(93)90213-4)
1422

1423 Salas, R., Guimerà, J., Mas, R., Martín-Closas, C., Meléndez, A., Alonso, Á., 2001. Evolution of
1424 the Mesozoic Central Iberian Rift System and its Cainozoic inversion (Iberian chain). In:
1425 Ziegler PA, Cavazza W, Robertson AHF, Crasquin-Soleau S (eds), *Peri-Tethys Memoir 6: Peri-*
1426 *Tethyan Rift/Wrench Basins and Passive Margins*, vol 186. *Mémoires du Museum National*
1427 *d'Histoire Naturelle*, Paris, pp 145–186
1428

1429 Saspiturry, N., Razin, P., Baudin, T., Serrano, O., Issautier, B., Lasseur, E., Allanic, C., Thion,
1430 I., Leleu, S., 2019. Symmetry vs. asymmetry of a hyper-thinned rift: Example of the Mauléon
1431 Basin (Western Pyrenees, France). *Mar. Pet. Geol.* 104, 86–105.
1432 <https://doi.org/10.1016/j.marpetgeo.2019.03.031>
1433

1434 Saura, E., Ardèvol i Oró, L., Teixell, A., Vergés, J., 2016. Rising and falling diapirs, shifting
1435 depocenters, and flap overturning in the Cretaceous Sopeira and Sant Gervàs subbasins
1436 (Ribagorça Basin, southern Pyrenees): Southern Pyrenees Cretaceous Diapirism. *Tectonics*
1437 35, 638–662. <https://doi.org/10.1002/2015TC004001>
1438

1439 Scotese, C.R. and Schettino, A., 2017. Late Permian-Early Jurassic paleogeography of
1440 Western Tethys and the world. In Soto et al., eds, *Permo-Triassic salt provinces of Europe,*
1441 *North Africa and the Atlantic margins. Tectonics and Hydrocarbon potential.* Elsevier, pp. 57-
1442 91.
1443

1444 Sibuet, J.-C., Srivastava, S.P., Spakman, W., 2004. Pyrenean orogeny and plate kinematics. *J.*
1445 *Geophys. Res. Solid Earth* 109, B08104. <https://doi.org/10.1029/2003JB002514>
1446

1447 Soto, J.I, Flinch, J.F. and Tari, G., 2017. Permo-Triassic salt provinces of Europe, North Africa
1448 and the Atlantic margins: A synthesis. In Soto et al., eds, *Permo-Triassic salt provinces of*
1449 *Europe, North Africa and the Atlantic margins. Tectonics and Hydrocarbon potential.*
1450 Elsevier, pp. 3-41.

2461
2462
2463 1451
2464 1452 Sutra, E., Manatschal, G., Mohn, G., Unternehr, P., 2013. Quantification and restoration of
2465 1453 extensional deformation along the Western Iberia and Newfoundland rifted margins. *Geoch.*
2466 1454 *Geoph. Geosys.* 14 (8), 2575e2597.
2467 1455
2468 1456 Teixell, A., 1998. Crustal structure and orogenic material budget in the west central
2469 1457 Pyrenees. *Tectonics* 17, 395–406. <https://doi.org/10.1029/98TC00561>
2470 1458
2471 1459 Teixell, A., Labaume, P., Lagabrielle, Y., 2016. The crustal evolution of the west-central
2472 1460 Pyrenees revisited: Inferences from a new kinematic scenario. *Comptes Rendus Geosci.* 348,
2473 1461 257–267. <https://doi.org/10.1016/j.crte.2015.10.010>
2474 1462
2475 1463 Teixell, A., Labaume, P., Ayarza, P., Espurt, N., de Saint Blanquat, M., Lagabrielle, Y., 2018.
2476 1464 Crustal structure and evolution of the Pyrenean-Cantabrian belt: A review and new
2477 1465 interpretations from recent concepts and data. *Tectonophysics* 724, 146–170.
2478 1466 <https://doi.org/10.1016/j.tecto.2018.01.009>
2479 1467
2480 1468 Thiébault J., Durand-Wackenheim C., Debeaux M. and Souquet P., 1992. Métamorphisme
2481 1469 des évaporites triasiques du versant nord des Pyrénées centrales et occidentales. *Bull. Soc.*
2482 1470 *Hist. Nat. Toulouse.* 128, 77-84.
2483 1471
2484 1472 Thinon, I., Matias, L., Réhault, J.P., Hirn, A., Fidalgo-González, L., Avedik, F., 2003. Deep
2485 1473 structure of the Armorican Basin (Bay of Biscay): a review of Norgasis seismic reflection and
2486 1474 refraction data. *J. Geol. Soc.* 160, 99–116. <https://doi.org/10.1144/0016-764901-103>
2487 1475
2488 1476 Tirel, C., Brun, J.-P. and Burov, E., 2008. Dynamics and structural development of
2489 1477 metamorphic core complexes. *Journal of Geophysical Research*, 113(B4): B04403.
2490 1478
2491 1479 Tomassimo, A., Marillier, F., 1997. Processing and interpretation in the tau-p domain of the
2492 1480 ECORS Bay of Biscay expanding spread profiles. *Mém. Société Géologique Fr.* 171, 31–43.
2493 1481
2494 1482 Tugend, J., Manatschal, G. and Kuszniir, N.J., 2015. Spatial and temporal evolution of
2495 1483 hyperextended rift systems: Implication for the nature, kinematics, and timing of the
2496 1484 Iberian-European plate boundary, *Geology*, 43(1), 15–18, doi:10.1130/G36072.1.
2497 1485
2498 1486 Tugend, J., Manatschal, G., Kuszniir, N.J., Masini, E., Mohn, G., Thinon, I., 2014. Formation
2499 1487 and deformation of hyperextended rift systems: Insights from rift domain mapping in the
2500 1488 Bay of Biscay-Pyrenees. *Tectonics* 33, 1239–1276. <https://doi.org/10.1002/2014TC003529>
2501 1489
2502 1490 Vergés, J., García-Senz, J., 2001. Mesozoic evolution and Cainozoic inversion of the Pyrenean
2503 1491 rift. *Mém. Muséum Natl. Hist. Nat.* 186, 187–212.
2504 1492
2505 1493 Vielzeuf, D., Kornprobst, J., 1984. Crustal splitting and the emplacement of Pyrenean
2506 1494 Iherzolites and granulites. *Earth Planet. Sci. Lett.* 67, 87–96. [https://doi.org/10.1016/0012-](https://doi.org/10.1016/0012-821X(84)90041-4)
2507 1495 [821X\(84\)90041-4](https://doi.org/10.1016/0012-821X(84)90041-4)
2508 1496
2509 1497 Vissers, R.L.M., Drury, M.R., Newman, J. and Fliervoet, T.F., 1997. Mylonitic deformation in
2510
2511
2512
2513
2514
2515
2516
2517
2518
2519
2520

2521
2522
2523
2524
2525
2526
2527
2528
2529
2530
2531
2532
2533
2534
2535
2536
2537
2538
2539
2540
2541
2542
2543
2544
2545
2546
2547
2548
2549
2550
2551
2552
2553
2554
2555
2556
2557
2558
2559
2560
2561
2562
2563
2564
2565
2566
2567
2568
2569
2570
2571
2572
2573
2574
2575
2576
2577
2578
2579
2580

1498 upper mantle peridotites of the North Pyrenean Zone (France) : implications for strength
1499 and strain localization in the lithosphere. *Tectonophysics*, 279, 303-325.

1500

1501 Wang, Y., Chevrot, S., Monteiller, V., Komatitsch, D., Mouthereau, F., Manatschal, G.,

1502 Sylvander, M., Diaz, J., Ruiz, M., Grimaud, F., Benahmed, S., Pauchet, H., Martin, R., 2016.

1503 The deep roots of the western Pyrenees revealed by full waveform inversion of teleseismic P

1504 waves. *Geology* 44, 475–478. <https://doi.org/10.1130/G37812.1>

1505

1506 Wernicke, B., 1981. Low-angle normal faults in the Basin and Range Province: nappe

1507 tectonics in an extending orogen. *Nature* 291, 645–648. <https://doi.org/10.1038/291645a0>

1508

1509 Wernicke, B., 1985. Uniform-sense normal simple shear of the continental lithosphere. *Can.*

1510 *J. Earth Sci.* 22, 108–125. <https://doi.org/10.1139/e85-009>

1511

1512 Ziegler, 1988. Evolution of Arctic-North Atlantic and western Tethys. Tulsa. AAPG Memoir,

1513 43, 198 pp.

1514

1515 Zamora, G., Fleming, M., Gallastegui, J., 2017. Salt Tectonics Within the Offshore Asturian

1516 Basin: North Iberian Margin, in Soto, J.I, Flinch, J.F. and Tari, G., 2017. Permo-Triassic salt

1517 provinces of Europe, North Africa and the Atlantic margins: A synthesis. In Soto et al., eds,

1518 Permo-Triassic salt provinces of Europe, North Africa and the Atlantic margins. *Tectonics and*

1519 *Hydrocarbon potential*. Elsevier, pp. 353-367.

1520

1521

1522

2581
2582
2583 **1523 Figure captions**
2584

2585 1524

2587 **1525 Figure 1. Location of the studied basins and their paleogeographic position during the**
2588
2589 **1526 Cretaceous at the onset of the Iberia drift.**

2590 1527 (a) Simplified structural map of the Cantabrian-Pyrenean orogenic system and adjoining
2592 Iberia showing Eurasia deformed and undeformed domain (modified from Verges and Garcia-
2593 Senz, 2001 and Teixell et al., 2018). (b) Hypothetical reconstruction at the onset of the Iberia
2594 drift (modified after Tugend et al., 2014).
2595
2596

2597 1531

2599 **1532 Figure 2. A compilation of Cretaceous basins architecture from the Cantabrian-Pyrenean**
2600 **1533 belt.**

2602 1534 Reconstructions from field and geophysical data collected by various authors in the Basque-
2603 Cantabrian basin (a, b, c) and in the North Pyrenean Zone (NPZ): Mauléon basin (d),
2604 Chainons Béarnais (e, f), Baronnies basin (g) and Agly massif-Boucheville basin (h).
2605
2606

2607 1537

2609 **1538 Figure 3. Structure and evolution of Iberia-Newfoundland-type and Alpine-type passive**
2610 **1539 margins** (modified from Péron-Pinvidic and Manatschal, 2009 and Mohn et al., 2012).

2613 1540 (a): two sketches showing the main concepts linked to Iberia-Newfoundland-type margin
2614 evolution, namely: (i) strong final asymmetry with upper and lower plates separated by a
2615 single detachment fault (HHD, Hobby High detachment), (ii) emplacement of extensional
2616 allochthons as rigid crustal blocks over the exhumed mantle. (b): strain distribution and
2617 strain partitioning during lithospheric thinning at magma-poor rifted margin, with example
2618 from the fossil Alpine Tethys margin. In this model, the pre-rift cover remains welded on the
2619 tilted crustal blocks; the middle crust is thinned to zero and the upper crust and upper
2620 mantle are juxtaposed at the break up stage. The concepts shown in (a) and (b) contrast with
2621 the concepts attached to the smooth-slopes basins evolution developed in this paper.
2622
2623
2624
2625
2626
2627

2628 1549

2630 **1550 Figure 4. The geological record of the Cretaceous extension in the Paleozoic basement and**
2631 **1551 exhumed mantle of the North Pyrenean Zone (NPZ).**

2633 1552 The map shows the location of mantle bodies and crustal units illustrated in photographs a
2634 to k. (a): dated crustal mylonites associated with the Urdach Iherzolites; thin section
2635
2636
2637
2638
2639
2640

2641
2642
2643 1554 microphotograph (natural light) of the leucocratic gneissic mylonite exposed at Col d'Urdach
2644
2645 1555 and containing numerous micafishes (dating by the Ar/Ar method at 105 Ma; after Asti et al.,
2646
2647 1556 2019). (b): thin section of typical ultramylonite from the lenses of Paleozoic material welded
2648
2649 1557 on the exhumed mantle rocks of the Sarailé lherzolite (Asti et al., 2019). (c): phacoidal fabric
2650
2651 1558 defined by anastomosing shear zones in the mantle body of Bestiac. This fabric is typical of
2652
2653 1559 the lenticular layer as defined by Lagabrielle et al. (2019a, 2019b). (d): phacoidal fabric in the
2654
2655 1560 lenticular layer of the lherzolite body of Moncaup. (e): phacoidal fabric in the lenticular layer
2656
2657 1561 of the lherzolite body of Sarailé (Lagabrielle et al., 2019b). (f): curved shear zones and
2658
2659 1562 elongated tectonic lenses in serpentinized lherzolites of the lenticular layer in the Moncaut
2660
2661 1563 peridotite body. (g and h): phacoidal fabric in the lenticular layer of the lherzolite body of
2662
2663 1564 Urdach: h shows pervasive carbonation (Lagabrielle et al., 2019a). (i and j): thin section and
2664
2665 1565 outcrop of anastomosing serpentinized shear bands in the lherzolites of Etang de Lers
2666
2667 1566 (Lherz). (k): anastomosing serpentinized shear bands in the lherzolites of Avezac.

2665
2666 1567

2667 1568 **Figure 5. The geological record of the Cretaceous extension in the pre-rift cover of the**
2668
2669 1569 **metamorphic North Pyrenean Zone (NPZ). Some field view of outcrops showing the layer**
2670
2671 1570 **perpendicular flattening and the S0/S1 syn-metamorphic foliation.**

2672 1571 (a): layer-parallel boudinage in the Calce quarry (Jurassic dolostones of the Agly massif
2673
2674 1572 cover, Eastern NPZ). (b): layer-parallel ductile stretching of the meta-laterite and carbonate
2675
2676 1573 breccia in the Benou quarry near Turon de la Tecouère lherzolite body (Chainons Béarnais,
2677
2678 1574 Western NPZ). (c): flattened fossils in the Jurassic meta-dolostones of the Saleix valley (Aulus
2679
2680 1575 basin, Central NPZ). (d): extreme stretching of a rudist-rich Urgonian marbles at Sarrance
2681
2682 1576 (Chainons Béarnais, Western NPZ) (see also fig. 6c). (e): tight normal faults affecting the
2683
2684 1577 early S0/S1 syn-metamorphic foliation in the pre-rift cover marbles of the Agly massif. These
2685
2686 1578 features characterize the ductile-brittle transition that occurred at the end of the rifting
2687
2688 1579 history. (f): same features as (e) but in the marbles of the detached Lherz body cover
2689
2690 1580 (southern side). (g): recumbent folds associated with the early ductile foliation in marbles
2691
2692 1581 from the detached cover of the Pays de Sault Paleozoic basement (Eastern NPZ). (h): tectonic
2693
2694 1582 brecciation with calcite veining marking the ductile-brittle transition in the marbles of the
2695
2696 1583 Lherz body cover (western side).

2694
2695 1584

2696 1585 **Figure 6 . A theoretical log of the lithological succession in the internal domain of the**

2701
2702
2703 **1586 Cretaceous NPZ rift basins.**
2704

2705 1587 The photographs illustrate the various rock-types forming the basin basement (crust and
2706 1588 mantle) and the pre-rift and syn-rift series. (a): Chaînons Béarnais (Saraillé massif, western
2707 1589 NPZ). (b): Boucheville basin (eastern NPZ). (c): Urgonian at Sarrance (western NPZ) (see also
2710 1590 fig. 5d). (d): Jurassic dolomites at Calce (eastern NPZ). (e): base of pre-rift series (Bestiac,
2711 1591 eastern NPZ). (f): base of pre-rift series (Moncaup, central NPZ). (g): crustal lenses of Saraillé
2713 1592 massif (western NPZ). (h): lenticular layer (Urdach mantle body, western NPZ).
2714

2715 1593

2716
2717 **1594 Figure 7. Interpreted and reconstructed profiles of peri-Pyrenean Cretaceous basins**
2718 **1595 architecture.**

2719
2720 1596 (a): Parentis basin. (b): Columbrets basin. (c and d): Cameros basin. See location of basins in
2721 1597 fig. 1.
2722

2723 1598

2724
2725 **1599 Figure 8. A compilation of model results and conceptual representations of extended to**
2726 **1600 hyper-extended continental crust.**

2727
2728 1601 This compilation aims enhancing the main mechanical concepts involved in the processes of
2729 1602 crustal extension and how they apply or not apply to the genesis and evolution of the
2730 1603 smooth-slopes basins defined in this article (see text for discussion).
2731
2732

2733 1604

2734
2735 **1605 Figure 9. A compilation of reconstructed architecture of Pyrenean Cretaceous basins and a**
2736 **1606 Basque-Parentis transect.**

2737
2738 1607 All represented sections are based on the activation of a restricted number of detachment
2739 1608 faults. As discussed in text, such representations do not match the newly defined smooth-
2740 1609 slopes architecture that characterize the Pyrenean and peri-Pyrenean Cretaceous basins.
2741
2742

2743 1610

2744
2745 **1611 Figure 10. Deformation regimes of the various units composing a typical smooth-slopes**
2746 **1612 basin.**

2747
2748 1613 (a): distribution of pure shear and simple shear regimes in a simplified smooth-slopes basin
2749 1614 system. (b): Detail of the very distal part of the hyper-extended crust (area shown in a). (b1):
2750 1615 simplified log showing the association of metric to hectometric crustal lenses separated
2751 1616 from the mantle rocks by the crust-mantle detachment and from the detached pre-rift cover
2752 1617 by the cover décollement (see definition in Lagabrielle et al., 2019a, 2019b). (b2): field view
2753
2754
2755
2756
2757
2758
2759
2760

2761
2762
2763 1618 of crustal sheets from the base of the Saraillé massif (western NPZ). (b3): field view of
2764
2765 1619 anastomosing shear zones cutting through the serpentinitized peridotite of the Saraillé body
2766
2767 1620 and forming the lenticular layer of the crust-mantle detachment (see also fig. 4c to k).

2768 1621

2770 1622 **Figure 11. A compilation of schematic architecture of selected Atlantic and Mediterranean**
2771
2772 1623 **passive margins.**

2773 1624 These margin profiles are selected because they offer architectures which do not fit with
2774
2775 1625 the Iberia-Newfoundland-type margin (see fig. 2). In particular, they show large scale crustal
2776
2777 1626 boudinage and lenticulation that are consistent with a ductile regime of extensional
2778
2779 1627 deformation. Sheets of hyper thinned crustal material is indicated by the orange arrow (see
2780
2781 1628 comments in text). Note that scale is similar in all profiles.

2782 1629

2784 1630 **Figure 12. Three numerical models of rift development compared to the Angola-Brazil and**
2785
2786 1631 **Iberia transects.**

2787 1632 All models highlight a mode of deformation that leads to the development of very thin and
2788
2789 1633 long sheets of crustal material also observed in the Angola-Campos transect but not in the
2790
2791 1634 Iberia transect. Such deformation necessarily imply a ductile behaviour of the crust
2792
2793 1635 consistent with processes acting in the central part of the smooth-slopes basins studied in
2794
2795 1636 this paper (see text for further comments).

2796 1637

2798 1638 **Figure 13. Paleogeography of Triassic deposits and Cretaceous rifting around the Iberia**
2799
2800 1639 **plate.**

2801 1640 (a): paleogeographic maps for the Triassic period (modified from Orti et al., 2017) and
2802
2803 1641 location of some further Cretaceous rifted regions. Note that by contrast to the area where
2804
2805 1642 Cretaceous smooth-slopes basins will open, the area corresponding to the future Iberia-
2806
2807 1643 Newfoundland conjugate margins are devoid of thick evaporitic series. (b): paleogeographic
2808
2809 1644 maps for the Ladinian and Carnian (Middle-early Late Triassic times, 242-227 Ma) modified
2810
2811 1645 after Scotese and Schettino (2017). (c): paleogeography of Upper Triassic deposits prepared
2812
2813 1646 after a compilation of unpublished data by D. Frizon de Lamotte (pers. com.) superimposed
2814
2815 1647 on a plate reconstruction by Olivet (1996).

2816 1648

2821
2822
2823 **1649 Figure 14. Correlation between the paleogeography of Triassic deposits and the mode of**
2824
2825 **1650 rifting around the Iberia plate.**

2826
2827 1651 (a): cartoons (a1 and a2) illustrating the contrasted rifting modes between the Iberia-
2828
2829 1652 Newfoundland-type and the Parentis-type margins (modified from Clerc and Lagabrielle,
2830
2831 1653 2014). (b): paleogeography of Triassic (Late Norian) deposits according to Marcoux et al. in
2832
2833 1654 the Dercourt et al. (1993) map atlas. As paleogeographic maps in fig. 13, this reconstruction
2834
2835 1655 points to the lack of thick evaporites deposits in the future Iberia-Newfoundland rifting
2836
2837 1656 domain (see text for discussion).

2838
2839
2840
2841
2842
2843
2844
2845
2846
2847
2848
2849
2850
2851
2852
2853
2854
2855
2856
2857
2858
2859
2860
2861
2862
2863
2864
2865
2866
2867
2868
2869
2870
2871
2872
2873
2874
2875
2876
2877
2878
2879
2880

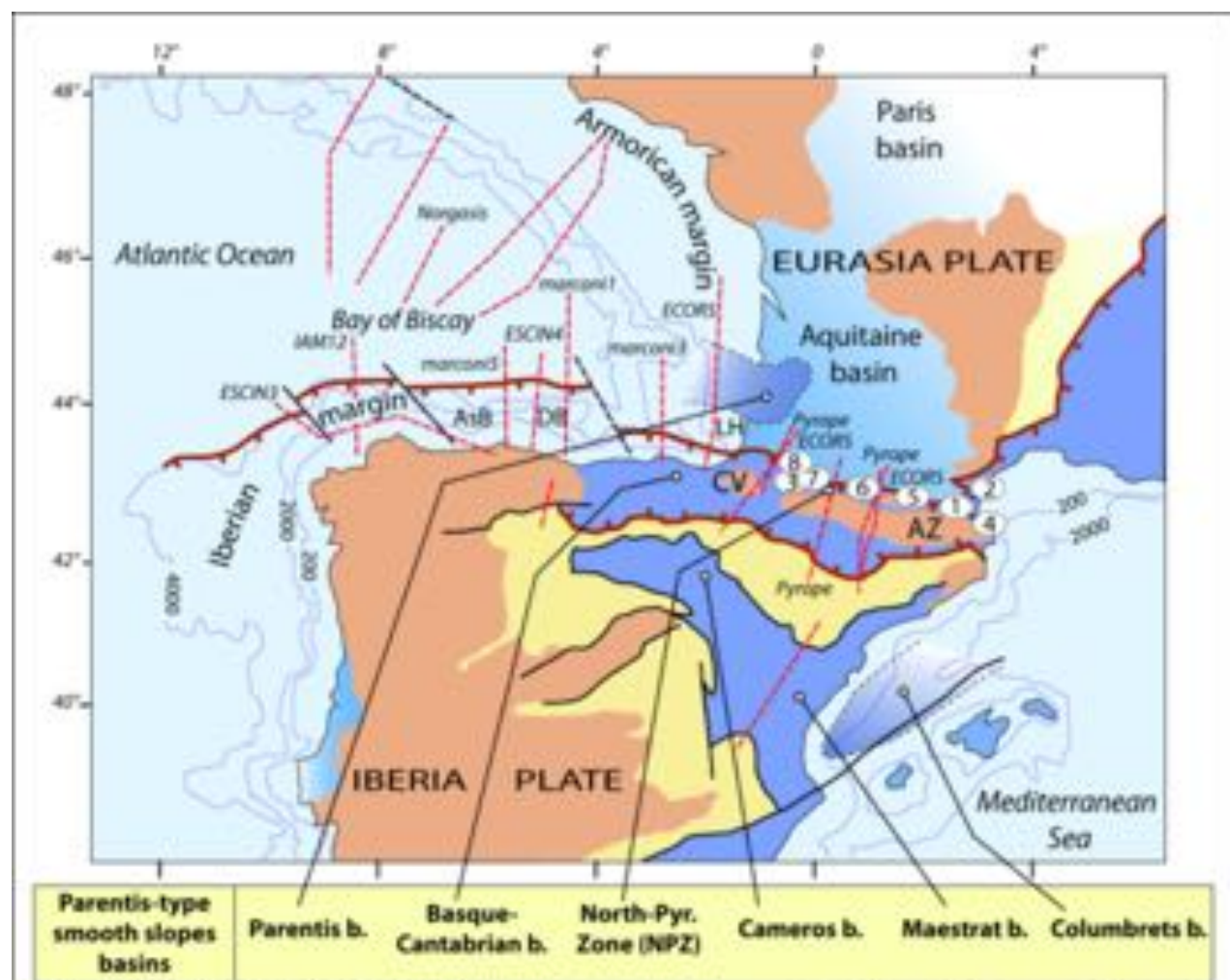
2838 **1658 Figure 15. Time-dependent rheological evolution of the Pyrenean rifting based on**
2839
2840 **1659 geological constraints from the North Pyrenean Zone and numerical results from a thermo-**
2841
2842 **1660 mechanical numerical modeling.**

2843
2844 1661 Sketches depicting the geological evolution are extracted from the Clerc et al. (2016) model.
2845
2846 1662 Rheological profiles derive from the Duretz et al., (2019) model. They are placed at critical
2847
2848 1663 locations (1, 2 and 3) of the rift in order to emphasize the drastic changes in the mechanical
2849
2850 1664 behaviour during its evolution from limited crustal extension to local mantle exhumation
2851
2852 1665 (see detailed description in text).

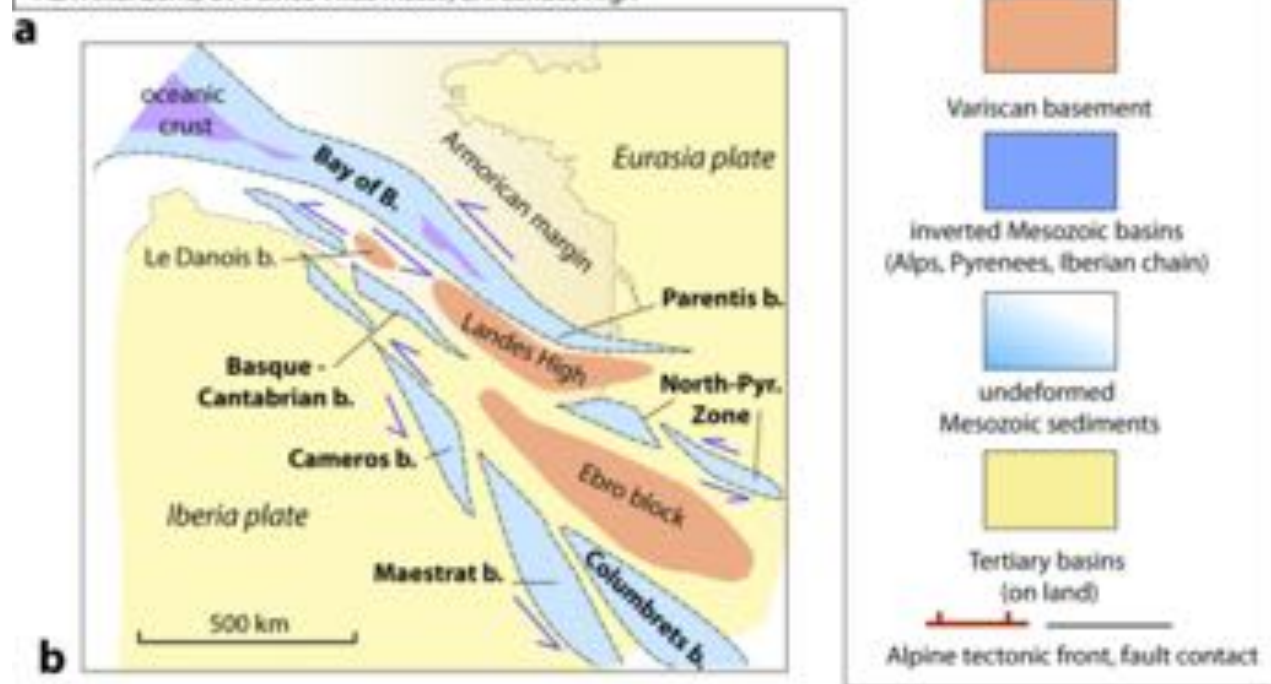
2853
2854
2855
2856
2857
2858
2859
2860
2861
2862
2863
2864
2865
2866
2867
2868
2869
2870
2871
2872
2873
2874
2875
2876
2877
2878
2879
2880

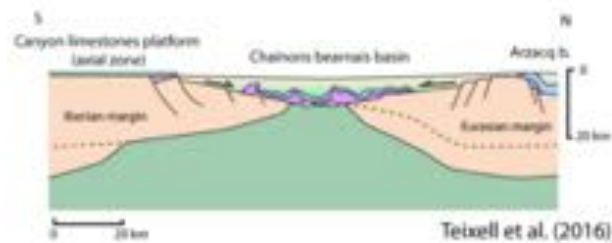
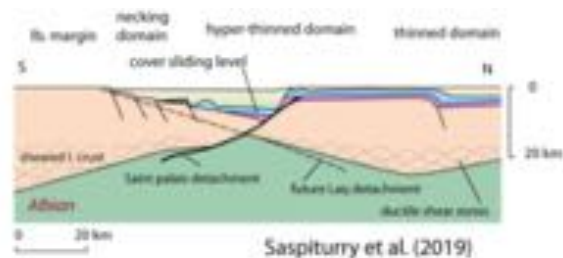
2854 **1667 Figure 16. A theoretical structural model for the Cantabrian, Pyrenean and Iberian**
2855
2856 **1668 symmetrical smooth-slopes basins based on the features and concepts discussed in this**
2857
2858 **1669 article.**

2859
2860
2861
2862
2863
2864
2865
2866
2867
2868
2869
2870
2871
2872
2873
2874
2875
2876
2877
2878
2879
2880



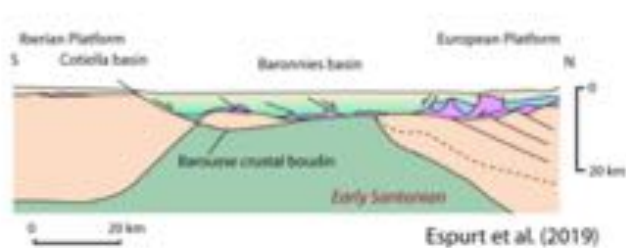
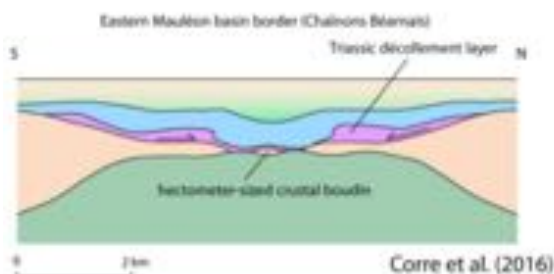
① location of photographs in figure 6





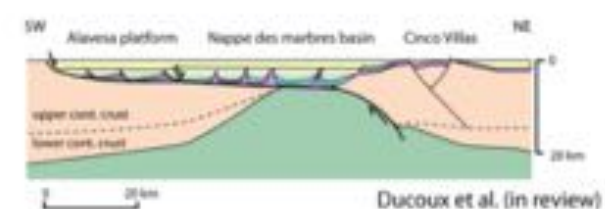
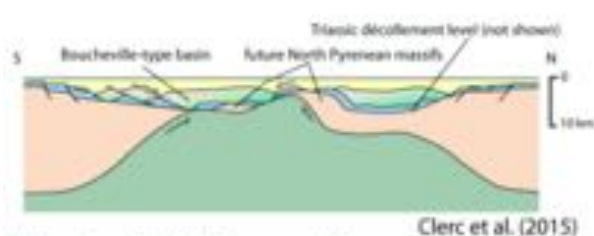
a. Western North Pyrenean Zone (1)

b. Western North Pyrenean Zone (2)



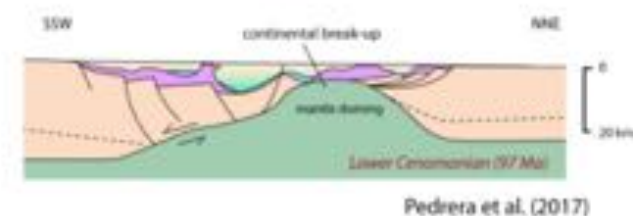
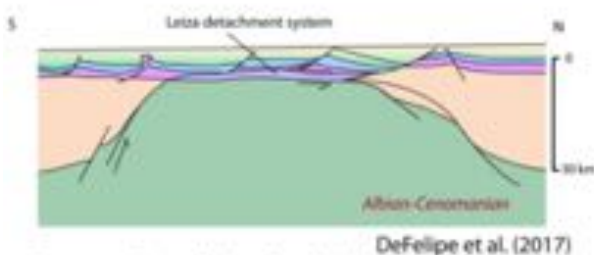
c. Western North Pyrenean Zone (3)

e. Central North Pyrenean Zone



h. Eastern North Pyrenean Zone

f. Basque-Cantabrian basin (1)

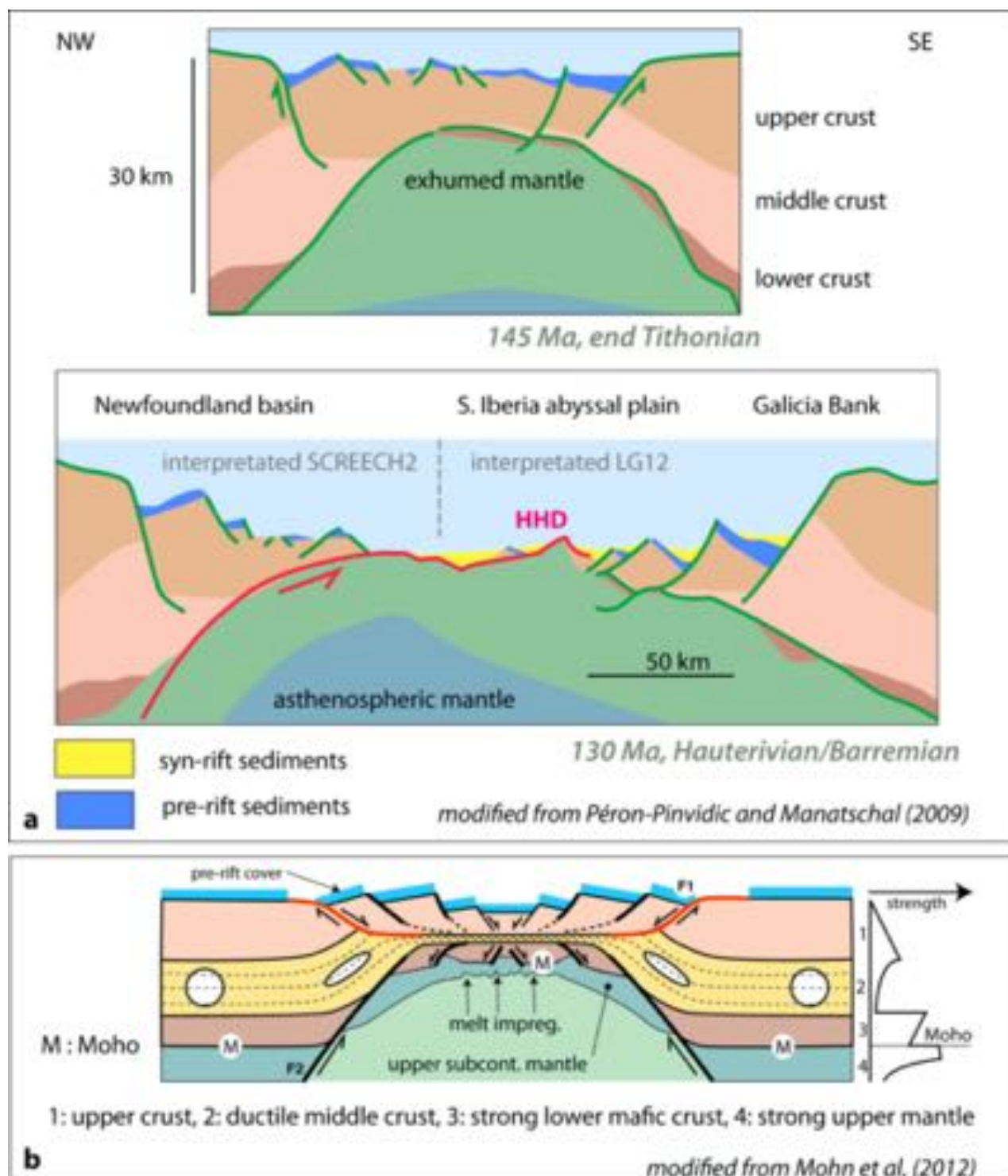


g. Basque-Cantabrian basin (2)

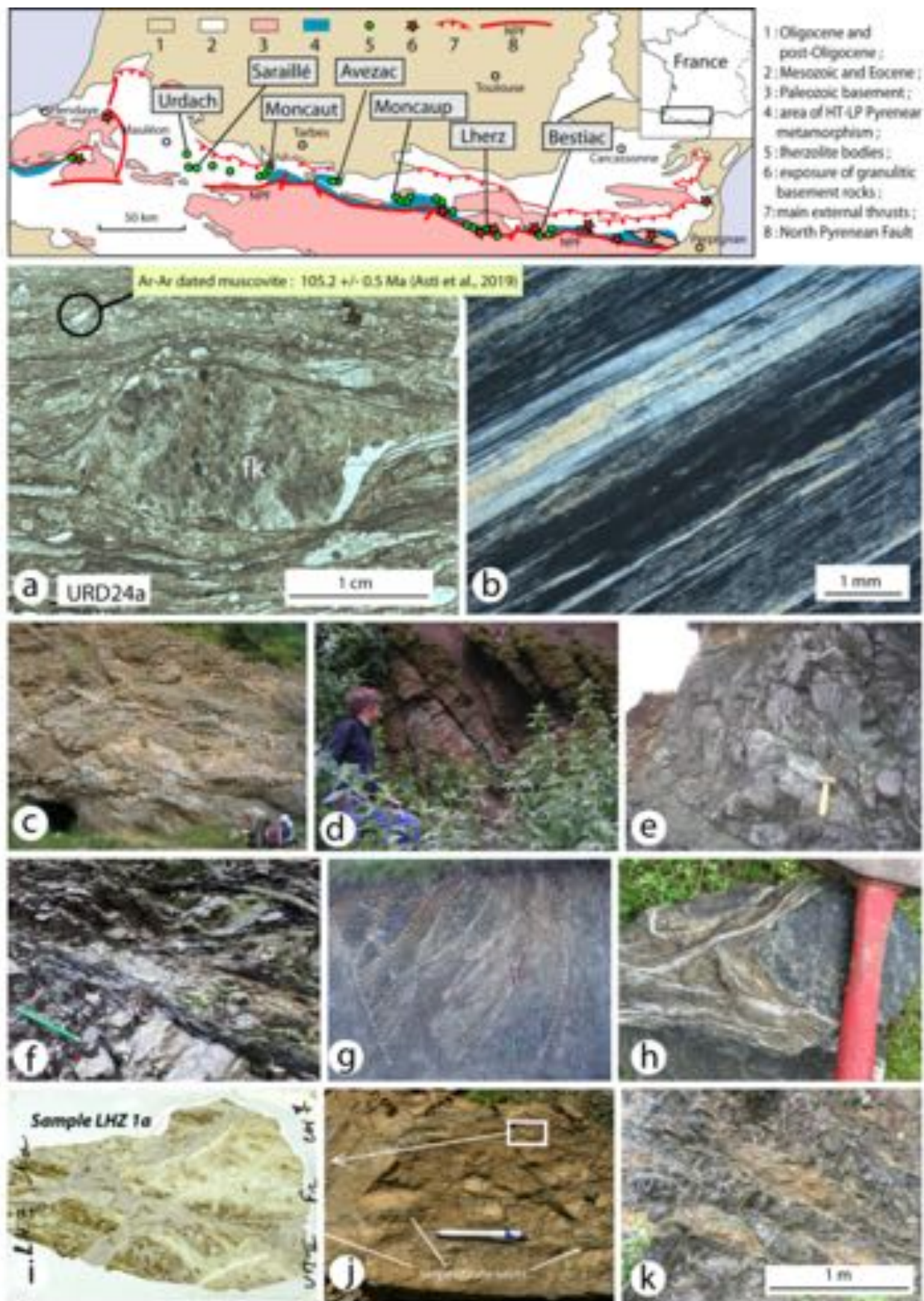
h. Basque-Cantabrian basin (3)



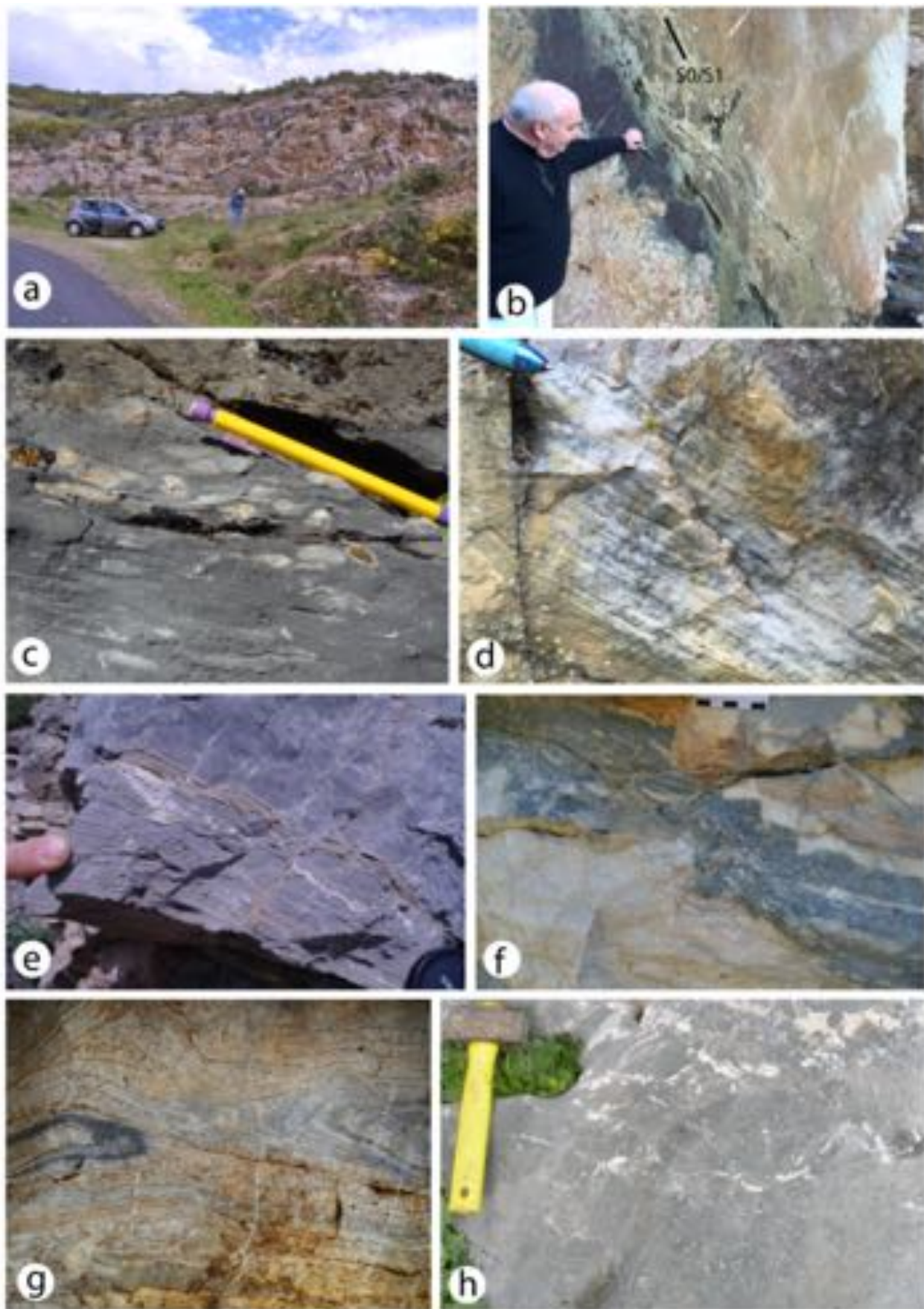
Lagabrielle et al., fig. 2, ESR, submitted



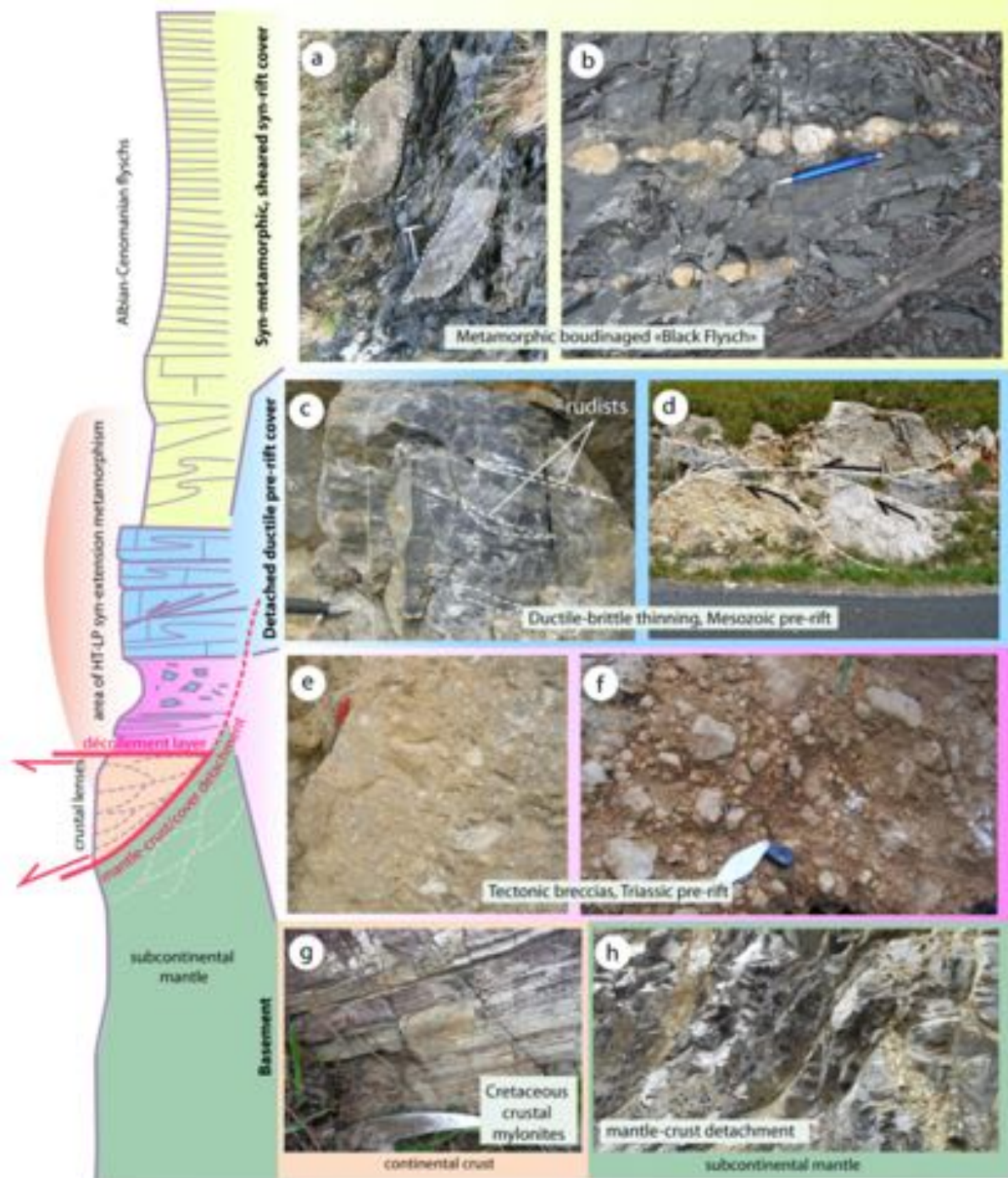
Lagabrielle et al., fig. 3, ESR, submitted



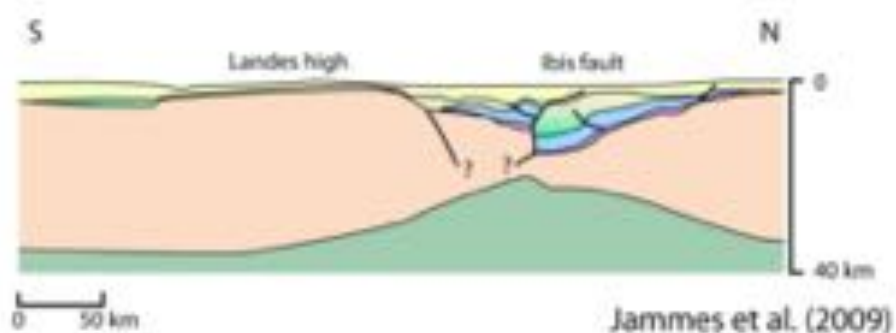
Lagabrielle et al., fig. 4, ESR, submitted



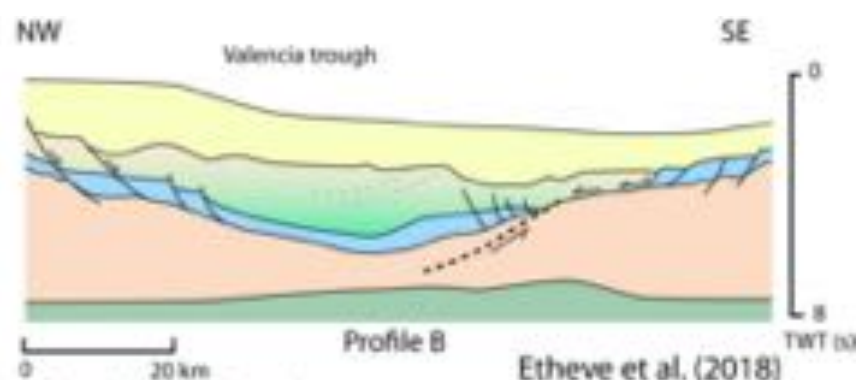
Lagabrielle et al., fig. 5, ESR, submitted



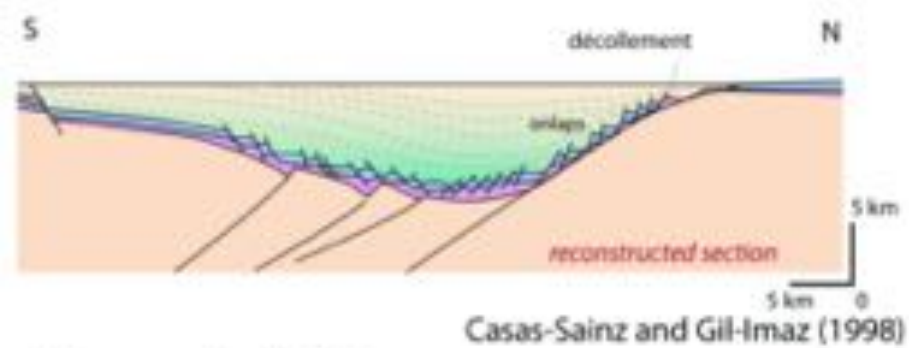
Lagabrielle et al., fig. 6, ESR, submitted



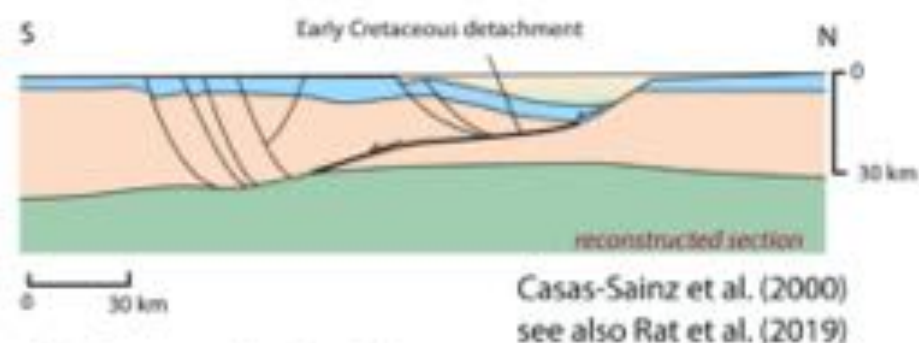
a. Parentis basin



b. Columbrets basin

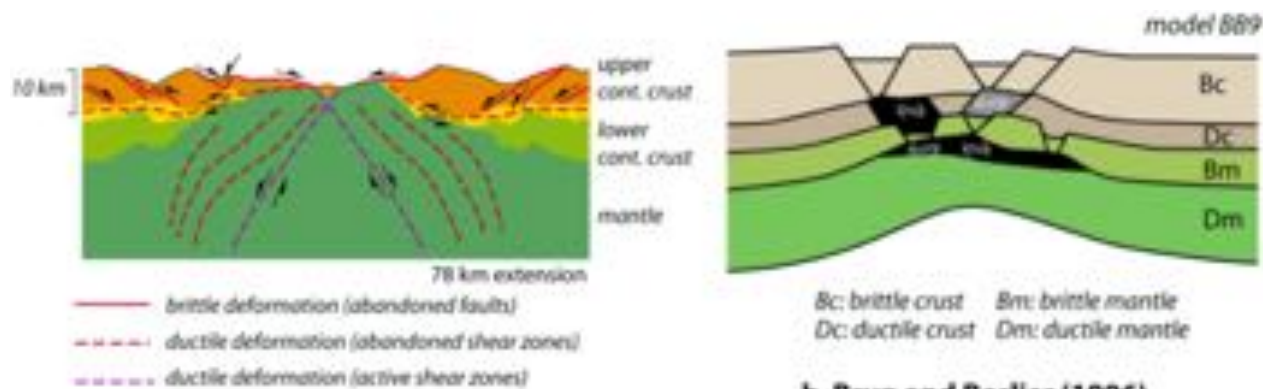


c. Cameros basin (1)

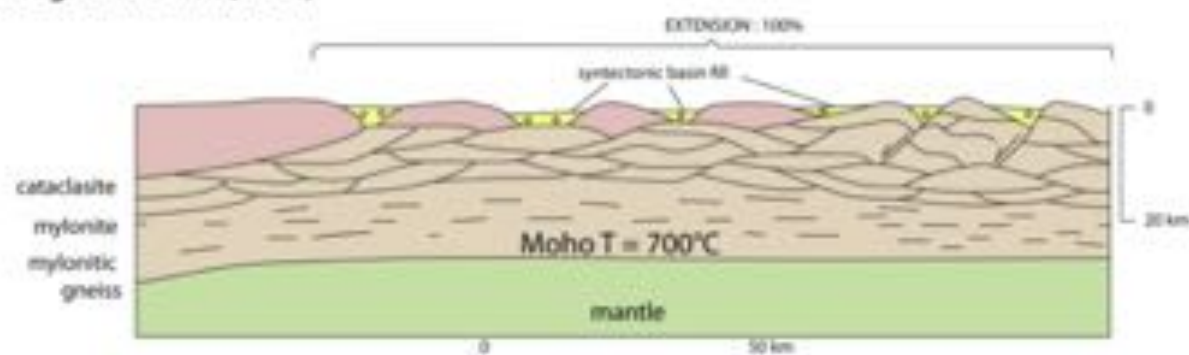


d. Cameros basin (2)

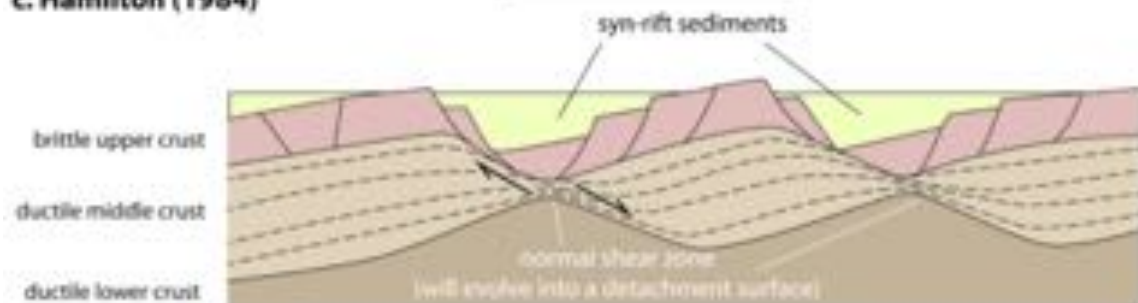




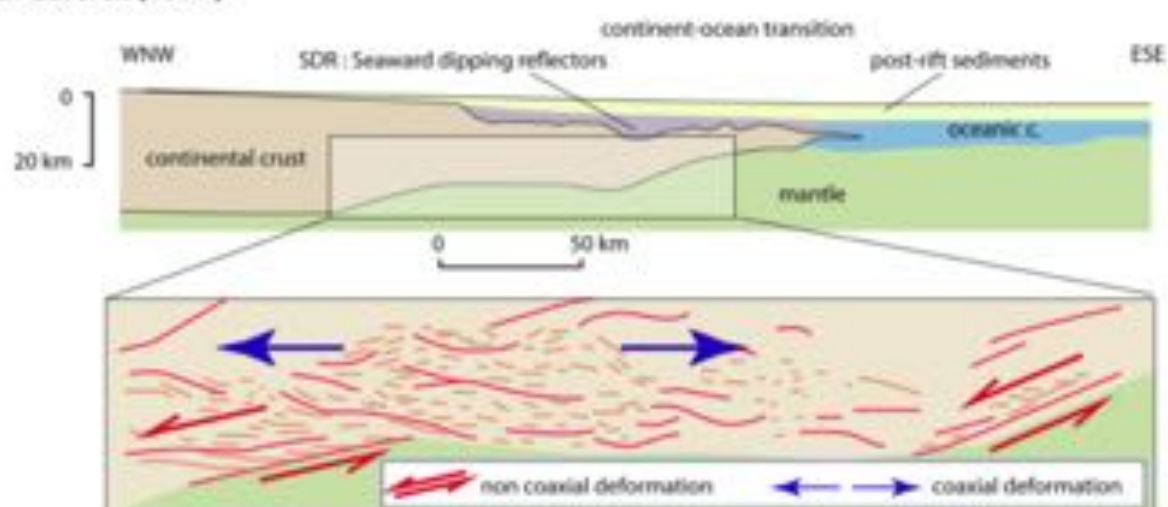
a. Nagel and Buck (2004)



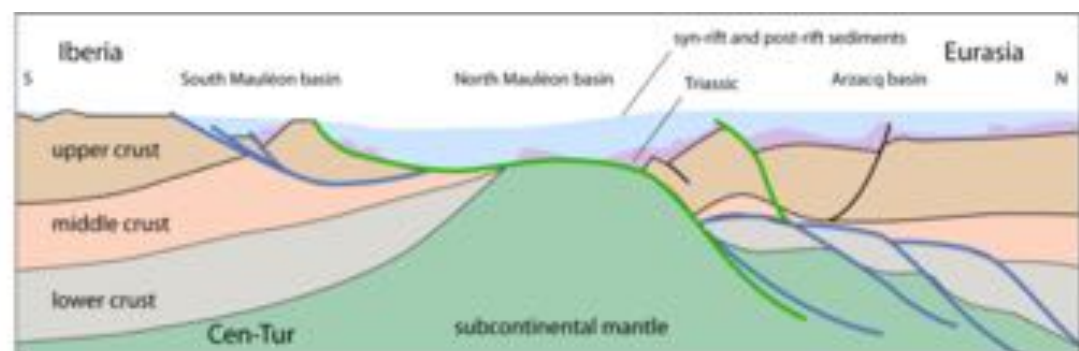
c. Hamilton (1984)



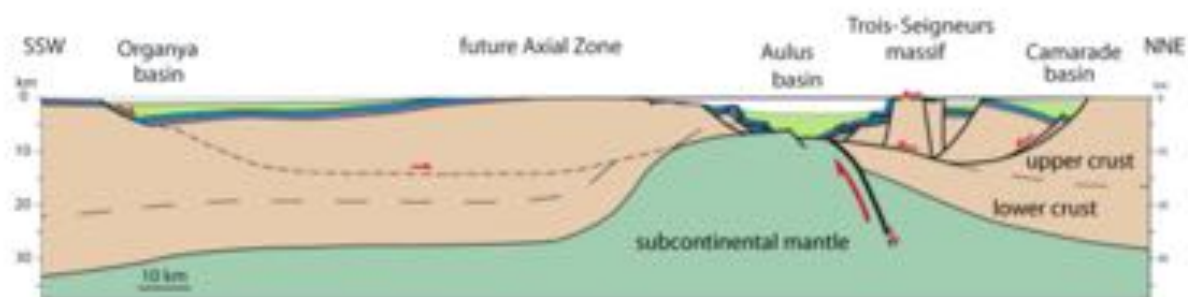
d. Gartrell (1997)



e. Clerc et al. (2018)



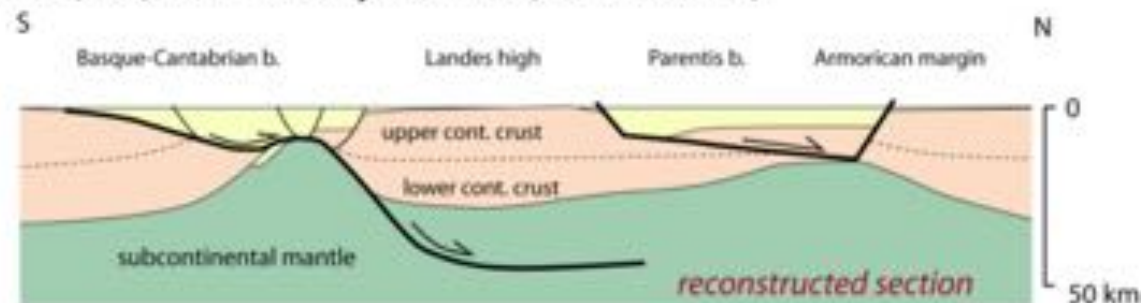
a. Masini et al. (2014): Mauléon basin



b. Lagabrielle et al. (2010): Central North Pyrenean Zone (Aulus basin, Etang de Lers)



c. Vauchez et al. (2013): Eastern North Pyrenean Zone (Boucheville basin)



d. Roca et al. (2011) : Basque-Parentis transect

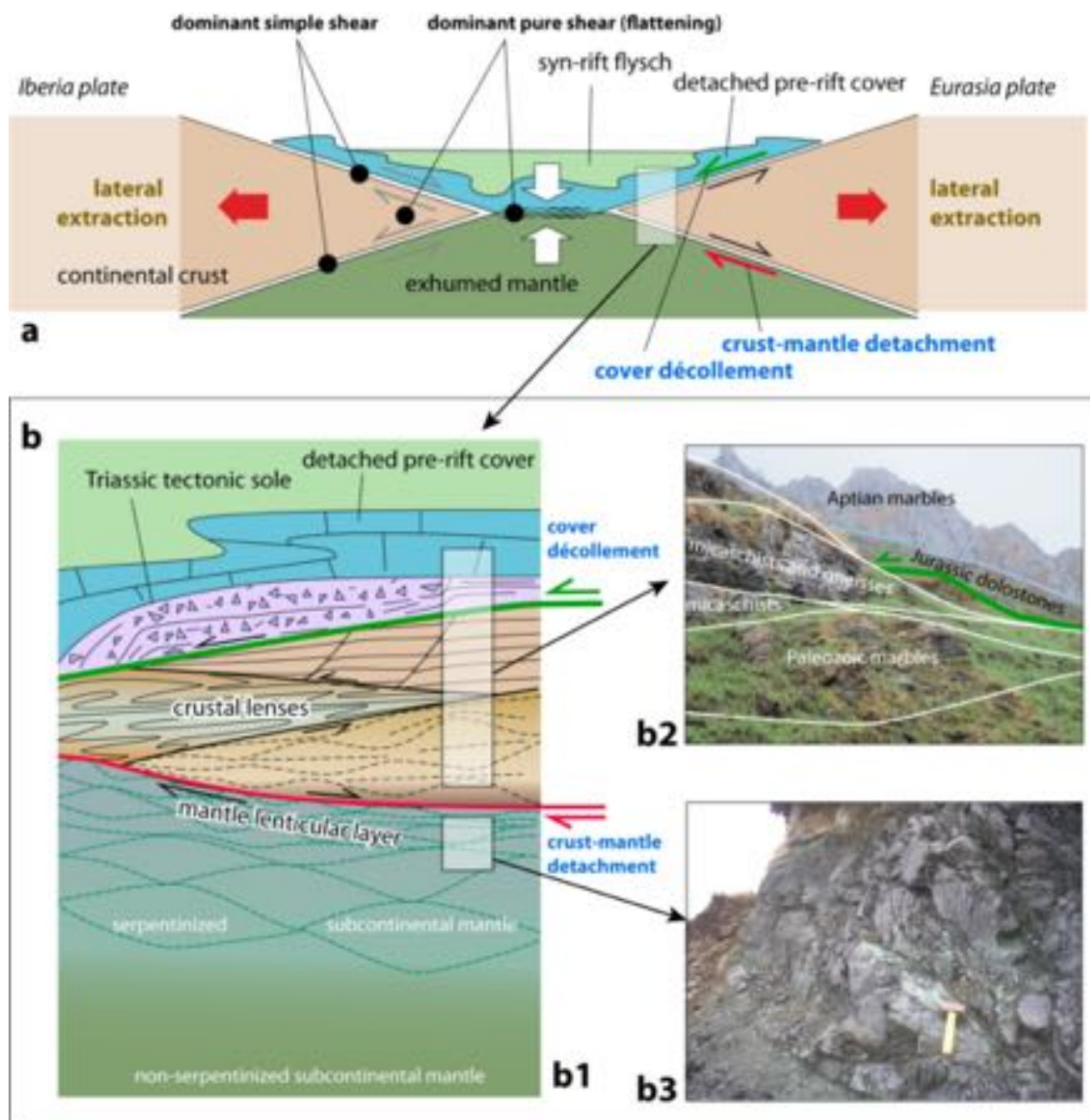
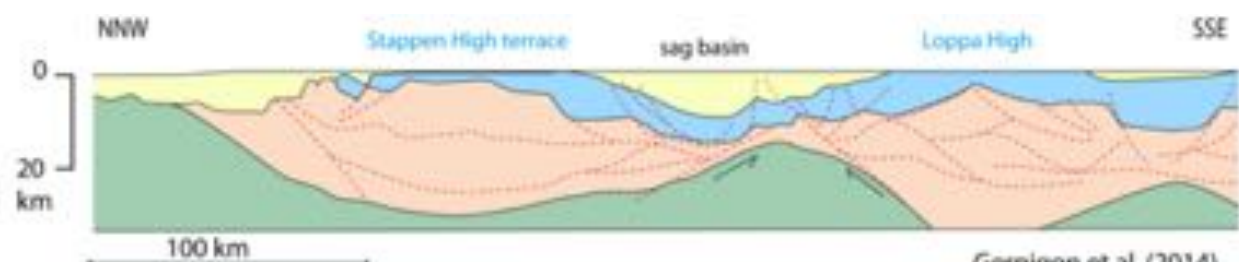
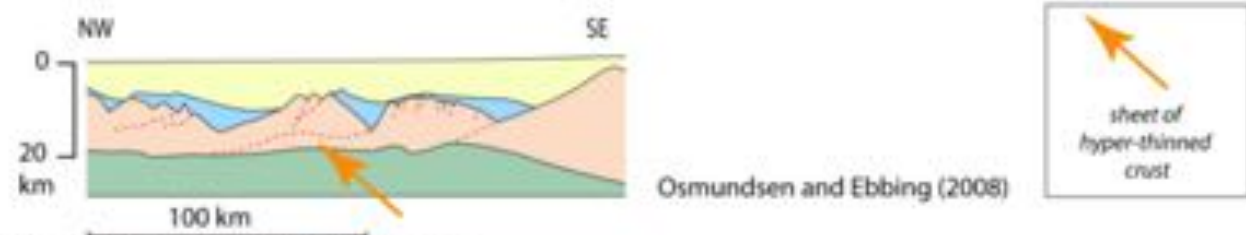


fig. 10

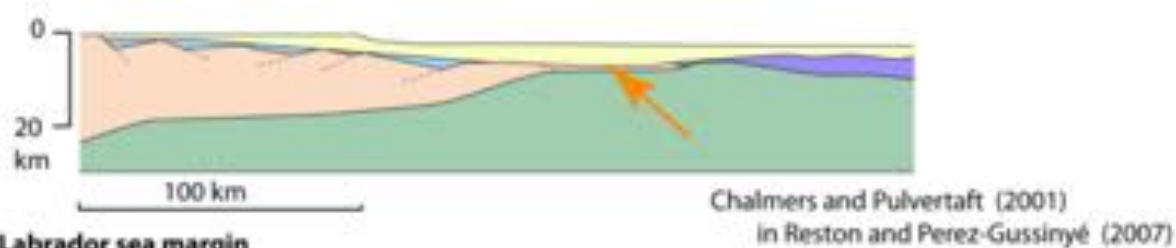
Lagabrielle et al., smooth slopes basins, submitted



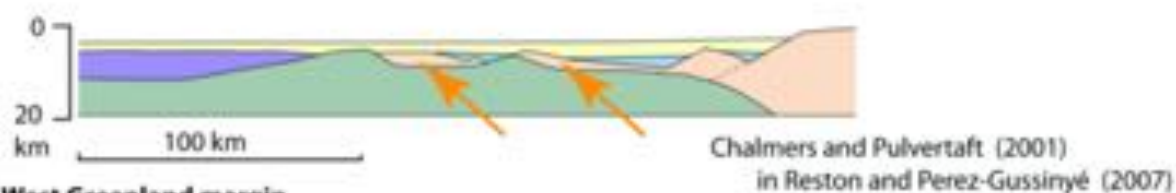
a. Barents margin



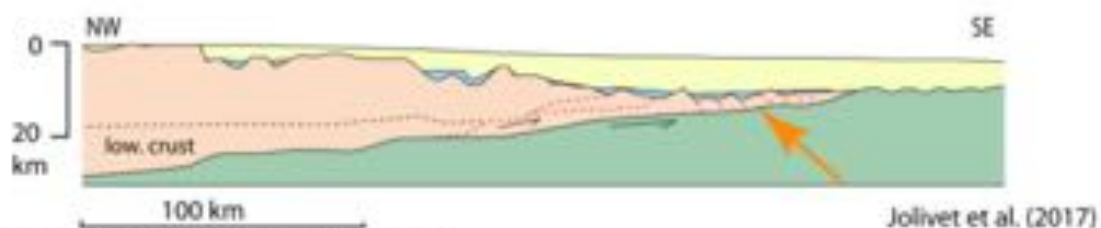
b. Northern More basin, Norway margin



c. Labrador sea margin

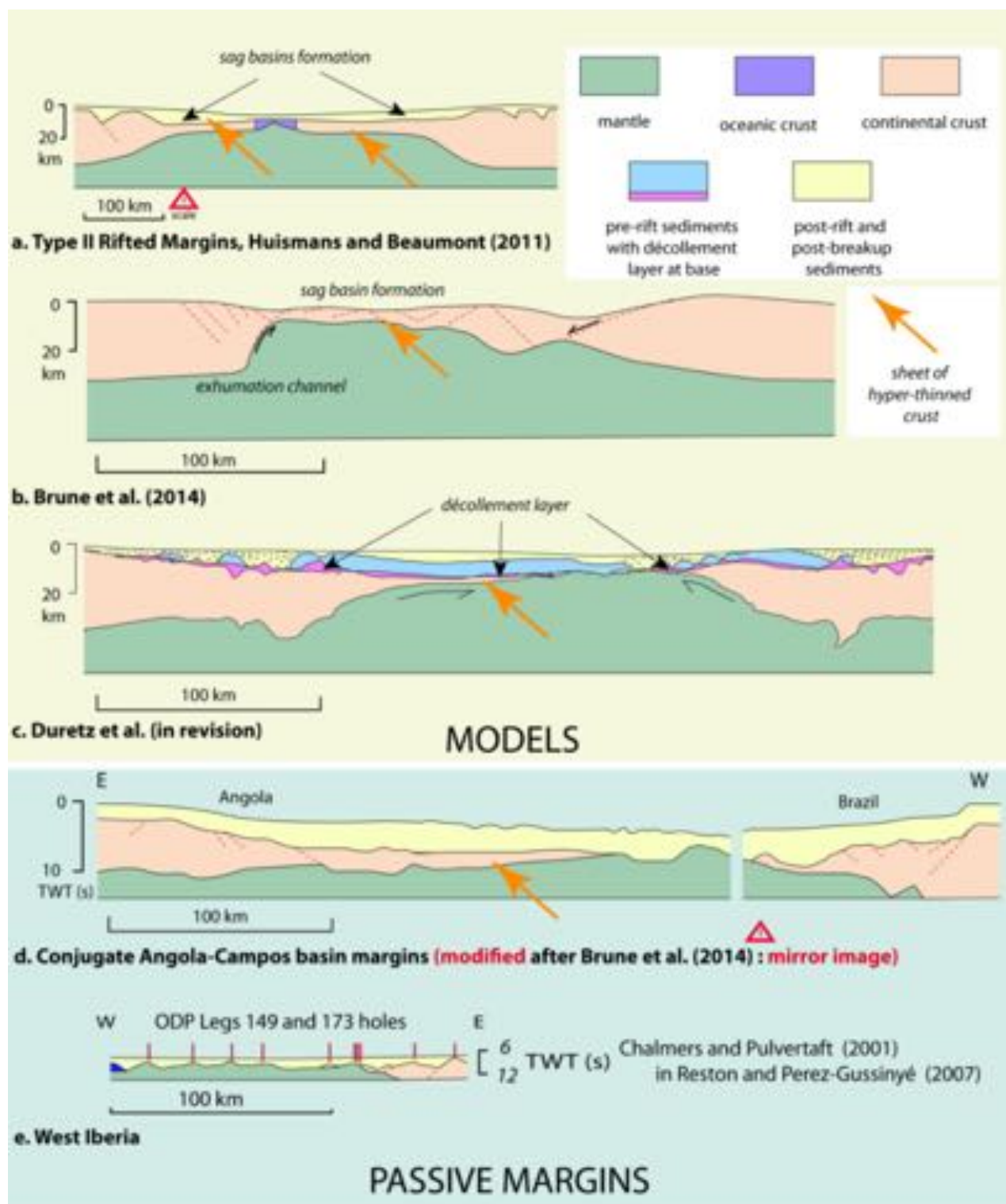


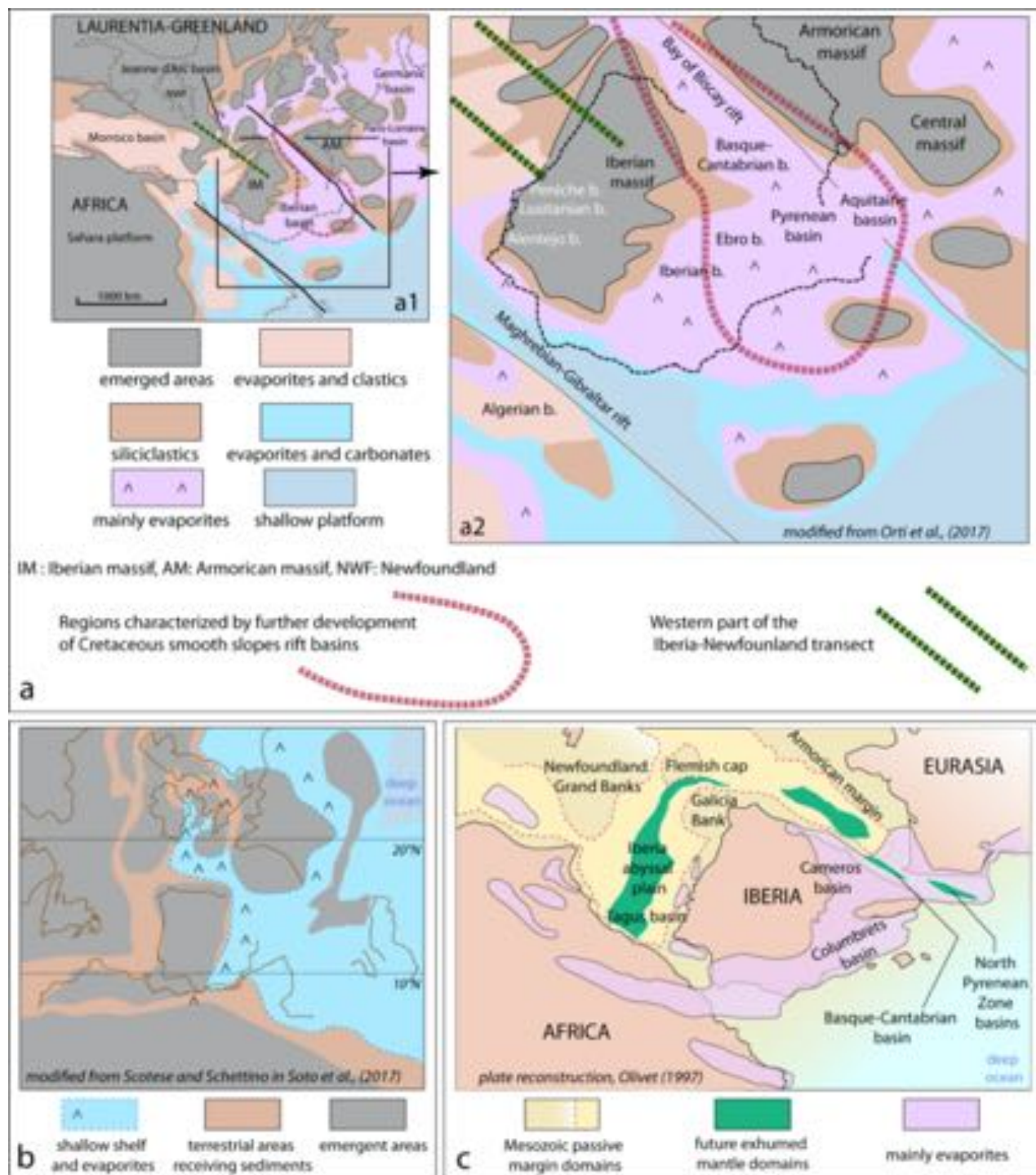
d. West Greenland margin



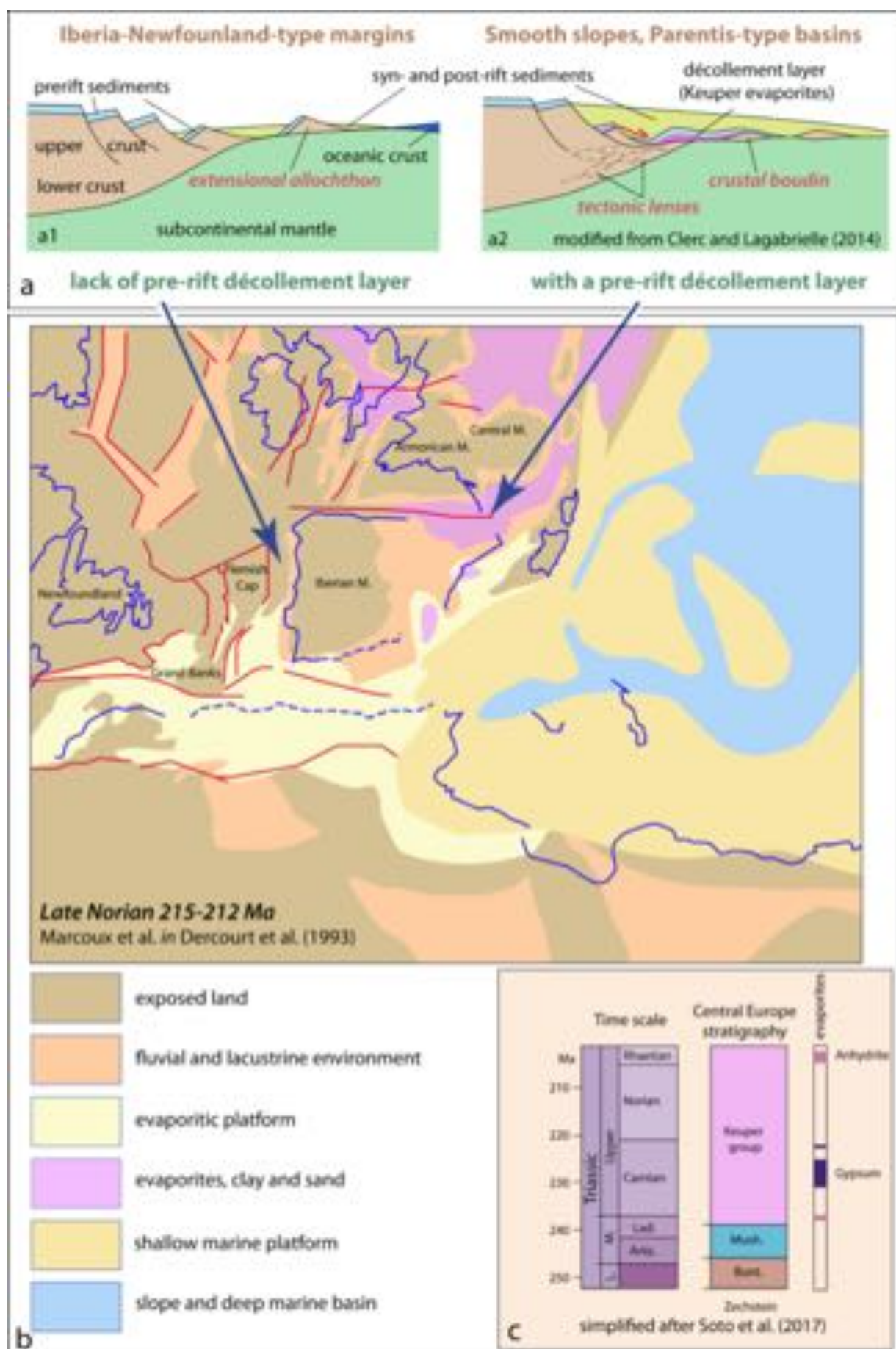
e. Western Mediterranean, Gulf of Lion

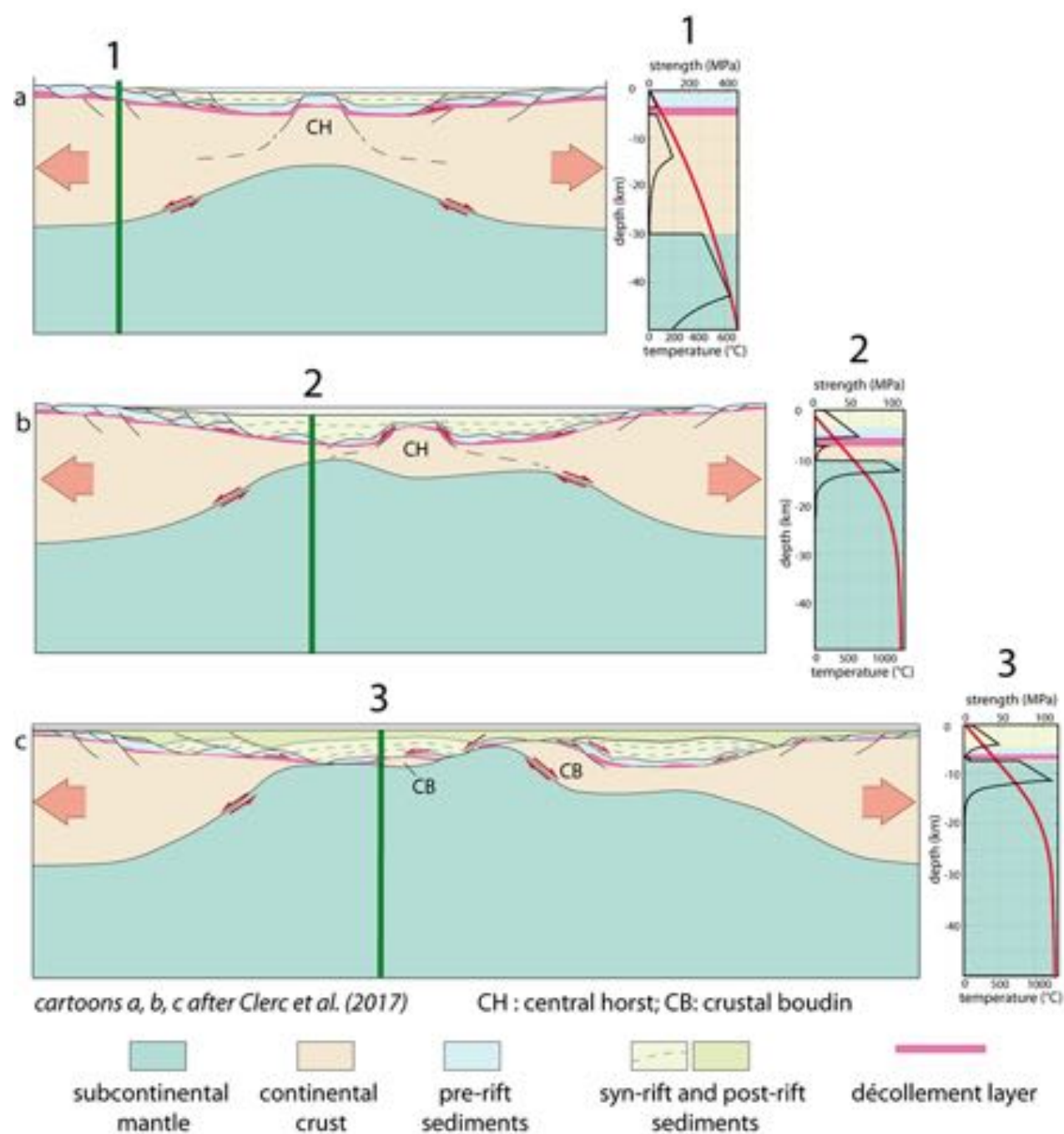




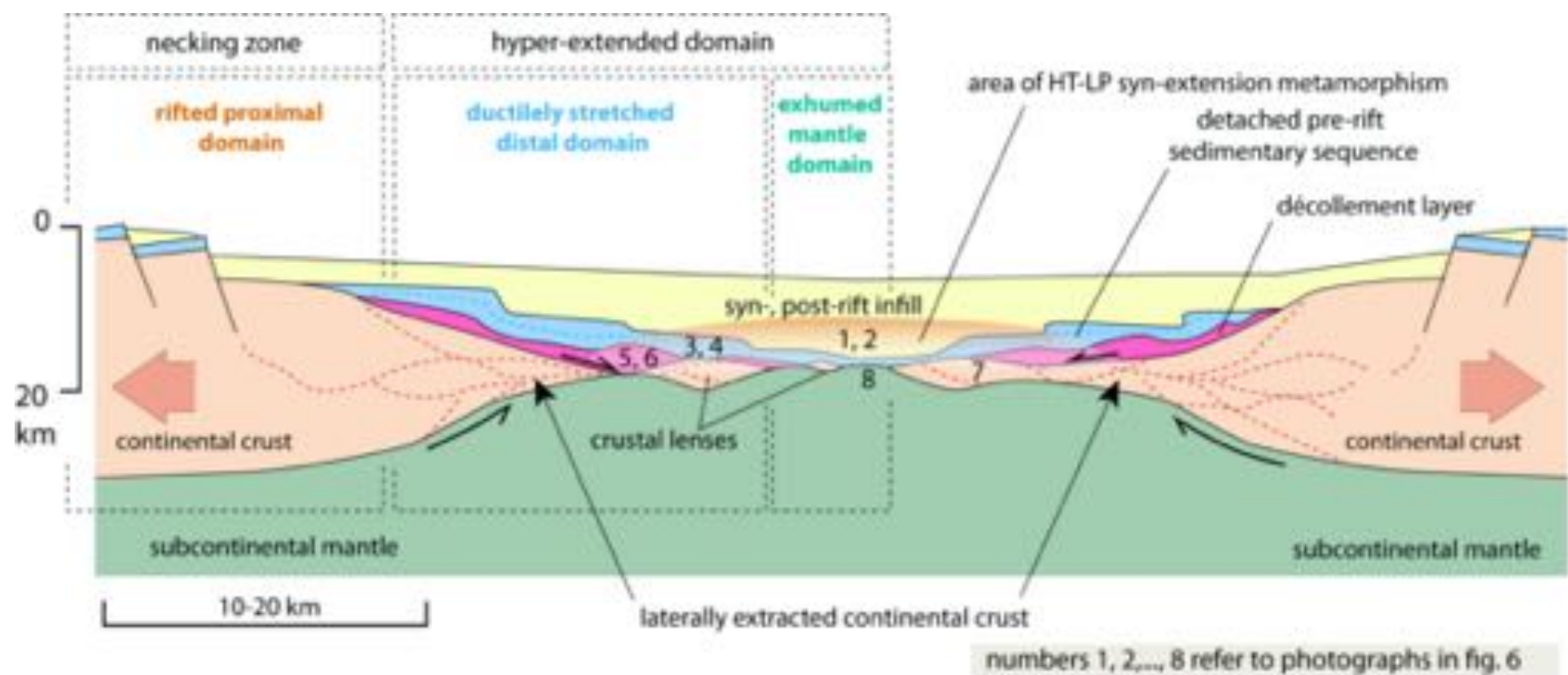


Lagabrielle et al., fig. 13, ESR, submitted





Lagabrielle et al., fig. 15, ESR, submitted



Lagabrielle et al., fig. 16, ESR, submitted